Hydrodynamics of Ciliary Systems

Dissertation for the award of the degree

Doctor Rerum Naturalium

of the Georg-August-Universität Göttingen

within the doctoral program

Physics of Biological and Complex Systems

of the Georg-August University School of Science

submitted by

David James Hickey

from

Epsom, The United Kingdom

GEORG-AUGUST-UNIVERSITÄT GÖTTINGEN IN PUBLICA COMMODA SEIT 1737

Göttingen 2023

Thesis committee

Member 1	Prof. Dr. Ramin Golestanian Living Matter Physics Max-Planck-Institut für Dynamik und Selbstorganisation
Member 2	Prof. Dr. Marcus Müller Institut für Theoretische Physik Georg-August-Universität Göttingen
Member 3	Prof. Dr. Annette Zippelius Institut für Theoretische Physik Georg-August-Universität Göttingen

Members of the examination board

First referee	Prof. Dr. Ramin Golestanian Living Matter Physics Max-Planck-Institut für Dynamik und Selbstorganisation
Second referee	Prof. Dr. Marcus Müller Institut für Theoretische Physik Georg-August-Universität Göttingen
Additional reviewer	Prof. Dr. Annette Zippelius Institut für Theoretische Physik Georg-August-Universität Göttingen
Additional reviewer	Prof. Dr. Stefan Klumpp Institute for Nonlinear Dynamics Georg-August-Universität Göttingen
Additional reviewer	Dr. David Zwicker Theory of Biological Fluids Max-Planck-Institut für Dynamik und Selbstorganisation
Additional reviewer	Dr. Aljaz Godec Mathematical Biophysics Group Max-Planck-Institut für Multidisziplinäre Naturwissenschaften

Date of oral examination: 2023-06-29

Abstract

The interactions of cilia with one another and their environment are central to many important questions in biology. These hairlike organelles are found in motile and immotile (or 'primary') variants, and have a variety of roles in sensing and fluid pumping. Primary cilia have long been known to act as chemosensors, but recent research has found that motile cilia also have this ability, and it is not known what benefit is conferred by combining all the complicated required molecular machinery. These chemosensitive motile cilia are often found in bundles, which is surprising, as one would expect each to deplete the local chemical concentration field, leading to a lower sensitivity per cilium. Motile cilia have long been known to synchronise with one another to produce metachronal waves, but the precise mechanism behind this synchronisation is still not well understood, except that hydrodynamics plays an important role.

In this thesis, we aim to make some headway in answering these open questions, by developing models of the interactions of cilia and the surrounding fluid flow. First, using both analytical and computational methods, we determine the mass transfer to individual cilia (both primary and motile) as well as bundles of motile cilia. We show that the cilium geometry alone is sufficient to dramatically increase chemosensitivity over chemosensors on the cell surface, especially if the fluid near the cilium is in motion. We also find that motility can increase chemosensitivity by a large factor at realistic cilium speeds, and that motile bundles are more chemosensitive per cilium, provided they are beating sufficiently quickly. We then use computational methods to focus on how cilia hydrodynamically interact with one another, and show that certain cilium beats can result in strongly nonreciprocal hydrodynamic interactions that can give rise to quickly emerging metachronal order with a single dominant wavevector, even in finite systems. When the near-field hydrodynamic interactions (and hence the nonreciprocity of interactions) is suppressed, synchronisation is much slower and multiple wavevectors are seen.

We have therefore uncovered several reasons why chemosensors may be advantageously located on both motile and primary cilia, and shown that a cilium beat fine-tuned to give strong nonreciprocal interactions can be extremely effective in inducing metachronal order. This amounts to a significant amount of evidence pointing to some potential answers to some of the open questions surrounding cilia.

Author contributions

This thesis contains two scientific articles, both included here in their original form.

Chapter 3 contains the article "Ciliary chemosensitivity is enhanced by cilium geometry and motility", published in the journal eLife, authored by David J Hickey, Andrej Vilfan, and Ramin Golestanian. The project on which the work was based was conceptualised by AV and RG; the analysis and simulation was designed and implemented by DJH and AV. The manuscript was written by DJH and AV, and edited by DJH, AV and RG. Supervision was contributed by AV and RG.

Chapter 4 contains the article "Nonreciprocal interactions give rise to fast cilium synchronisation in finite systems", currently under review in the journal PNAS, authored by David J Hickey, Ramin Golestanian, and Andrej Vilfan. The project on which the work was based was conceptualised by AV and RG; the analysis and simulation was designed and implemented by DJH and AV. The manuscript was written by DJH and AV, and edited by DJH, AV and RG. Supervision was contributed by AV and RG.

All other work and writing presented in the thesis is entirely the work of DJH.

Acknowledgements

This thesis summarises work conducted over a period of over three years, beginning in 2019 and ending now in 2023. Without the support I have received from others, this work could never have existed, so I would like to take this space to acknowledge their contributions:

I am grateful to my thesis advisory committee members, Prof. Dr. Marcus Müller and Prof. Dr. Annette Zippelius, as well as my supervisors, Prof. Dr. Ramin Golestanian and Dr. Andrej Vilfan, for their constant guidance and support. Of these, I would especially like to thank Andrej Vilfan – I could not have asked for a better supervisor. These people have been the dynein arms that have been propelling me in the right direction.

I am grateful to everyone who proofread this thesis to make sure it was the best it could be, especially my parents, who have probably read through it more times than I have. Without them, this piece of writing would be like a kidney with no mechanosensitive cilia, i.e. missing some very important parts and being dramatically worse off as a result.

Lastly, if my time spent here has taught me anything, it is that collective behaviour is important at all scales of living systems: just as motile cilia are more efficient when they work in a group, life is much better when your friends have your back. For that reason, I'd like to thank everyone who I've enjoyed spending time with during the last three-and-a-bit years, in Göttingen and elsewhere. You know who you are!

Best wishes,

David

Contents

1 Introduction

If one were to go through some of the anatomical sketches made by Leonardo da Vinci, one might find something unexpected: a drawing of someone with their heart on the right side of their chest, as opposed to the more usual left side. It's not certain whether he simply reflected the sketch as he famously reflected his handwriting, but this inversion is a real condition, known as *situs inversus*[1]. Approximately one in ten thousand people are born with this condition, where some or all the organs in the body are reflected left to right. Most patients have all their organs reflected and thus experience no major health issues, as the relative position of all organs is unchanged – they might never even know of their unusual organ arrangement. However, an unlucky few will experience only a partial reflection, leading to potentially life-altering complications [4]. Even centuries on from the first descriptions, we still don't know exactly what causes this to happen. We do, however, know that tiny hairlike organelles named cilia play a central role [5, 6], just as they will play a central role in the work described in this thesis.

1: If he really did observe *situs inversus*, he didn't leave any record to indicate that he found it interesting or unusual. Partial inversions (usually called *situs ambiguous*) were later explicitly described by Hieronymus Fabricius [1] and Marco Aurelio Severino [2], with the full inversion probably being first described later by Matthew Baillie [2, 3].

[1]: Pennekamp *et al.* (2015), *Situs inversus and ciliary abnormalities*

[2]: Ogunlade *et al.* (2015), *The role of electrocardiogram in the diagnosis of dextrocardia with mirror image atrial arrangement and ventricular position in a young adult Nigerian in Ile-Ife: a case report*

[3]: Baillie (1788), *An account of a remarkable transposition of the viscera.*

[4]: Eitler *et al.* (2022), *Situs Inversus Totalis*

[5]: Essner *et al.* (2002), *Conserved function for embryonic nodal cilia*

[6]: McGrath *et al.* (2003), *Cilia are at the heart of vertebrate left–right asymmetry*

One can hardly blame the physician Matthew Baillie for describing this inversion as 'remarkable' in a letter to a friend [3], but *situs inversus* is far from the only fascinating or unexpected thing in biology. The billions of years that have been spent by natural selection tweaking and optimising living organisms have left us some incredibly complex and robust active systems that we are only just beginning to understand. Cilia and the associated disorders are just one very narrow example – the wider field of active matter research concerns itself with systems from scales much smaller than cells (such as cilia or swimming microorganisms) to scales much greater than the size of organisms (such as flocking behaviour in sheep or crowd dynamics at sports venues). Nature has something of a head start on us, as the field of active mat-

ter research has existed for barely three decades – possibly the best known model in active matter is the Vicsek model of flocking, which was only defined in 1995 [7]) – whereas life on this planet may have existed for close to 4.5 billion years. However, there is a bright side to the rather daunting problem we find ourselves with, as we are presented with a unique opportunity to dig into these systems and begin to unravel the mysteries that life has left for us.

[7]: Vicsek *et al.* (1995), *Novel Type of Phase Transition in a System of Self-Driven Particles*

1.1 Motivation

But despite (or because of) the plethora of systems that fall under the purview of active matter, we have to focus our efforts somewhere, and in this thesis that focus will fall on cilia. These are tiny hairlike organelles[2] which can be found on the membranes of most eukaryotic cells [8], i.e. cells within the group of eukaryotes, organisms whose cells have nuclei. This group includes all animals and many unicellular organisms. Within those organisms, cilia have an astounding array of tasks to perform; if they were to suddenly disappear, the lungs would stop working [9], the brain would cease to function [10], reproduction would grind to a halt [11, 12], little microorganisms would stop moving and subsequently starve to death [13], and much more besides.

2: An organelle is a specialised part of a cell, analogous to how an organ is a specialised part of an organism. Examples include the nucleus, the cell membrane, or the ribosome.

[8]: Nachury *et al.* (2019), *Establishing and regulating the composition of cilia for signal transduction*

[9]: Yaghi *et al.* (2016), *Airway Epithelial Cell Cilia and Obstructive Lung Disease*

[10]: Faubel *et al.* (2016), *Cilia-based flow network in the brain ventricles*

[11]: Lyons *et al.* (2006), *The reproductive significance of human Fallopian tube cilia*

[12]: Girardet *et al.* (2019), *Primary cilia: biosensors of the male reproductive tract*

[13]: Funfak *et al.* (2015), *Paramecium swimming and ciliary beating patterns: a study on four RNA interference mutations*

Given the ubiquity and importance of these little organelles, one would hope that we understood them quite well, but this isn't really the case, despite having known about them for centuries. The first of the two broad types of cilia, termed 'motile cilia' due to their ability to wave under their own power, was probably first discovered in 1675 at the earliest. We now know that they have roles pumping fluid, and under certain circumstances can coordinate their beating with other nearby cilia (since they are usually found in large patches called 'carpets', there are other cilia nearby more often than not) to improve their energetic pumping efficiency [14, 15]. The much-maligned second type, named 'primary cilia' and

[14]: Osterman *et al.* (2011), *Finding the ciliary beating pattern with optimal efficiency*

[15]: Elgeti *et al.* (2013), *Emergence of metachronal waves in cilia arrays*

typically found with only one per cell, were discovered a century later and immediately ignored by the scientific community at large, as their lack of motion meant they were assumed to be useless and vestigial. Only more recently, some two centuries after the initial discovery of cilia, was it realised that primary cilia have sensory roles in the body, such as detection of forces and chemicals, leading to a surge in interest. Later still, it was found that motile cilia also have sensory roles, but the implications of this aren't yet clear [16].

[16]: Bloodgood (2010), *Sensory reception is an attribute of both primary cilia and motile cilia*

There are a number of open questions around these tiny structures, concerning how they interact with each other and the environment, despite numerous studies investigating them. A few that are addressed in this thesis include:

- Why are chemical detectors (more commonly called 'chemoreceptors') on cilia at all? Building and maintaining cilia to host chemoreceptors comes with an energetic cost that could be spent elsewhere in the organism.
- Is there a reason that motile cilia are sometimes chemosensitive? This combination of motility and chemosensing puts a lot of complexity in one small compartment. Is motility somehow beneficial to the chemosensitivity of the cilia?
- Could there be a benefit to having chemosensitive motile cilia in bundles or carpets? It seems like each cilium would deplete the local concentration field, leading to a lower sensitivity per cilium.
- How do cilia coordinate their waving? They are typically submerged in fluid; are hydrodynamic interactions between cilia sufficient to explain the relatively fast synchronisation seen in biological systems?

1.2 Thesis outline

The outline of the remainder of this thesis is as follows:

Chapter 2: Background

I discuss the background biology and physics required to understand cilia and the later chapters of this thesis. The structure of cilia is explained, and the peculiar behaviour of fluids at the microscopic scales of cilia is covered in detail. I also delve into some of the approaches that have been taken in modelling the interaction between cilia and fluid.

Chapter 3: Particle capture

By developing analytical and computational models, we investigate the interactions of both primary and motile cilia (in the latter case considering bundles of motile cilia as well as isolated individual motile cilia) with chemicals at a known concentration, with a view to better understand how cilium geometry and motility affects their ability to sense chemicals. We consider how well the model reflects reality, and the biological implications for chemoreception by cilia.

Chapter 4: Ciliary synchronisation

We develop a model of cilium synchronisation via hydrodynamic interactions, and use it to carry out an investigation of how hydrodynamic interactions lead to synchronisation, and what factors of the cilia, their arrangement, and their motion are essential for synchronisation. Most importantly, we find that our modelled intercilium hydrodynamic interactions are nonreciprocal, and we discuss the importance of this fact. We finally consider the extent to which these results reflect real-world cilia, and what our model leaves out.

Chapter 5: Conclusion

I summarise the work presented, and discuss some related potential future research. The implications of this work are considered.

Background 2

2.1 Hydrodynamics

At the length scales of cilia (generally between one and a few tens of micrometres [17]) fluid flow looks very different to what is seen at a human scale. For a human in a swimming pool, inertial forces are hugely important, allowing a competent swimmer to glide several metres on a single stroke. A bacterium in a puddle of water sees a very different world, where the environment is dominated by viscous forces; if a swimming bacterium were to stop actively propelling itself, it would only coast approximately 10 pm (slightly less than the diameter of a hydrogen atom), and come to a halt in under a microsecond [18], as the friction is so much more important than the bacterium's minuscule momentum. Despite this, the swiftest bacteria can swim at hundreds of body lengths per second [19].

[17]: Saggese *et al.* (2012), *Development of a method for the measurement of primary cilia length in 3D*

[18]: Purcell (1977), *Life at low Reynolds number*

[19]: Zhang *et al.* (2014), *Swimming behaviour and magnetotaxis function of the marine bacterium strain MO-1*

This dominance of viscous forces over inertia is quantified by the dimensionless Reynolds number, defined as

$$\mathrm{Re} = \frac{Lu\rho}{\mu}, \tag{2.1}$$

where L is the length scale, u is the speed of motion, ρ is the fluid density, and μ is the dynamic viscosity of the fluid. Plugging in reasonable numbers, we find that for a cilium or bacterium, the Reynolds number is around $\sim 10^{-5} - 10^{-4}$, which, being much less than one, tells us that inertial forces are tiny enough to be entirely negligible compared to fluid viscosity. For comparison, a human in a swimming pool experiences a Reynolds number of $\sim 10^{3} - 10^{4}$, around a hundred million times greater than the cilium. For a human to experience this same viscous dominance that a cilium feels, they would have to swim at their normal swimming speed,

but in a fluid around 10 − 100 times more viscous than even the thickest peanut butter [20].

[20]: Citerne *et al.* (2001), *Rheological properties of peanut butter*

2.1.1 Stokes flow

The Navier-Stokes equation for an incompressible fluid, describing the velocity $\mathbf{u}$ and pressure p of a fluid experiencing an external force per unit volume $\mathbf{f}$, can be written as

$$\rho\left(\frac{\partial \mathbf{u}}{\partial t} + (\mathbf{u}\cdot\nabla)\,\mathbf{u}\right) = -\nabla p + \mu\nabla^2\mathbf{u} + \mathbf{f}. \tag{2.2}$$

1: The proof of the existence of a smooth and globally defined solution to the Navier-Stokes equations is one of the Millennium Prize Problems. Anyone who is able to prove such a solution exists in every case will receive a prize of $1,000,000.

This equation is nonlinear and famously hard to solve[1]. However, as previously mentioned, inertia is negligible at the scale of cilia. Many of the terms in this equation represent inertial forces that are not relevant, so we can simplify this equation heavily to obtain the Stokes equation:

$$\mu\nabla^2\mathbf{u} - \nabla p + \mathbf{f} = 0, \tag{2.3}$$

$$\nabla\cdot\mathbf{u} = 0. \tag{2.4}$$

This equation has no explicit time dependence, which means that a change in the force $\mathbf{f}$ or boundary conditions propagates instantly to the fluid, but if the force and boundary conditions are unchanged, the flow field $\mathbf{u}$ is constant in time. The form of the equations also ensures that if $\mathbf{u}$ is a solution for a given $\mathbf{f}$, then so is $-\mathbf{u}$ for $-\mathbf{f}$; the equations are 'reversible'. This leads to an interesting consequence known as Purcell's scallop theorem: at low Reynolds number, any series of actions followed by the reverse of those actions can't generate a net motion. The organism that gives the theorem its name, the scallop, swims by opening and closing its shell, and is therefore unable to swim in a Stokes fluid [18]. For motile cilia, this lesson is of the utmost importance: if fluid is to be pumped, waving back and forth in a plane without bending is insufficient. The motion needs to be cyclic, but not reversible.

[18]: Purcell (1977), *Life at low Reynolds number*

2.1.2 Solving the Stokes equations

Computing the flow due to a moving cilium is complicated, and in practice requires some simplifying assumptions that change depending on the context and what kind of accuracy is needed. The simplest possible solution to the Stokes equations is the Stokeslet, which represents the fluid flow a displacement $\mathbf{r}$ from a point force $\mathbf{F}$:

$$\begin{aligned} \mathbf{u}(\mathbf{r}) &= \mathcal{S}(\mathbf{r}) \cdot \mathbf{F} \\ &\equiv \frac{1}{8\pi\mu}\left(\frac{\mathbb{1}}{|\mathbf{r}|} + \frac{\mathbf{rr}}{|\mathbf{r}|^3}\right) \cdot \mathbf{F}, \end{aligned} \tag{2.5}$$

under the assumption that the flow speed and pressure decays to zero infinitely far away. However, this is a very poor approximation of a cilium, and would almost never be a sufficiently good simplification for practical purposes.

For a start, the cilium is found on the surface of a cell, which means that one has to account for the effect of the cell on the fluid flow. Generally, the best boundary condition to use in this case is the no-slip condition, wherein the fluid flow relative to the cell's surface is stationary. This has fairly significant experimental backing for fluids where viscosity dominates over inertia [21], so we will adopt it here as well.

[21]: Day (1990), *The no-slip condition of fluid dynamics*

To compute the flow due to a point force in the presence of a no-slip boundary, we can use a solution sometimes called the Blakelet [22]. In much the same way that it is possible to find the electric field due to a charged particle in the presence of a conducting boundary by introducing a second imaginary 'image' particle with the opposite charge reflected in the conducting boundary, Blake realised it was possible to model the flow due to a Stokeslet in the presence of a no-slip boundary by creating an 'image system', consisting of multiple flow singularities (one of which is a Stokeslet with equal magnitude and opposite direction), located where the mirror image of the real particle would be: see Fig. 2.1 for a diagram of the image system. The derivation is complicated,

[22]: Blake (1971), *A note on the image system for a stokeslet in a no-slip boundary*

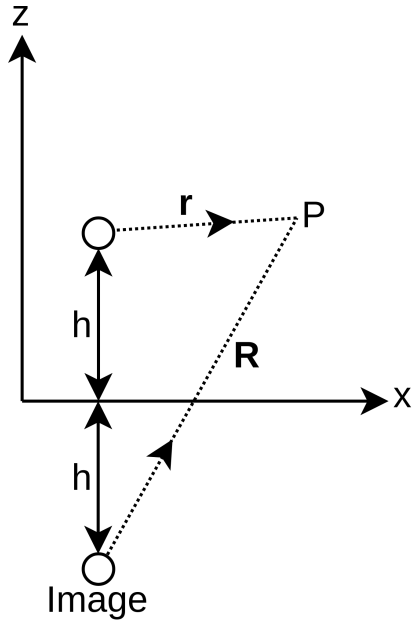

Figure 2.1: The image system that underpins the Blake tensor. The real Stokeslet is a distance h above the no-slip boundary at $z = 0$, and the image system is found a distance h below the boundary. P is the observation point at which we want to compute the flow.

and the full treatment can be found in Blake [22], but the result is incredibly useful for modelling the hydrodynamics of cilia: if we have a point force in a fluid at a position (r_1, r_2, h) above a no-slip boundary, we also introduce an 'image particle' which is reflected in the $z = 0$ axis from the real particle. In other words, the image will be located at $(r_1, r_2, -h)$. We denote the displacement from the image particle to the position where we are interested in the fluid flow as $\mathbf{R}$, and thus the Blakelet can be written as:

$$\begin{aligned} u_j(\mathbf{r}, \mathbf{R}) &= \mathcal{B}_{jk} F_k \\ &= \frac{1}{8\pi\mu} \left[\left(\frac{1}{r} - \frac{1}{R} \right) \delta_{jk} + \frac{r_j r_k}{r^3} - \frac{R_j R_k}{R^3} \right. \\ &\left. + 2h \left(\delta_{k\alpha}\delta_{\alpha\beta} - \delta_{k3}\delta_{3\beta} \right) \frac{\partial}{\partial R_\beta} \left(\frac{h R_j}{R^3} - \left\{ \frac{\delta_{j3}}{R} + \frac{R_j R_3}{R^3} \right\} \right) \right] \cdot F_k. \end{aligned} \tag{2.6}$$

Note the use of Einstein summation notation, meaning that repeated indices are summed over[2], i.e. $r_i r_i = r_1^2 + r_2^2 + \cdots = r^2$.

This can be rewritten as a Stokeslet plus an 'image' contribution:

$$u_j(\mathbf{r}, \mathbf{R}) = (\mathcal{S}_{jk} + \mathcal{B}^{\text{im}}_{jk}) F_k. \tag{2.7}$$

[22]: Blake (1971), *A note on the image system for a stokeslet in a no-slip boundary*

2: In the same notation, the Stokeslet would become:

$$\begin{aligned} u_j(\mathbf{r}) &= \mathcal{S}_{jk} F_k \\ &= \frac{1}{8\pi\mu} \left(\frac{\delta_{jk}}{r} + \frac{r_j r_k}{r^3} \right) F_k. \end{aligned}$$

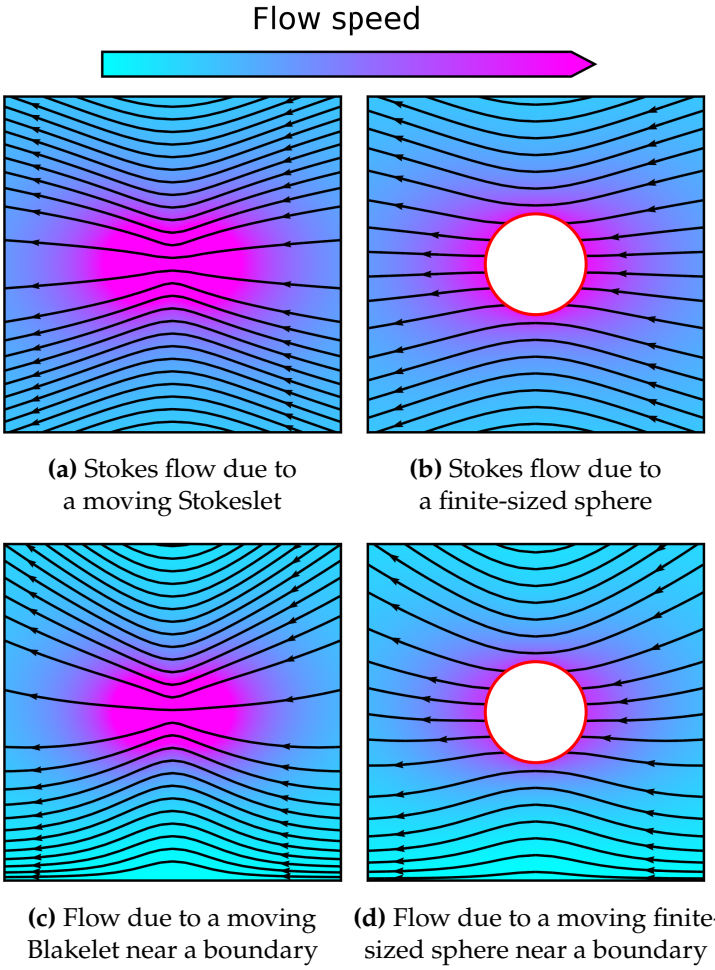

(a) Stokes flow due to a moving Stokeslet

(b) Stokes flow due to a finite-sized sphere

(c) Flow due to a moving Blakelet near a boundary

(d) Flow due to a moving finite-sized sphere near a boundary

Figure 2.2: Different solutions to the Stokes equations corresponding to various Green's functions. (a) and (b) show the flows far away from a boundary, whereas (c) and (d) show the flow field near a no-slip boundary. One can see how the fluid is much slower near the boundary at the bottom edge of the plots, and how the fluid flow is altered.

The image contribution decays to zero if the particle is far enough from the boundary.

Far away from the cilium, the Blakelet is a very good approximation for the fluid flow due to a moving sphere or even a whole cilium, despite assuming a single point force – in fact, in the far-field[3] limit, it is exactly the same as the flow due to a sphere acted upon by a force [23]. However, closer to the cilium, something more accurate is required; to achieve this, we can integrate the Blakelet over the surface of a sphere of radius a to obtain a version of the Rotne-Prager tensor, modified to include a no-slip boundary. This new mobility satisfies the no-slip boundary on the surface of the sphere. The Rotne-Prager tensor can be written in terms of the Blake

3: 'Far-field' refers to the fluid behaviour far from the cilium, where only the terms in the force response that decay very slowly with distance are important. 'Near-field' refers to the fluid behaviour much closer to the cilium, where the higher order terms are also relevant.

[23]: Vilfan (2012), *Generic flow profiles induced by a beating cilium*

tensor as:

$$\mathcal{M}_{jk} = \left(1 + \frac{a^2}{6}\nabla^2_{\mathbf{r}_j}\right)\left(1 + \frac{a^2}{6}\nabla^2_{\mathbf{r}_k}\right)\mathcal{B}(\mathbf{r}_j, \mathbf{r}_k) \tag{2.8}$$

for the off-diagonal elements, and

$$\mathcal{M}_{jj} = \frac{1}{6\pi\mu a}\mathbb{1} + \left(1 + \frac{a^2}{6}\nabla^2_{\mathbf{r}_j}\right)\left(1 + \frac{a^2}{6}\nabla^2_{\mathbf{R}_j}\right)\mathcal{B}^{\text{im}}(\mathbf{r}_j, \mathbf{R}_j) \tag{2.9}$$

for the diagonal elements [24]. The full form of the tensor is much too long to write here, but see for example Vilfan *et al.* [25]. Some of the fluid flow solutions discussed here are shown in Fig. 2.2. Our work in later chapters will make extensive use of this corrected Rotne-Prager tensor.

[24]: Gauger *et al.* (2009), *Fluid transport at low Reynolds number with magnetically actuated artificial cilia*

[25]: Vilfan *et al.* (2010), *Self-assembled artificial cilia*

Rotne-Prager derivation

The Rotne-Prager tensor can be derived (following [24]) by integrating the Blakelet over the surface of a sphere of radius a and its centre at $\mathbf{r_s}$:

$$\mathbf{u}(\mathbf{r}) = \int_S \mathcal{B}(\mathbf{r}, \mathbf{r}')\mathbf{f}(\mathbf{r}')\,\mathrm{d}S'. \tag{2.10}$$

To first order, the force density $\mathbf{f}$ is just the total force $\mathbf{F}$ divided by the surface area of the sphere, which means that we can expand the force and the Blake tensor around $\mathbf{r}' = \mathbf{r}_s$ to get

$$\mathbf{u}(\mathbf{r}) \approx \left[\left(1 + \frac{a^2}{6}\nabla^2_{\mathbf{r}'}\right)\mathcal{B}(\mathbf{r}, \mathbf{r}')\right]_{\mathbf{r}'=\mathbf{r}_s} \cdot \mathbf{F}. \tag{2.11}$$

Now, Faxén's law tells us that the velocity of a sphere of radius a experiencing a hydrodynamic force $\mathbf{F}$ in a flow is given by:

$$\mathbf{F} = 6\pi\mu a\left[\left(1 + \frac{a^2}{6}\nabla^2\right)\mathbf{u}_0 - \mathbf{u}_s\right] \tag{2.12}$$

where $\mathbf{u}_0$ is the fluid flow that would be at the centre of the sphere if the sphere was not there [26], so we can

[24]: Gauger *et al.* (2009), *Fluid transport at low Reynolds number with magnetically actuated artificial cilia*

[26]: Guazzelli *et al.* (2011), *A Physical Introduction to Suspension Dynamics*

combine this with Eq. (2.11), eliminating $\mathbf{u}(\mathbf{r}) = \mathbf{u}_0$ to find the diagonal and off-diagonal terms of the Rotne-Prager tensor.

2.1.3 Modelling the motile cilium

Slender bodies are of great interest in a lot of fields, especially within biophysics: cilia and the superficially similar bacterial flagella are used for swimming and pumping, and many bacteria or other microorganisms have elongated shapes [27]. Outside of biophysics, certain materials (both natural and artificial) such as clays [28] or fibre-reinforced composites [27] are composed of elongated components. However, there are some problems when trying to numerically model elongated bodies. For example, the boundary element model divides the body's surface into many small elements and then makes assumptions about the hydrodynamic stress on each element to determine the fluid flow around the cilium [26], but since the width of the elongated body is very small, a high resolution (i.e. a lot of surface elements) is required to achieve good accuracy. Then, because the other length scale is much larger, this high-resolution has to be extended over a large area, resulting in heavy performance penalties [28]. As such, it comes as no surprise that there are a great many ways to model the hydrodynamics of cilium-like structures that attempt to sidestep these computational pitfalls.

[27]: Borker *et al.* (2019), *Slender body theory for particles with non-circular cross-sections with application to particle dynamics in shear flows*

[28]: Koens (2022), *Tubular-body theory for viscous flows*

[26]: Guazzelli *et al.* (2011), *A Physical Introduction to Suspension Dynamics*

One of the conceptually simplest of these approaches is slender body theory, in which an elongated body is approximated by a line of Stokeslets (and other related flow solutions, in order to enforce a no-slip condition), and the fluid flow is then found by summing over the length of the elongated body [26]. This exploits the linearity of the Stokes flow, which means that a superposition of solutions to the Stokes flow is also a valid solution to the Stokes flow. In the case of a series of Stokeslets with position $\mathbf{r}_j$, the total fluid flow at $\mathbf{r}$ would

be

$$\mathbf{u}^{\text{total}}(\mathbf{r}) = \sum_j \mathcal{S}(\mathbf{r}, \mathbf{r}_j) \cdot \mathbf{F}_j. \tag{2.13}$$

Summing up the velocity responses due to a line of point forces is equivalent to considering the much less tractable case where one must find the velocity response due to a line of forces directly. This approach has seen use in modelling bacterial swimming [29] and cilium beating [30]. However, the presence of singularities in the flow can pose problems for numerical integration, and it can be expensive to try to determine the (potentially huge) set of forces required to reproduce a given motion coupled with the boundary condition, so other methods have been developed that try to improve upon the numerical practicality.

[29]: Lauga (2016), *Bacterial Hydrodynamics*

[30]: Fulford *et al.* (1986), *Muco-ciliary transport in the lung*

Other approaches include the numerically much simpler resistive force theory, in which the slender body is divided into (usually infinitesimal) length elements. The force components on each length element are computed using drag coefficients which are known in advance, and the velocity of the length element relative to the fluid at infinity. However, this approximation does not account for self-interaction, so tightly curved filaments can pose issues, and it begins to break down if the slender body is anchored to a much larger cell body (which is almost always the case with cilia) [31]. Nonetheless, this method has seen success in modelling of ciliary hydrodynamics [32]. The method of regularised Stokeslets seeks to fix the issues created by the singularities in slender body theory, by replacing each Stokeslet point-force with a 'blurry' force distribution called a regularised Stokeslet; the Dirac delta function that characterises the point force is instead replaced by a smooth approximation called a 'cut-off' function, which solves the problems introduced by flow singularities. However, there is an issue with 'leaking' whereby the no-slip boundary condition is not very well satisfied, which might prove fatal depending on the requirements of the model [33]. Nonetheless, this method has also been applied to cilia [34, 35]. Various other methods

[31]: Johnson *et al.* (1979), *Flagellar hydrodynamics. A comparison between resistive-force theory and slender-body theory.*

[32]: Gueron *et al.* (1992), *Ciliary motion modeling, and dynamic multicilia interactions*

[33]: Cortez (2018), *Regularized Stokeslet segments*

[34]: Smith (2009), *A boundary element regularized Stokeslet method applied to cilia- and flagella-driven flow*

[35]: Pedley *et al.* (1992), *Hydrodynamic Phenomena in Suspensions of Swimming Microorganisms*

have been developed, such as the recent tubular-body-theory developed by Koens [28].

[28]: Koens (2022), *Tubular-body theory for viscous flows*

However, there is a simpler way to solve the issues arising from flow singularities, which is to avoid creating any in the first place. The primary method we use in this work is to replace the cilium with a sphere or chain of non-overlapping spheres as appropriate, depending on the requirements of the model.

In Ch. 3, where the near-field flow extremely close to the cilium is of great relevance, we approximate the cilium as a chain of beads. Exploiting the linearity of the Stokes flow, we can superpose the flow solution given by the modified Rotne-Prager mobility tensor for each individual sphere, and hence compute the flow due to a chain of spheres in the presence of a no-slip boundary. This is both numerically efficient and a very good approximation to a cilium, even in the near field, that does not suffer strongly from 'leaking' effects.

In the work we will present in Ch. 4, we are less concerned with the fluid flow very close to the cilium. Even a single sphere is a good approximation in the far field, and by putting it on a titled circular trajectory, the asymmetry between the power and recovery stroke is reproduced. This is an extremely effective simplification that allows for a great improvement in computational efficiency, which is necessary due to the large numbers of interacting cilia we must simulate.

[8]: Nachury *et al.* (2019), *Establishing and regulating the composition of cilia for signal transduction*

2.2 Cilia

Cilia are hairlike organelles found on the surface of most eukaryotic cells [8] and certain microorganisms such as *Paramecium*. They can be broadly divided into two types: primary cilia, which do not move under their own power, and motile cilia, which do.

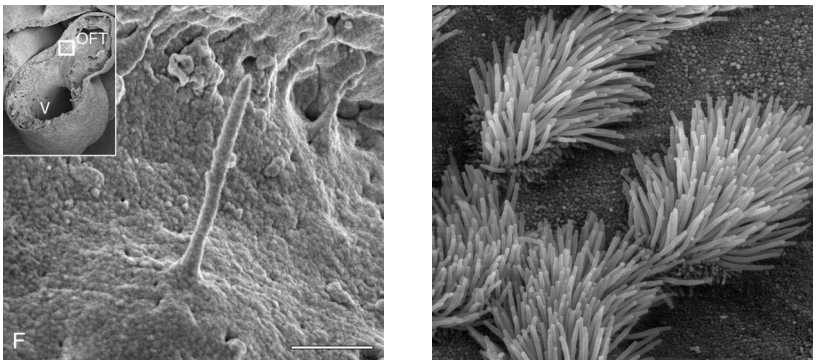

(a) Primary cilium in a developing chicken heart. Image from Van der Heiden *et al.* [45]. Reproduced here with permission of the copyright holder via Rightslink. © 2005 Wiley-Liss, Inc.

(b) Motile cilia in the human trachea. Image by Charles Daghlian and released to the public domain.

Figure 2.3: Scanning electron microscope images of a single primary cilium (a) and bundles of motile cilia (b). The primary cilium stands alone whereas the motile cilia are found in bundles, which is typical for the two types.

Primary cilia (imaged in Fig. 2.3a) usually have roles in sensing, normally of mechanical forces or chemicals: primary cilia on bone cells detect mechanical stresses [36], primary cilia in the kidneys and blood vessels detect fluid flow [37, 38], many chemical signals such as serotonin are mainly detected by cilia [39], and even the olfactory receptors in the human nose are primary cilia [40]. Modified primary cilia also sense light [41] and temperature [42]. All of this sensing ability gives them their nickname of the 'cell's antenna' [43]. In fact, nearly every cell in the human body has exactly one primary cilium. Since they are found on most cell types, it is no surprise that they are found in many different tissues, or that when defective, they can cause a large number of diseases (including *situs inversus*) known as ciliopathies [44].

Motile cilia, on the other hand, mostly have roles in fluid pumping, though recent research has also revealed that they have sensory capacity as well [16]; this revelation is examined in much more detail in Ch. 3. They are usually found in 'bundles' or 'carpets', where one cells hosts many cilia (imaged in Fig 2.3b); for example, in the lungs, multiciliated cells have around 200 cilia per cell [46]. They are also found in many places in the body: as previously mentioned, they are found in the lungs and trachea [9], where their waving works to

[36]: McGlashan *et al.* (2006), *Localization of Extracellular Matrix Receptors on the Chondrocyte Primary Cilium*

[37]: Nauli *et al.* (2008), *Endothelial Cilia Mediate Low Flow Sensing during Zebrafish Vascular Development*

[38]: Nauli *et al.* (2008), *Primary Cilia Are Fluid Shear Sensors That Regulate Calcium Signaling and Nitric Oxide Production Through Polycystin-1*

[39]: Brailov *et al.* (2000), *Localization of 5-HT6 receptors at the plasma membrane of neuronal cilia in the rat brain*

[40]: Marshall *et al.* (2006), *Cilia: Tuning in to the Cell's Antenna*

[41]: Insinna *et al.* (2008), *Intraflagellar transport and the sensory outer segment of vertebrate photoreceptors*

[42]: Kuhara *et al.* (2008), *Temperature Sensing by an Olfactory Neuron in a Circuit Controlling Behavior of C. elegans*

[43]: Malicki *et al.* (2017), *The Cilium: Cellular Antenna and Central Processing Unit*

[44]: Waters *et al.* (2011), *Ciliopathies: an expanding disease spectrum*

[16]: Bloodgood (2010), *Sensory reception is an attribute of both primary cilia and motile cilia*

[46]: Horani *et al.* (2018), *Advances in the Genetics of Primary Ciliary Dyskinesia*

[9]: Yaghi *et al.* (2016), *Airway Epithelial Cell Cilia and Obstructive Lung Disease*

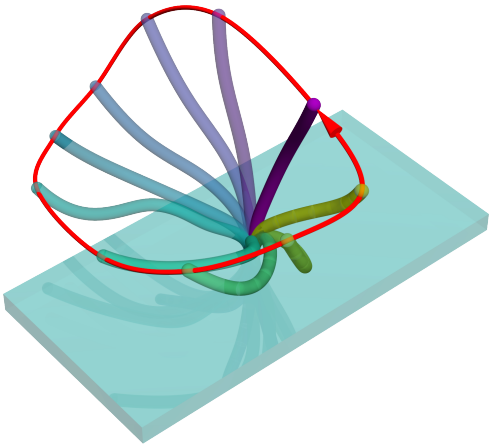

Figure 2.4: Motile cilium beat. The cilium performs a power stroke (solid dark blue colour), then curls up and pulls back along the cell surface. The trajectory breaks time reversal symmetry, so it can produce a net flow without falling afoul of scallop theorem.

move mucus out of the lungs to remove trapped pathogens and particulates. They are also found pumping fluid in the brain to move signalling molecules [47], in the reproductive system (both male [48] and female [11]) and on the surface of microscopic organisms where they help with feeding and swimming [13, 49]. As with primary cilia, defective motile cilia lead to a large number of diseases [50].

The beat of a motile cilium is asymmetric and irreversible, meaning that the problem posed by scallop theorem is avoided. The beat begins with a straightened cilium performing a power stroke, intended to move as much fluid as possible as fast as possible. The cilium then curls up and returns to its original position in a so-called recovery stroke, staying as close to the cell surface as possible [51]. Due to the curled-up shape of the recovery stroke, and the no-slip condition on the cell surface, the cilium doesn't move much fluid during the recovery stroke compared to the amount moved during the power stroke, giving a net pumping effect. This beating pattern is illustrated in Fig. 2.4. At sufficient density, motile cilia can coordinate their beating to improve their efficiency and minimise intercilium collisions [14, 52]; the mechanisms underpinning this behaviour are examined in Ch. 4.

Both primary and motile cilia consist of a basal body affixed to the cell, and a protruding structure with a microtubule skeleton, all covered in cell membrane. The basal body works to organise and support the microtubules. The microtubule

[47]: Olstad *et al.* (2019), *Ciliary Beating Compartmentalizes Cerebrospinal Fluid Flow in the Brain and Regulates Ventricular Development*

[48]: Yuan *et al.* (2019), *Motile cilia of the male reproductive system require miR-34/miR-449 for development and function to generate luminal turbulence*

[11]: Lyons *et al.* (2006), *The reproductive significance of human Fallopian tube cilia*

[13]: Funfak *et al.* (2015), *Paramecium swimming and ciliary beating patterns: a study on four RNA interference mutations*

[49]: Mannan *et al.* (2020), *Minimal model of the hydrodynamical coupling of flagella on a spherical body with application to Volvox*

[50]: Afzelius (2004), *Cilia-related diseases*

[51]: Gueron *et al.* (1999), *Energetic considerations of ciliary beating and the advantage of metachronal coordination*

[14]: Osterman *et al.* (2011), *Finding the ciliary beating pattern with optimal efficiency*

[52]: Ringers *et al.* (2023), *Novel analytical tools reveal that local synchronization of cilia coincides with tissue-scale metachronal waves in zebrafish multiciliated epithelia*

'skeleton' of the cilium is called the axoneme, and consists of a series of nine microtubule doublets, shown in Fig. 2.5a-b for the two cilium types. The primary cilium and the motile cilium have slightly different axonemes: the motile cilium has an additional pair of microtubules in the centre (hence the name 9+2 axoneme, for the nine outer doublets and the two inner microtubules), and some radial spokes that connect it to the outer doublets, along with some dynein arms that are responsible for sliding the microtubules relative to one another to generate bending [53]. The primary cilium lacks the central pair of microtubules, leading to it being named a 9+0 axoneme, as well as lacking the dynein arms and radial stokes. The structure of the motile cilium, including the additional apparatus required for motility, is shown in cross-section in Fig. 2.5c.

[53]: Falk *et al.* (2015), *Specialized Cilia in Mammalian Sensory Systems*

There are, however, exceptions to this seemingly neat classification: in the structure responsible for the left-right differentiation of mammalian embryos (creatively named the left-right organiser), specialised motile cilia (called 'nodal cilia') lack the central pair, and they have a very different (and simpler) beating pattern compared to regular motile cilia. Kinocilia, found in the inner ear, have a 9+2 axoneme, like motile cilia, but they don't have the dynein arms and they don't move under their own power; they simply bend under the influence of external vibrations, and are usually considered to be a variant of primary cilia. There can therefore be said to be four types of cilia depending on the combination of axoneme type and motility [53].

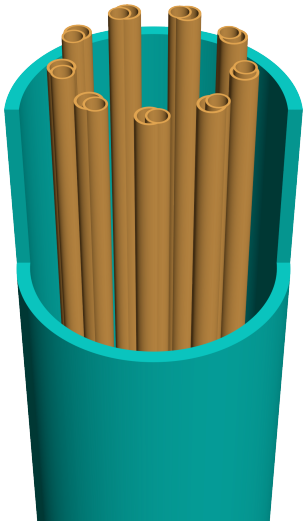

(a) Render of the microtubule structure of a primary cilium. Because it has nine doublets and no central pair, this arrangement is often referred to as a 9+0 axoneme.

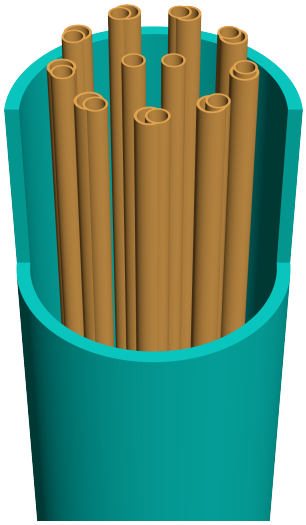

(b) Render of the microtubule structure of a motile cilium; note the two central microtubules (which are absent in the primary cilium case) which along with the nine doublets give this axoneme arrangement its designation as a 9+2 axoneme.

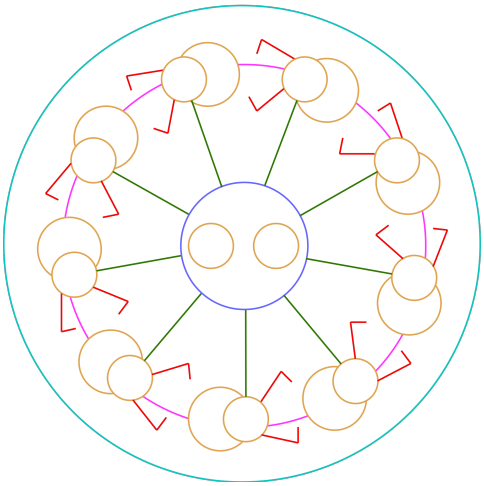

(c) Top-down view of motile cilium axoneme. The outer tubule doublets and central microtubules (yellow) are visible, along with the spokes connecting them. The dynein arms that give rise to the motility of the cilium are shown in red; these generate sliding motion between the doublets and thus create the cilium's bending motion. The primary cilium lacks almost all of the structure shown in this diagram, except for the outer doublets.

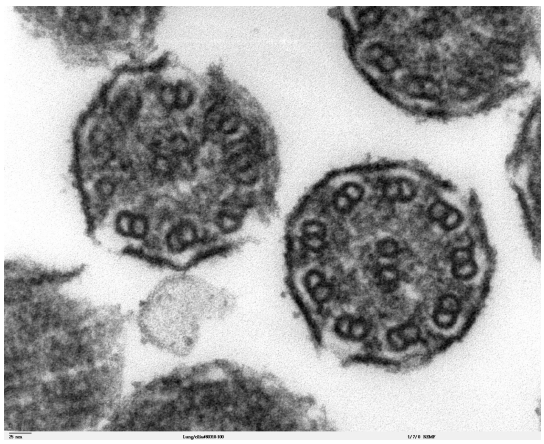

(d) Photo showing the axoneme of some motile cilia in the mammalian lung from above. The doublets are clearly visible, as is the central microtubule pair. Taken by Louisa Howard and released to the public domain.

Figure 2.5: Structure of the two types of cilia.

2.3 Chapter summary

- At the length scale of cilia, fluid behaviour is dominated by viscosity, which greatly simplifies the equations of fluid motion.
- These simplified equations can be solved using various mobility tensors, the most relevant of which is the Rotne-Prager tensor. This approach results in high computational efficiency, even when accounting for no-slip boundaries on the surfaces of spherical bodies, or including planar no-slip boundaries.
- The linearity of the Stokes flow permits a lot of approaches to modelling slender bodies, and we favour an approach based on superposing Green's function solutions.
- Cilia come in two main types: primary and motile cilia. Both can be chemosensitive but only the motile cilia have roles in pumping.
- Motile cilia break time-reversal symmetry with an asymmetric beat consisting of a power and recovery stroke.

3 Particle capture

The ability to sense chemicals was one the earliest kinds of environment sensing to evolve, and chemosensing abilities are known to be present in organisms spanning all biological kingdoms [54]. Humans have chemosensory abilities, most obviously in the forms of a sense of smell and taste, but in myriad other ways such as detecting blood carbon dioxide level [55]. For certain microorganisms, chemosensing is integral to their ability to swim along chemical gradients to find nutrients (in a process called 'chemotaxis') [56]. Even plants can sense chemicals in their environment, for example to trigger a response to dangerous pathogens [57]. Within organisms, chemosensing is everywhere, for example in the form of signalling chemicals that can convey messages between cells. Chemosensing is therefore an incredibly important facet of life as we know it, and in eukaryotes, many of these chemosensors are found on cilia [40].

[54]: Sokolinskaya *et al.* (2020), *Molecular principles of insect chemoreception*

[55]: Cummins *et al.* (2020), *Mechanisms and Consequences of Oxygen and Carbon Dioxide Sensing in Mammals*

[56]: Sarvestani *et al.* (2016), *Simulation of Paramecium Chemotaxis Exposed to Calcium Gradients*

[57]: Zipfel (2014), *Plant pattern-recognition receptors*

[40]: Marshall *et al.* (2006), *Cilia: Tuning in to the Cell's Antenna*

When the primary cilium was first discovered, it was widely assumed to be useless and vestigial. A sensory role was first proposed for it at the end of the 19th century [16, 58], but it took many years for this idea to be taken seriously, whereupon the primary cilium experienced a huge explosion in popularity. More recently, it was realised that motile cilia are also chemosensory, though the evidence has been piling up for a long time [16].

[16]: Bloodgood (2010), *Sensory reception is an attribute of both primary cilia and motile cilia*
[58]: Zimmermann (1898), *Beiträge zur Kenntniss einiger Drüsen und Epithelien*

Primary cilia have a high density of receptors, in particular G-protein-coupled receptors (often shortened to GPCRs) [59]. G-proteins are a family of proteins found inside cells, that act as molecular switches. The G-protein-coupled receptors are transmembrane structures that bind to a specific extracellular signalling molecule. This binding causes the GPCR to change its shape (i.e. undergo a conformational change) which affects the shape of the intracellular part of the GPCR, which allows

[59]: Mykytyn *et al.* (2017), *G-Protein-Coupled receptor signaling in cilia*

this intracellular part to alter the environment within the cilium [59], which can in turn affect the cellular behaviour. It is estimated that close to half of all drugs available target these GPCRs [60], so understanding ciliary chemoreception is extremely useful.

[59]: Mykytyn *et al.* (2017), *G-Protein-Coupled receptor signaling in cilia*

[60]: Cheng *et al.* (2010), *Luciferase Reporter Assay System for Deciphering GPCR Pathways*

There are several reasons why primary cilia have a high chemosensor density: the environment very close to the cell is often not a good representation of the actual intercellular medium, because cells have charged lipids on their surfaces that can repel or attract various chemicals and ions [40]. Many cells are also surrounded by a so-called glycocalyx, a several micrometre thick covering of sugars, lipids, proteins [61] that acts as a physical barrier to protect and control entry to the cell, as well as filling various other roles [62]; however, this covering will also alter the chemical environment close to the cell [40]. The no-slip condition on the cell's surface could also mean that the role of advection very close to the cell's surface is almost totally suppressed, thus limiting fluid mixing and therefore chemosensitivity [40]. There is also the fact that, because the cilium has a very high surface area to volume ratio compared to the rest of the cell, only a small number of chemosensors and signalling molecules are required to create large changes in the concentration of second messengers[1] in the cilium's cytoplasm; by comparison, an enormous number of chemosensors would be required to achieve a similar increase [40]. Our work aims to see if there are further geometric reasons for placing chemosensors on cilia, as well as determining what advantages arise when combing chemosensing with motility.

[40]: Marshall *et al.* (2006), *Cilia: Tuning in to the Cell's Antenna*

[61]: Ebong *et al.* (2011), *Imaging the Endothelial Glycocalyx In Vitro by Rapid Freezing/Freeze Substitution Transmission Electron Microscopy*

[62]: Reitsma *et al.* (2007), *The endothelial glycocalyx*

1: These are signalling molecules that are released inside cells in response to some extracellular signalling molecule that is detected by a chemosensor on the cell (or 'first messengers').

3.1 Physics of chemoreception

In 1827, the famous botanist Robert Brown was looking through his microscope at some grains of pollen in water, and noticed that they were jiggling, moving in seemingly random directions with seemingly random speeds [63]. This

[63]: Feynman *et al.* (2006), *The Feynman lectures on physics*

random motion, eponymously called Brownian motion, was later used by Albert Einstein to prove the existence of atoms. He (correctly) proposed that this random jiggling was caused by the particles that make up the water, moving around and colliding with the pollen grains. At some times the pollen would be bombarded more on one side than another, giving a net force. Since this bombardment is constantly in flux, the direction of pollen motion changes constantly and unpredictably [64]. This random motion will eventually cause chemicals to become spread out and mixed: a drop of ink in a glass of water will eventually diffuse to tint the entire glass equally.

[64]: Einstein (1905), *Über die von der molekularkinetischen Theorie der Wärme geforderte Bewegung von in ruhenden Flüssigkeiten suspendierten Teilchen*

At the scale of cells and cilia, this process of diffusion is extremely fast, with a timescale given by

$$\tau_D = \frac{L_c^2}{D}, \tag{3.1}$$

for some characteristic length L_c. D is the diffusion constant of the molecule being transported. For something the size of a small signalling molecule being absorbed by a cilium, this timescale is of the order of ~ 0.1 seconds[2].

2: At the synapses between nerve cells, diffusion carries the signal across the gap junction, a distance of a few tens of nanometres [65]. Since human reaction time is only a few hundred milliseconds, this gives an idea of how fast diffusion can happen.

[65]: Widrow *et al.* (2019), *Chapter 1 - Nature's Learning Rule*

The dominance of advection over diffusion can be quantified by the dimensionless Péclet number:

$$\mathrm{Pe} = \frac{L_c v_c}{D}, \tag{3.2}$$

where a large Péclet number means advection is dominant, and vice versa. Humans barely notice diffusion, so for a human this number is incalculably large, but for something like a signalling molecule close to the no-slip boundary of a cell, this number is much smaller than one. The length scale L_c in the expression for the Péclet number, as well as the fact that D tends to be larger for smaller, lighter particles, means that diffusion is an incredibly powerful force at small scales, and is often the dominant factor in molecular transport [66].

[66]: Berg *et al.* (1977), *Physics of chemoreception*

This leads neatly to the concept of diffusion-limited reactions.

If we have some perfectly reactive body with a surface S, such that any particle of interest that touches it is immediately absorbed[3] (or converted to other molecules, or adsorbed, or otherwise removed from the population of particles) then this can be represented as a boundary condition where the concentration of those particles is zero ($c(|\mathbf{r}| \in S, t) = 0$). Far away from this absorbing body, there is some representative unperturbed concentration $c(|\mathbf{r}| \to \infty, t) = c_0$. In the steady state, the advection-diffusion equation, which describes the concentration field, is very simply

$$D\nabla^2 c(\mathbf{r}, t) - \mathbf{u}(\mathbf{r}, t) \cdot \nabla c(\mathbf{r}, t) = \frac{\partial c(\mathbf{r}, t)}{\partial t} = 0, \tag{3.3}$$

subject to the boundary conditions above, and where $\mathbf{u}$ is the fluid velocity. Fick's law, which relates the concentration gradient to the average particle flux, means that the rate at which this body absorbs particles can be written as

$$R = \iint_S \mathrm{d}\mathbf{S} \cdot (D\nabla c). \tag{3.4}$$

R is proportional to c_0, but we can define a rate constant $k = R/c_0$ which is independent of the far-field concentration.

In the absence of advection, the diffusion equation reduces to

$$D\nabla^2 c(\mathbf{r}) = 0, \tag{3.5}$$

which is exactly analogous to the source-free Laplace equation for the potential ϕ in electrostatics:

$$\nabla^2 \phi(\mathbf{r}) = 0. \tag{3.6}$$

It is possible to find the concentration field by finding pre-existing solutions for the electrostatic problem in the scientific literature, as electrostatics is a much more widely-studied field. Alternatively, and as shown in the appendix of the article below, one can show that the self-capacitance C of the

3: As shown by Berg *et al.* [66], even if chemosensors only cover 1% of the area of a body, one still has near-perfect absorption, so this is a surprisingly accurate assumption for real systems.

[66]: Berg *et al.* (1977), *Physics of chemoreception*

body can be straightforwardly converted to a rate constant:

$$k = \frac{D}{\varepsilon_0} C, \tag{3.7}$$

where ε_0 is the dielectric permittivity of free space. It is relatively straightforward to adapt this for the case of a particle near a no-slip boundary, using the method of images. One can introduce a second equally-charged 'image' particle, reflected in the no-slip boundary, and then compute the self-capacitance (and hence reaction rate constant) of the particle in the presence of its image.

This rate of absorption due to pure diffusion is called the diffusion limit, and puts an upper bound on how fast microorganisms and cilia can detect chemicals in the absence of advection. However, microorganisms can swim and cilia can pump fluid. The interesting question, which our work presented in this chapter seeks to answer, is to what extent that additional advection can increase sensitivity. The degree to which a body is breaking the diffusion limit may be quantified by the Sherwood number, defined as the ratio of advective mass transfer to diffusive mass transfer. For the advection-diffusion reaction described above, it could be written in terms of the parameters as:

$$\mathrm{Sh} = \frac{L_c k}{D c_0 A} \sim \frac{k}{D c_0 L_c}, \tag{3.8}$$

where A is the surface area of the body in question. If $\mathrm{Sh} \ll 1$, there is a strong dominance of diffusion-related mass transfer over advective mass transfer, but once $\mathrm{Sh} \gtrsim 1$, advection begins to dominate. At this point, the advection is sufficient to begin to break the diffusion limit. There is also the analogous Nusselt number (often abbreviated to Nu), which is the equivalent quantity for heat transfer. Since the diffusion equation is identical to the heat equation, there are a lot of helpful similarities between the two problems, and solutions to heat transfer problems can often be straightforwardly transformed to get the solution to the equivalent mass transfer problem.

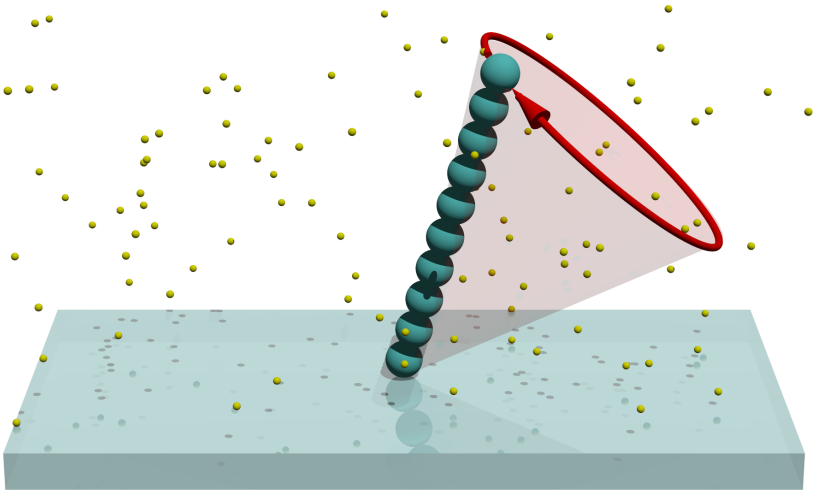

Figure 3.1: An illustration of the hydrodynamic simulation. Tracer particles are shown in yellow, and the cilium, simplified to a chain of spheres, is also shown. The trajectory swept out by the cilium is indicated.

3.2 Our work

In our work, we studied the interaction between a chemosensitive cilium and an arbitrary chemical species of interest. We initially assumed that the cilium was perfectly chemosensitive over its entire surface, and would immediately adsorb any signalling molecule that touched it, and that it was attached to a cell that was not itself chemosensitive. Beginning with some analytical calculations that take advantage of the electrostatic analogy, we determined that the elongated shape of the cilium, even in the absence of motility, means it can have a much higher chemosensitivity compared to a flat chemosensitive patch on the cell surface. In a quiescent fluid, for typical cilium dimensions, a chemosensitive cilium is equivalently sensitive to a chemosensitive surface patch with 4× the surface area of the cilium. A more complicated calculation (see the appendix of the article below) revealed that this chemosensitivity advantage is even more pronounced in a shear flow, with the equivalently chemosensitive patch having an area of around 6× the surface area of the cilium. In both cases, we also find that the longer the cilium, the more chemosensitive it becomes, even if we keep its surface area constant. This increase in sensitivity that we have seen purely because of the elongated cilium geometry gives one reason why primary cilia are so often host to chemoreceptors.

We then developed a numerical hydrodynamics simulation,

wherein individual tracer particles move due to advection and diffusion, and the cilium is approximated by a chain of spheres. The fluid flow due to the motion of these spheres can be computed using superpositions of the Rotne-Prager tensor (Eqs. (2.9–2.8)), due to the linearity of the Stokes flow. An illustration of the simulation setup is shown in Fig. 3.1.

We used this simulation to understand how much of a gain in chemosensitivity can be achieved by a motile cilium, and found that, provided the cilium beats nonreciprocally in a way that generates a net flow across the cilium, motility can produce a five-fold increase in chemosensitivity compared to a stationary cilium (at realistic cilium Péclet numbers). The increase in chemosensitivity due to cilium motility is even more pronounced than the increase due to cilium geometry, with the chemosensitivity of a motile cilium approaching a factor of 5 over a stationary cilium at the highest reasonable Péclet numbers a cilium could approach (and hence hugely more sensitive than a chemosensory patch on the cell's surface). At very low Péclet, the cilium barely breaks the diffusion limit, but as the cilium beats faster, the sensitivity rapidly increases. In the high-Péclet regime, the reaction rate scales with $\mathrm{Pe}^{1/3}$, which astoundingly is the same rate that would be found for a sphere in a flow (see box below). The fact that a motile cilium that must pump the fluid itself can reach the same high-Péclet rate scaling as a sphere suspended in a flow is a testament to the efficacy of combining motility with chemosensitivity. This result could go some way to explaining why motile cilia are now known to be chemosensory. The asymmetric beating stroke of the cilium is important, as the net flow it generates is crucial to this increase in chemosensitivity; if a beat is chosen that produces no net flow past the cilium, there is very little increase in chemosensitivity.

Reaction rate for a sphere

We can make a scaling argument to derive how the reaction rate R for a sphere in a moving fluid scales with the Péclet number. To begin with, we consider a sphere of radius a in a moving fluid:

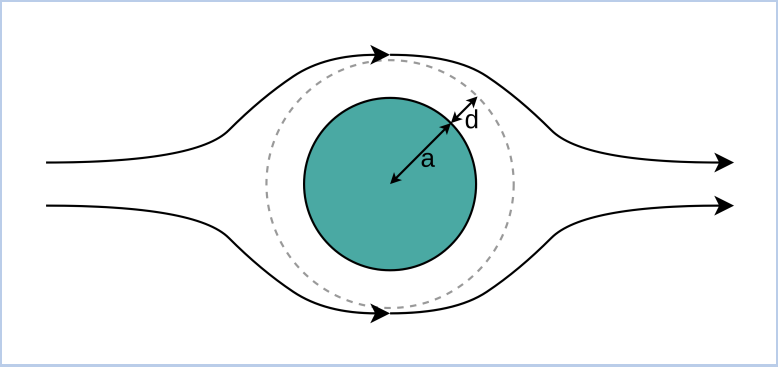

We assume that any chemical particles that enter some thin boundary layer of thickness d will make contact with the sphere and be absorbed. Since we know how the diffusion timescale relates to the diffusion length scale (Eq. (3.1)), we know that if the particles take some time τ to pass the sphere, then

$$d^2 \sim D\tau.$$

We also know that due to the no-slip condition on the surface of the sphere, the fluid flow very close to the sphere will be well-approximated by a shear flow, and therefore the characteristic flow speed in the boundary layer is $d\dot{\gamma}$ (where $\dot{\gamma}$ is the shear rate), which tells us that $\tau \sim 2\pi a/(d\dot{\gamma})$.

The reaction rate is then the product of the rate of particle influx ($\sim d\dot{\gamma}$) with the cross-sectional area of this boundary layer, i.e.

$$R \sim 2\pi a d \cdot d\dot{\gamma} \sim \left(\frac{a\dot{\gamma}}{D}\right)^{1/3} = \mathrm{Pe}^{1/3},$$

where we have dropped any purely numerical prefactors, as this scaling argument is not nearly precise enough for them to be relevant. Note that we have assumed that $d \ll a$,

so that the cross-sectional area of the boundary area can be written as $2\pi ad$; at very high Péclet, this condition is satisfied by definition, so this argument only tells us the scaling behaviour in the high-Péclet limit. Obviously this is an incredibly simplified argument, but much more complicated treatments of the problem give the same result [67].
It is quite surprising that our results show that a cilium that must pump the fluid itself can reach the same scaling rate as this sphere in a flow, but it is illustrative of just how far motility can increase chemosensitivity.
A similar (albeit more complicated) scaling argument can be made for a cylinder, but due to the Stokes paradox (i.e. there is no well-behaved flow field around a disc in two dimensions at zero Reynolds number) a force density has to be introduced. In this way, a scaling argument can be derived up to a proportionality constant. An approximate value for the proportionality constant had already been found by others [68], but we derived an exact value of this constant for the rate per unit length:

$$\frac{dk}{dz} = 3\left(\frac{6}{\pi}\right)^{1/3} \frac{\Gamma(3/4)^{4/3}}{\Gamma(1/3)} D \cdot \mathrm{Pe}^{1/3}.$$

The derivation can be found in the appendix of the article below.

[67]: Bowman *et al.* (1961), *Mass transfer from fluid and solid spheres at low Reynolds numbers*
[68]: Friedlander (1957), *Mass and heat transfer to single spheres and cylinders at low Reynolds numbers*

Lastly, we used the same hydrodynamic simulation to investigate the behaviour when placing several chemosensitive motile cilia close together, and found that a bundle motile cilia can be more sensitive together than the same number of individual motile cilia could be apart, i.e. the per-cilium chemosensitivity is higher in a bundle. This result is extremely counter-intuitive, as one would naively expect that many cilia together would all deplete the concentration of signalling molecules and result in a lower per-cilium sensitivity. Instead, every cilium benefits from the fluid flow generated by every other cilium, resulting in the surprising

result seen.

All this shows that by putting chemosensors on cilia, the cell can increase the diffusion limit significantly, and by combining chemosensing with motility, it can break the diffusion limit entirely. This goes some way towards closing some of the open questions introduced in Ch. 1. There are, however, some questions that remain unanswered, which open some possibilities for future work. As previously established, bundles of motile cilia often synchronise, and this work did not examine the impact of metachronal waves on the per-cilium chemosensitivity of a bundle.

There is also potential for a more efficient approach to numerically solving this problem. One consequence of the reciprocal theorem in hydrodynamics is that the particle flux through a surface is invariant under flow reversal, as long as the particle concentration at that surface is uniform [69]. If we apply this flow reversal symmetry to the absorption problem, and then apply time-reversal symmetry as well, we have essentially mapped from an absorption problem to an emission problem, where the cilium is now emitting particles but has not changed its trajectory. By inserting and removing particles near the cilium to maintain this concentration, and measuring the flux of particles that escape to infinity, it should be possible to infer the reaction rate. There remain details to be worked out, but it is possible that this approach would increase the efficiency over directly simulating the absorption problem.

[69]: Masoud *et al.* (2019), *The reciprocal theorem in fluid dynamics and transport phenomena*

RESEARCH ARTICLE

Ciliary chemosensitivity is enhanced by cilium geometry and motility

David Hickey[1], Andrej Vilfan[1,2]*, Ramin Golestanian[1,3]*

[1]Max Planck Institute for Dynamics and Self-Organization (MPIDS), Göttingen, Germany; [2]J. Stefan Institute, Ljubljana, Slovenia; [3]Rudolf Peierls Centre for Theoretical Physics, University of Oxford, Oxford, United Kingdom

Abstract Cilia are hairlike organelles involved in both sensory functions and motility. We discuss the question of whether the location of chemical receptors on cilia provides an advantage in terms of sensitivity and whether motile sensory cilia have a further advantage. Using a simple advection-diffusion model, we compute the capture rates of diffusive molecules on a cilium. Because of its geometry, a non-motile cilium in a quiescent fluid has a capture rate equivalent to a circular absorbing region with ~4× its surface area. When the cilium is exposed to an external shear flow, the equivalent surface area increases to ~6×. Alternatively, if the cilium beats in a non-reciprocal way in an otherwise quiescent fluid, its capture rate increases with the beating frequency to the power of 1/3. Altogether, our results show that the protruding geometry of a cilium could be one of the reasons why so many receptors are located on cilia. They also point to the advantage of combining motility with chemical reception.

***For correspondence:**
andrej.vilfan@ds.mpg.de (AV);
Ramin.Golestanian@ds.mpg.de (RG)

Competing interests: The authors declare that no competing interests exist.

Funding: See page 13

Received: 07 January 2021
Preprinted: 14 January 2021
Accepted: 03 August 2021
Published: 04 August 2021

Reviewing editor: Raymond E Goldstein, University of Cambridge, United Kingdom

Introduction

Cilia are small hairlike organelles with a microtubule-based core structure that protrude from the cell surface. They are found on most eukaryotic cells (***Nachury and Mick, 2019***) and can be broadly classified into two categories: primary and motile. Primary cilia, of which there is only one on each cell, have primarily sensory functions (as receptors for chemical, mechanical, or other signals) (***Zimmermann, 1898***; ***Berbari et al., 2009***; ***Hilgendorf et al., 2016***; ***Spasic and Jacobs, 2017***; ***Ferreira et al., 2019***). Due to their shape and their role in signalling, they are often referred to as 'the cell's antenna' (***Marshall and Nonaka, 2006***; ***Malicki and Johnson, 2017***). Motile cilia, typically appearing in larger numbers (***Brooks and Wallingford, 2014***; ***Spassky and Meunier, 2017***), move the surrounding fluid by beating in an asymmetric fashion (***Golestanian et al., 2011***; ***Gilpin et al., 2020***), and often with some degree of coordination (***Uchida and Golestanian, 2010***; ***Elgeti and Gompper, 2013***). They play a key role in a number of processes, including the swimming and feeding of microorganisms (***Guasto et al., 2012***; ***Lisicki et al., 2019***), mucus clearance in airways (***Bustamante-Marin and Ostrowski, 2017***), fluid transport in brain ventricles (***Faubel et al., 2016***), and egg transport in Fallopian tubes. However, there are exceptions to this classification. Primary cilia in the vertebrate left-right organiser are motile and drive a lateral fluid flow that triggers, through a mechanism that is not yet fully understood, a distinct signalling cascade determining the body laterality (***Essner et al., 2002***). There is also mounting evidence that motile cilia can have various sensory roles (***Bloodgood, 2010***), including chemical reception (***Shah et al., 2009***). Adversely, receptors localised on motile cilia, such as ACE2, can also act as entry points for viruses including SARS-CoV-2 (***Lee et al., 2020***). Some chemosensory systems, including vomeronasal (***Leinders-Zufall et al., 2000***) and olfactory neurons (***Bhandawat et al., 2010***) and marine sperm cells (***Kaupp et al., 2003***), are known to achieve a sensitivity high enough to detect a small number of molecules.

The sensitivity of a chemoreceptor is characterised by its binding affinity for the ligand, as well as its association/dissociation kinetics. If the time-scale of ligand dissociation is longer than the time-

scale of the changes in ligand concentration, or if the ligands bind irreversibly, the sensitivity is determined by the binding rate alone. It has been shown that the theoretical limit of sensing accuracy is achieved when the receptors detect the frequency of binding events and when re-binding is excluded (**Bialek and Setayeshgar, 2005**; **Endres and Wingreen, 2009**) Because diffusion is fast on very short length scales, only 1% of the surface area of a cell or cilium needs to be covered in high-affinity receptors to obtain near-perfect adsorption (**Berg and Purcell, 1977**). Even if this condition is not satisfied, the membrane itself could non-specifically bind the ligands with near-perfect efficacy, which then reach the receptors in a two-stage process. In either of these cases, as long as there is no advection, the binding rates can be estimated using the theory of diffusion-limited reactions (**Adam and Delbruck, 1968**). This binding rate is known as the diffusion limit, and it has already been shown that flagella-driven swimming microorganisms can break the diffusion limit in order to increase their access to nutrients (**Short et al., 2006**).

The increasingly overlapping functions of sensory and motile cilia lead to the natural question about the advantage of placing receptors on a cilium, or in particular on a motile cilium. Because of its small volume, a cilium forms a compartment that facilitates efficient accumulation of second messengers (**Marshall and Nonaka, 2006**; **Hilgendorf et al., 2016**). Placing receptors on a protrusion, away from the flat surface, could have other advantages, like avoiding the effect of surface charges or the glycocalycx. It has also been suggested that the location of chemoreceptors on cilia exposes them to fluid that is better mixed (**Marshall and Nonaka, 2006**). A recent study suggests that the hydrodynamic interaction between motile and sensory cilia can enhance the sensitivity of the latter (**Reiten et al., 2017**). However, the question of how the geometry and motility of cilia affect their ability to capture and detect ligands has still remained largely unexplored.

In this paper, we investigate the theoretical limits on association rates of ligands on passive and motile cilia. In particular, we address the question of whether the elongated shape of a cilium and its motility can improve its chemosensory effectiveness. By using analytical arguments and numerical simulations, we show that the capture rate of a cilium is significantly higher than that of a receptor located on a flat epithelial surface. Motile cilia can further improve their chemosensitivity. Finally, we show that a cilium within an immotile bundle has a lower capture rate than an isolated cilium, but a higher one when the cilia are sufficiently motile.

Results

In this study, we calculate the second-order rate constant for diffusive particle capture on a cilium. We discuss scenarios where the fluid and the cilium are at rest, where the fluid exhibits a shear flow, where the cilium is actively beating, and where a bundle of hydrodynamically interacting cilia absorbs particles.

We consider a perfectly absorbing cilium protruding from a non-absorbing surface, in a fluid containing some chemical species with a concentration field c. Far from the cilium, the unperturbed concentration has a constant value c_0. The rate constant k is defined such that

$$I = c_0 k, \tag{1}$$

where I is the capture rate, defined as the number of captured particles per unit time.

Since the aforementioned cilium is perfectly absorbing, we define an absorbing boundary condition such that the concentration of the chemical species is zero at every point on the cilium's surface. We assume that the flat membrane surrounding the cilium does not absorb particles and it is therefore described with a reflecting boundary condition at $z = 0$. The geometry and boundary conditions are illustrated in **Figure 1**.

Cilium in quiescent fluid

We consider a cilium (modelled as a cylinder next to a boundary at $z = 0$) in a quiescent fluid, with the goal of determining its capture rate constant in the absence of advection. In the case where there is a steady state with no advection, the advection-diffusion equation reduces to

$$D\nabla^2 c = 0, \tag{2}$$

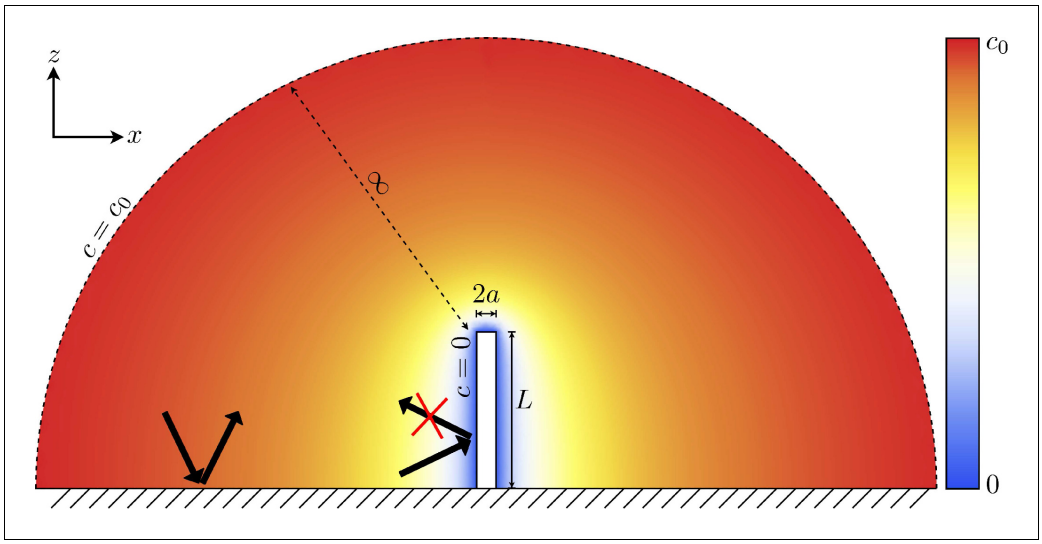

Figure 1. The concentration boundary conditions and general setup of the problem to be solved. The cilium satisfies an absorbing boundary condition, and there is a constant concentration an infinite distance from the cilium. The coloured overlay shows the concentration field in the absence of any fluid flow.

where D is the diffusion constant. The rate constant is determined by the integral of the current density $\mathbf{J}$ over the surface, which follows from Fick's law:

$$k = -\frac{1}{c_0}\int \mathrm{d}\mathbf{S}\cdot\mathbf{J} = \frac{1}{c_0}\int \mathrm{d}\mathbf{S}\cdot(D\nabla c). \tag{3}$$

As we show in Appendix 1, the rate constant can be evaluated using an analogy between particle diffusion and electrostatics (***Berg and Purcell, 1977***). Up to a prefactor, the capture rate is determined by the self-capacitance C of a conducting body of the same shape as $k = DC/\varepsilon_0$.

To determine the capture rate of a cilium embedded in a non-absorbing surface, we first eliminate the reflective boundary condition at the surface by symmetrically extending the problem to a cylinder of length $2L$ in open space and considering $1/2$ of its capacitance. There is no closed-form expression for the capacitance of a cylinder, so we loosely approximate this cylinder as a prolate spheroid with semi-major axis L and semi-minor axis a. Using its self-capacitance in the limit $L \gg a$ (***Snow, 1954***), we find the rate constant:

$$k_{\mathrm{cilium}} = 2\pi D\frac{L}{\ln(2L/a)}. \tag{4}$$

This value agrees well with simulations: the ratio of the simulated to this analytical rate constant is 1.02.

The finding that the capture rate scales almost linearly with the length of the cilium can be compared to experimental data obtained on olfactory cilia from the nasal cavity of mouse, whose lengths in different regions vary from a few micrometers to tens of micrometers. ***Challis et al., 2015*** have used patch-clamp recordings on olfactory sensory neurons and measured the response to pulses of an odorant (eugenol or a mixture of 10 odorants), lasting $5 - 400\,\mathrm{ms}$. Regions with different lengths show very different sensitivity thresholds, differing by an order of magnitude. The results are qualitatively consistent with the predicted length dependence of the capture rate.

To quantify the advantage of localising the receptors on a cilium, we compare it with a case where the receptors form a circular patch on a flat surface (***Figure 2a***). Again, we assume that the receptor patch has a perfectly absorbing surface, while the surface surrounding it is reflective. We determine the size of the patch needed to attain the same rate constant as the cilium. The rate constant for a circular patch on the reflective boundary can be found by applying the electrostatic analogy to the well-known result for the self-capacitance of a thin conducting disc of radius R (***Berg and Purcell, 1977***):

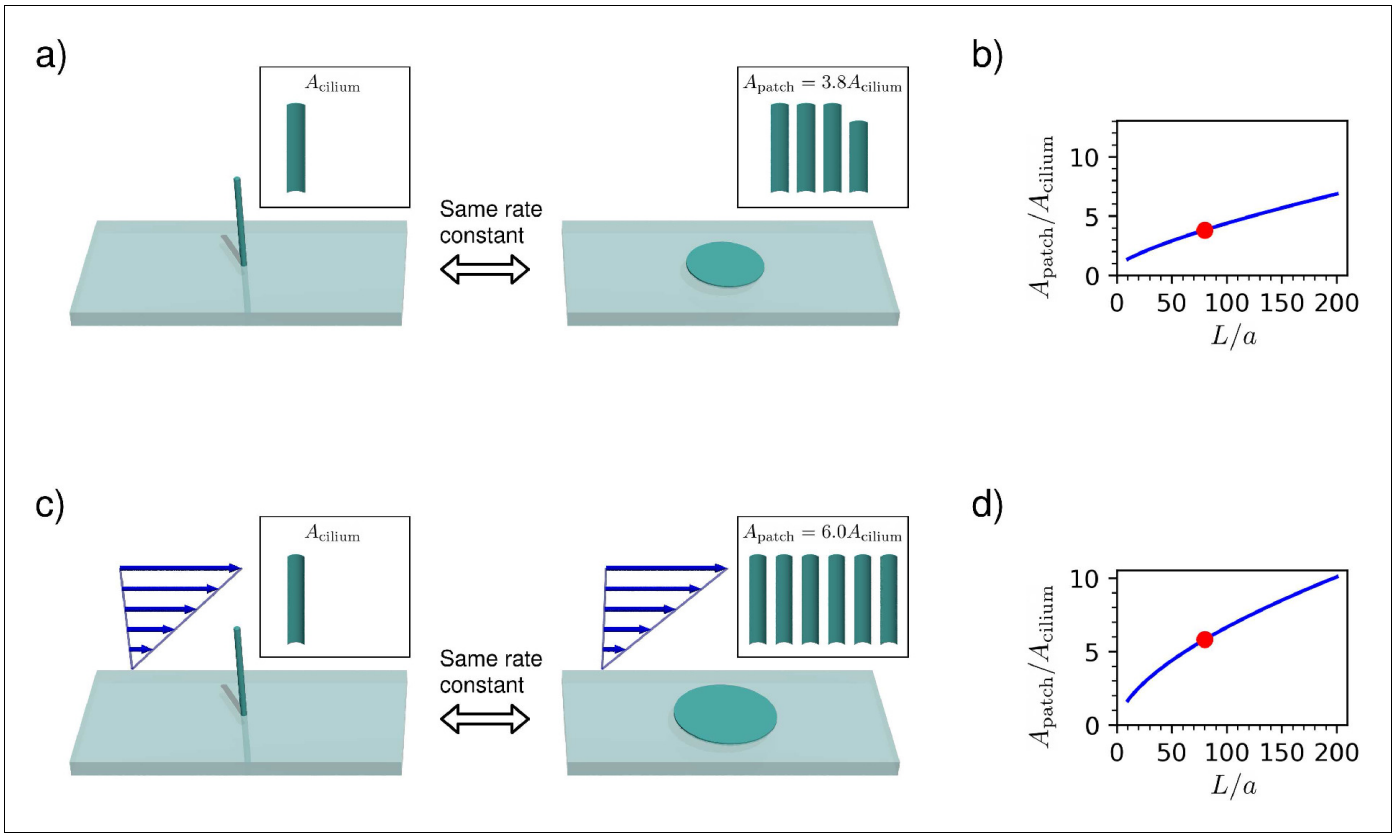

Figure 2. Comparison between capture rates of a non-motile cilium and a circular patch on the surface. All diagrams use $L/a = 80$, indicated on the graphs by a red dot. (**a**) In a quiescent fluid, the cilium has the same capture rate as a surface patch with 3.8 times the surface area. (**b**) The area ratio $A_{\text{patch}}/A_{\text{cilium}}$ as a function of the cilium aspect ratio L/a in a quiescent fluid, given by ***Equation (6)***. (**c**) In a shear flow at a high Péclet number, the capture rate of the cilium reaches that of a surface patch with 6.0 times the surface area. (**d**) The area ratio as a function of the aspect ratio in the high Péclet number limit (***Equation 14***).

The online version of this article includes the following source data and figure supplement(s) for figure 2:

Figure supplement 1. Capture rate as a function of the Péclet number for passive cilia in a shear flow, obtained from numerical simulations.

Figure supplement 1—source data 1. Event counts and calculated rates as shown in ***Figure 2—figure supplement 1***.

$$k_{\text{patch}} \approx 4DR. \tag{5}$$

We find that the patch has a much larger surface area than the cilium with the same rate constant. We can calculate this area ratio:

$$\frac{A_{\text{patch}}}{A_{\text{cilium}}} \approx \frac{\pi^2}{8} \cdot \frac{L}{a} \frac{1}{\ln^2(2L/a)}. \tag{6}$$

The area ratio as a function of the aspect ratio L/a is shown in ***Figure 2b***. For a typical cilium aspect ratio of $L/a = 80$ (with $L = 10\,\mu\text{m}$, and $a = 125\,\text{nm}$), this area ratio is 3.8, implying that the cilium is much more effective per unit area than a receptor on the surface of the cell. Olfactory cilia have a great variation of lengths, ranging from $2.5\,\mu\text{m}$ to $100\,\mu\text{m}$ (***Challis et al., 2015***; ***Williams et al., 2014***). If we neglect the fact that long cilia are not straight, the calculated area ratio ranges from 2.7 to 18. Using an exact numerical result for the capacitance of a cylinder (***Paffuti, 2018***), the ratio becomes 4.5 for $L/a = 80$. With the dimensions given above, the radius of the circular patch with the same capture rate is $R = 3.4\,\mu\text{m}$.

Cilium in shear flow

At the scale of cilia, the flow is characterised by a low Reynolds number, meaning that viscous forces dominate over inertia. The fluid motion is well-described by the Stokes equation, together with the incompressibility condition:

$$\eta\nabla^2\mathbf{u}-\nabla p=0 \tag{7}$$

$$\nabla\cdot\mathbf{u}=0 \tag{8}$$

in which $\mathbf{u}$ is the fluid velocity, η is the dynamic viscosity, and p is the pressure. The concentration field of some chemical species suspended within this fluid is governed by the advection-diffusion equation:

$$\frac{\partial c}{\partial t}+\mathbf{u}\cdot\nabla c=D\nabla^2 c \tag{9}$$

where c is a function of both position and time.

The ratio of advection to diffusion is described by the dimensionless Péclet number. This is usually written as some characteristic flow speed multiplied by some characteristic length scale, all divided by the diffusion constant.

Because the cilium grows from a flat surface with a no-slip boundary condition, the flow can be described as a uniform shear flow with the shear rate $\dot{\gamma}$. To estimate the capture rate constant of a cilium in a shear flow, we make use of the fact that the radius of the cylinder is much smaller than the length scale over which the shear flow varies. We therefore approximate the local rate density at any point on the cilium with that of an infinitely long cylinder in a uniform flow with velocity $v(z)=\dot{\gamma}z$. The capture rate per unit length is

$$\frac{\mathrm{d}k_{\mathrm{cilium}}}{\mathrm{d}z}=\beta D\cdot\left(A\frac{av}{D}\right)^{1/3}, \tag{10}$$

where $\beta=2.50$ is a numerical constant (see Appendix 2 for derivation).

Now the total rate constant is obtained by integration over the cilium length

$$k_{\mathrm{cilium}}=\int_0^L \mathrm{d}z\beta D\cdot\left(\frac{a\dot{\gamma}z}{D}\right)^{1/3}=\frac{3}{4}\beta DL\cdot\left(\frac{L}{a}\right)^{-1/3}\mathrm{Pe}_{\mathrm{cilium}}^{1/3}. \tag{11}$$

We take the characteristic velocity to be the speed of the cilium's tip relative to the surrounding fluid, and hence the Péclet number for the extended cilium is

$$\mathrm{Pe}_{\mathrm{cilium}}=\frac{\dot{\gamma}L^2}{D}. \tag{12}$$

This expression for the rate once again shows a strong positive relationship between cilium length and sensitivity, as is known to be the case in real biological systems (***Challis et al., 2015***). The characteristic Péclet number for the cross-over between the diffusive and the convective capture is of the order $\sim L/a\approx 80$.

Once again we determine the size of a circular surface patch offering an equivalent effectiveness to the cilium in a flow with the same shear rate (***Figure 2c***). The high-Pe rate constant for a patch in a shear flow is (***Stone, 1989***):

$$k_{\mathrm{patch}}\approx DR\left[\zeta\cdot\mathrm{Pe}_{\mathrm{patch}}^{1/3}+O\left(\mathrm{Pe}_{\mathrm{patch}}^{-1/6}\right)\right], \tag{13}$$

where $\mathrm{Pe}_{\mathrm{patch}}\equiv\dot{\gamma}R^2/D$ and $\zeta=2.157$ is a purely numerical constant. We can calculate the ratio of the area of the equivalent patch to the area of the cilium for these high-Pe asymptotic results:

$$\frac{A_{\mathrm{patch}}}{A_{\mathrm{cilium}}}\approx\frac{1}{2}\left(\frac{3\beta}{4\zeta}\right)^{6/5}\cdot\left(\frac{L}{a}\right)^{3/5}\approx 0.42\left(\frac{L}{a}\right)^{3/5}. \tag{14}$$

The area ratio is shown in ***Figure 2d*** and compared with the results in a quiescent fluid. For a

typical cilium aspect ratio $L/a = 80$ (with $L = 10\,\mu\mathrm{m}$, and $a = 125\,\mathrm{nm}$), this area ratio is 6.0 – much larger than the area ratio in a quiescent fluid, which was 3.8. This means that a cilium is better per area than a patch at both low and high Péclet numbers, but the cilium excels when the Péclet number is large.

We additionally investigated the question how robust the results are if the receptors are localised to only one segment of the cilium. In a model, we assumed that of the total length L, the distal part νL is absorbing, while the proximal $(1-\nu)L$ is reflective. At high Péclet numbers, we can modify the integration limits in ***Equation (11)*** and obtain a theoretical capture rate $k_{\mathrm{cilium}}(\nu) = k_{\mathrm{cilium}} \cdot (1-(1-\nu)^{4/3})$. The result is compared to simulations in ***Figure 2—figure supplement 1***. A cilium with receptors over the distal 50% of its length therefore achieves 60% of the maximal capture rate.

Active pumping

A mounting collection of evidence suggests that both primary and motile cilia have sensory roles (***Bloodgood, 2010***). We are interested in the extent to which cilium motility can increase their ability to detect particles. To this end, we numerically simulate various different possible types of ciliary motion in otherwise quiescent fluids.

Because of the complex flow patterns and time-dependent boundary conditions, the absorption by a beating cilium is not analytically tractable. Instead, we use numerical simulations to determine the rate constants. We consider four different active pumping scenarios: a purely reciprocally moving cilium, a cilium tracing out a cone around an axis perpendicular to the surface, a cilium tracing out a tilted cone, and a cilium with a trajectory that includes bending, to raise the pumping efficiency (all shown in their respective order in ***Figure 3a–d***).

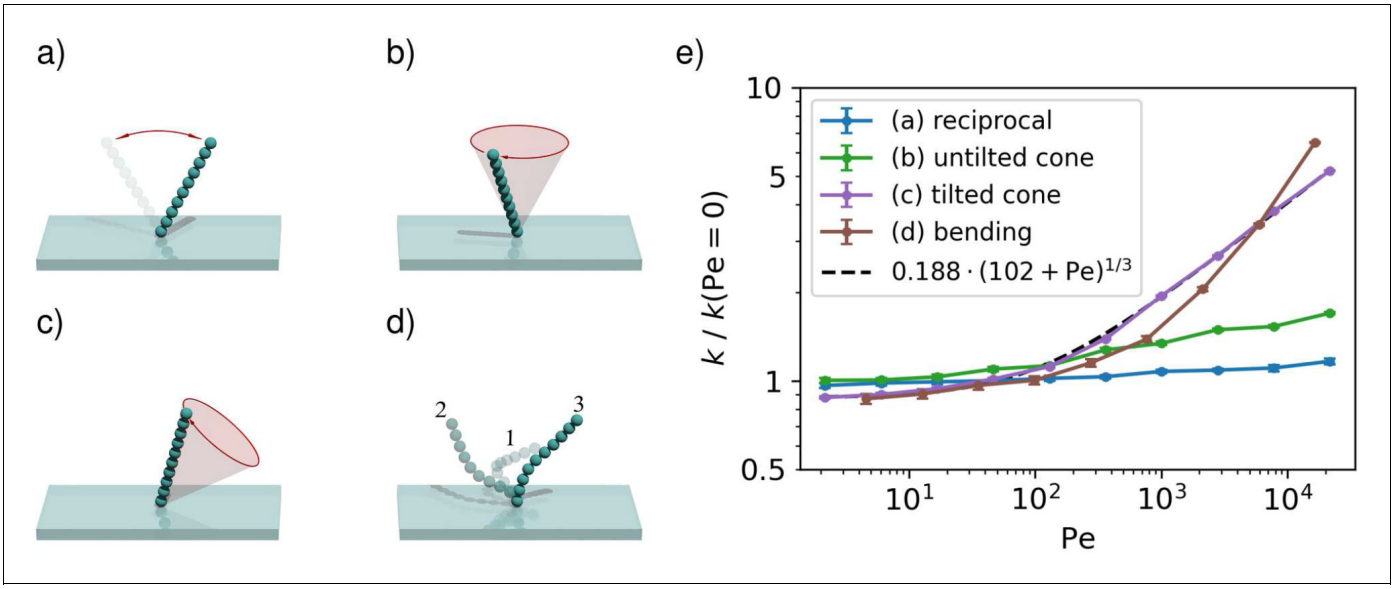

Figure 3. The capture rate of an active cilium for four types of motion. (**a**) The cilium is undergoing reciprocal motion, which is not generating any net flow. (**b**) The cilium moves along a cone with its axis perpendicular to the surface, such that it produces a rotational flow, but no long-range fluid transport. (**c**) The cilium moves along a tilted cone, which generates a long-range volume flow. (**d**) The cilium follows a realistic trajectory, beginning with a recovery stroke along the no-slip surface in 1, then performing an overhead power-stroke from 2 to 3 before returning to one in another recovery stroke. (**e**) The capture rate constants k of a beating cilium as a function of the Péclet number. The rates are determined using stochastic simulations. The error bars denote 95% confidence intervals and the dashed line shows a fit function that interpolates between the high and low-Péclet limits. All rates are normalised to the rate constant for a diffusion-limited capture with a cylindrical cilium with the same length and width.
The online version of this article includes the following source data and figure supplement(s) for figure 3:

Source data 1. Event counts and calculated rates as shown in ***Figure 3e***.
Figure supplement 1. Capture rate of an actively beating cilium tracing out a tilted cone, plotted as a function of the Péclet number.
Figure supplement 1—source data 1. Event counts and calculated rates as shown in ***Figure 3—figure supplement 1***.

The rate constants in these scenarios, relative to that of a non-moving cilium, are plotted in ***Figure 3e***. Analogously to the cilium in a shear flow, we define the Péclet number using the maximum tip velocity during the cycle:

$$\mathrm{Pe} = \frac{v_{\mathrm{tip}}^{\max} L}{D}. \tag{15}$$

The reciprocally moving cilium (***Figure 3a***) displays almost no improvement over several orders of magnitude of the Péclet number. This is expected, because Purcell's scallop theorem (***Purcell, 1977***) states that purely reciprocal motion does not create any net flow, so the particle intake is largely diffusive in nature. A minor increase of the rate constant with the Péclet number is caused by the local shear flow that facilitates absorption on the surface.

The cilium moving around a vertical cone (***Figure 3b***) induces a net rotational flow, but no inflow or outflow (by symmetry, the time-averaged flow can only have a rotational component [***Vilfan, 2012***]). Nevertheless, the constant motion of the cilium through the fluid leads to a higher local capture efficiency. The rate constant therefore shows more improvement; over a few orders of magnitude of the Péclet number, the rate constant increases by a factor of two.

The tilted cone (***Figure 3c***) shows a much higher capture rate, which is unsurprising. When the cilium is near to the plane, the no-slip boundary screens the flow, whereas when it is far from the plane, its pumping is unimpeded. This results in the cilium inducing a long range flow in one direction, characterised by a finite volume flow rate (***Smith et al., 2008***). The long range flow causes a constant intake that replenishes the depleted particles. At high Péclet numbers, the capture rate scales $k \sim \mathrm{Pe}^{1/3}$, which is the same dependence as in an external shear-flow, although with a prefactor that is lower by a factor of ~2. Locally, the relative flow around the cilium is the same whether a cilium is pivoting or resting in a shear flow. The pumping effect of the tilted cilium, on the other hand, provides sufficient inflow that the concentration around a cilium sees only a small depletion effect.

We finally simulated the capture process on a cilium exerting a realistic beating pattern, consisting of a stretched working stroke and a bent, sweeping recovery stroke (***Figure 3d***). The capture rate is close to that of the tilted cone, but surpasses it at very high Péclet numbers.

Collective active pumping

We consider seven cilia on a hexagonal centred lattice with lattice constant $0.95L$, with a view to understand how the presence of multiple cilia affects performance. We quantify the performance gain using a quantity Q, which we define as

$$Q = \frac{k_{\mathrm{multiple}}}{k_{\mathrm{cilium}}(\mathrm{Pe}) \cdot N_{\mathrm{cilia}}}, \tag{16}$$

which represents the fractional per-cilium improvement in rate constant compared to a single isolated cilium at the same Péclet number.

Using numerical simulations, we find that at zero Péclet number (***Figure 4a–b***), $Q \approx 0.5$, which means that the cilia locally deplete the concentration field, harming the per-cilium effectiveness; in a quiescent fluid, it is most efficient for cilia to stand far away from their neighbours.

However, when the cilia actively move (with each tracing out a tilted cone with a different randomly-chosen phase lag compared to its neighbours, as in ***Figure 4e***) the trend is reversed: we find that at $\mathrm{Pe} \approx 10000$, $Q \approx 1.53$, meaning that per cilium, the capture rate is around 50% higher in the collective when compared to an isolated cilium with the same Péclet number. We find that over the range of Péclet numbers simulated, the Q increases monotonically with the Péclet number (***Figure 4h***).

When comparing these randomly chosen phases to a patch of cilia which beat in uniform, we find that cilia which beat in phase (***Figure 4d***) see an improvement over the stationary case with $Q \approx 1.16$, but are much less effective than the cilia patch that beats with random phases. The random phases give a higher volume flow, and complex hydrodynamic interactions between the randomly-phased cilia result in a slightly higher capture chance for any given particle. Similar levels of improvement are also seen for other arrangements of cilia forming a bundle, that is, $N_{\mathrm{cilia}} = 19$ on a hexagon (***Figure 4f***) or $N_{\mathrm{cilia}} = 4$ on a square (***Figure 4g***). Furthermore, an improvement of randomly beating over uniformly-beating cilia has been observed in previous work with finite-sized particles (***Ding and***

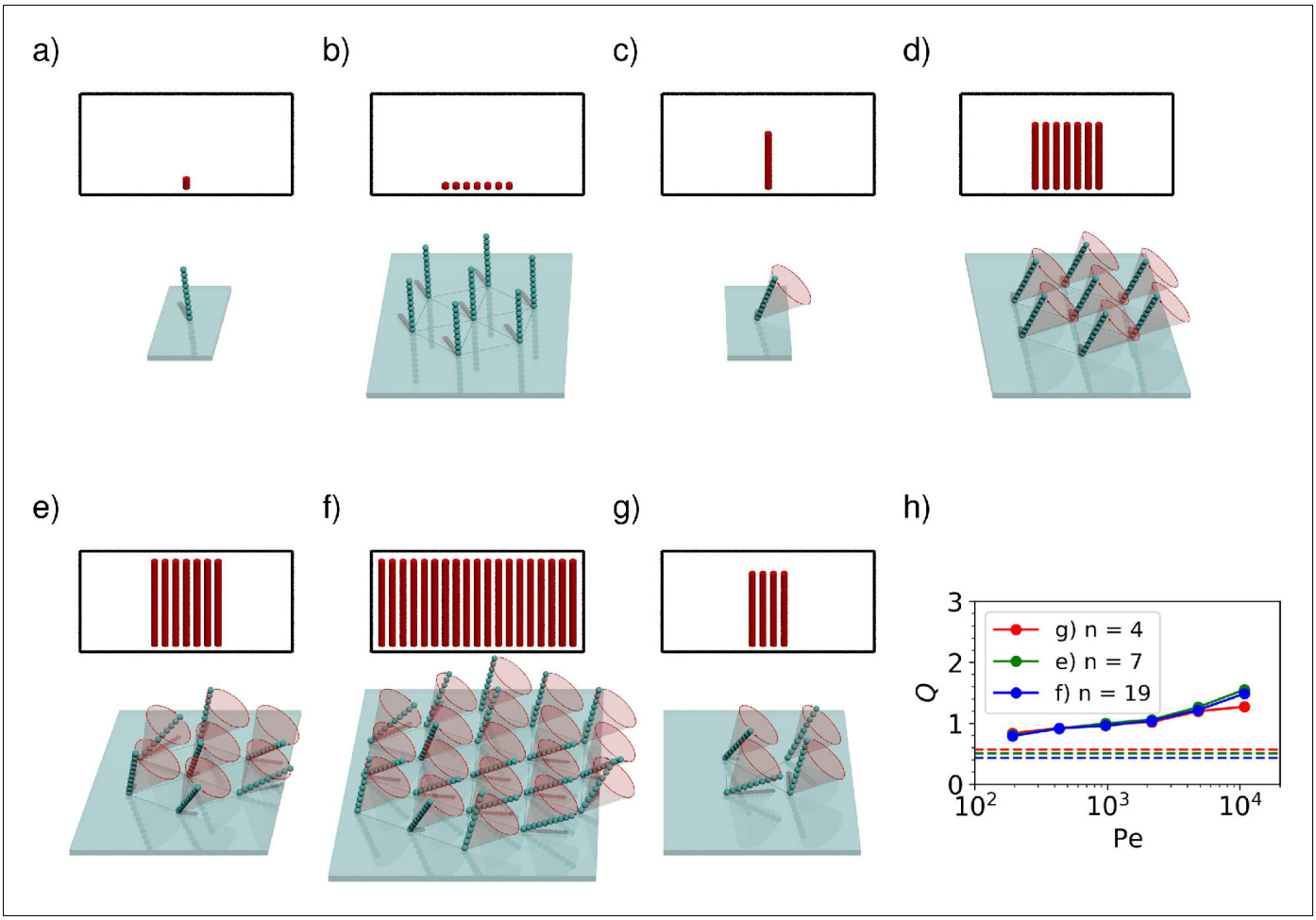

Figure 4. Comparison between the capture rate constant of a single cilium (**a**, **c**) and a bundle of $N_{\text{cilia}} \in \{4, 7, 19\}$ cilia (**b**, **d–g**). In the insets, the height of each red cylinder indicates the rate constant per cilium at $\text{Pe} \approx 10000$, and the number of cylinders represents the number of cilia. For immotile cilia (**a**, **b**), a bundle has a lower per-cilium capture rate than an isolated cilium, although the the total rate constant of the bundle is higher. The reduced capture rate per cilium is caused by the depletion of ligands close to the bundle. For motile cilia (**d–g**), the situation is reversed and the capture rate per cilium in a bundle (**d–g**) can be significantly higher than for an isolated cilium (**c**). The increase can be explained by the collective flow generation, which helps the capture on all cilia. In (**d**) the cilia all beat with the same frequency corresponding to $\text{Pe} \approx 10000$ but with identical phases. In (**e–g**) all cilia beat with the same frequency corresponding to $\text{Pe} \approx 10000$, but their phases are chosen randomly. It can be seen that the random phases give a higher rate constant than the uniform phases. (**h**) shows how the performance gain Q varies with the Péclet number for different configurations. The rates shown at each point are the average of 30 random phase configurations like the one shown in (**e**). The dashed line is the Q-value for $\text{Pe} = 0$ for each configuration.

The online version of this article includes the following source data for figure 4:

Source data 1. Event counts and calculated rates as shown in ***Figure 4h***.

Kanso, 2015; ***Nawroth et al., 2017***). The results suggest that mutual enhancement of capture rates is a robust phenomenon and does not depend on a specific geometry.

Discussion

Our results address a simple question: does the location of so many chemical receptors on cilia bring them an advantage in sensitivity? Besides the well-known advantages of compartmentalisation, which facilitates the downstream signal processing, we show that the elongated shape of a cilium provides an advantage for the capture rate of molecules in the surrounding fluid. The advantages can be summarised as follows:

1. If neither the fluid nor the cilium move and the process of particle capture is purely diffusive, the elongated shape improves the capture rate of the cilium by giving it better access to the diffusing ligands. The length dependence of the capture rate has the sub-linear form $k \sim L/\log L$. With typical parameters, the cilium achieves a capture rate equivalent to that of a circular patch of receptors on a flat surface with 4× the surface area of the cilium.
2. When a non-moving cilium is exposed to a shear flow, the advantage increases, mainly because the tip of the cilium is exposed to higher flow velocities. The capture rate scales with $k \sim L^{4/3}$ and becomes equivalent to that of a surface patch with approximately 6× the surface area at high flow rates.
3. An actively beating cilium can achieve capture rates comparable to those by a passive cilium in a shear flow with the same relative tip velocity, but only if the beating is non-reciprocal, that is, if the cilium generates a long range directed flow. The capture rate can scale with the beating frequency to the power of 1/3 or higher.
4. Without motility, a bundle of sensory cilia achieves a capture rate *per cilium* that is lower than that of a single cilium, because of the locally depleted ligand concentration. However, the situation can become reversed if the cilia are beating: then each cilium benefits from the flow produced by the bundle as a whole, and the per-cilium capture rate can be significantly higher than in an isolated beating cilium. Cilia beating with random phases achieve significantly higher capture rates than when beating in synchrony.

Our results are based on a few assumptions. We assumed that the particles get absorbed and detected upon their first encounter of the cilia surface – an assumption that is justified if the receptors are covering the surface at a sufficient density (**Berg and Purcell, 1977**), or if the particles bind non-specifically to the membrane of the cilium first. We also treat the particles as point-like (their size only has an influence on their diffusivity), which is accurate for molecules up to the sizes of a protein and we do not expect a significant error even for small vesicles. The Rotne-Prager tensor approximation used to determine the flow fields does not exactly satisfy the no-slip boundary condition on the surface of the cilium, especially at high Péclet numbers.

With the typical dimensions of a cilium ($L = 10\,\mu\mathrm{m}$, $a = 0.125\,\mu\mathrm{m}$) and a diffusion constant of a small molecule $D = 10^{-9}\,\mathrm{m^2 s^{-1}}$, we obtain $k_{\mathrm{cilium}} = 7\,\mathrm{pM^{-1}s^{-1}}$. A chemosensory cilium working at the physical limit is therefore capable of detecting picomolar ligand concentrations on a timescale of seconds. Sensitivity thresholds in the sub-picomolar range have been measured in some olfactory neurons (**Frings and Lindemann, 1990**; **Zhang et al., 2013**), indicating that some olfactory cilia work close to the theoretical sensitivity limit. If the cilia are embedded in mucus with a viscosity at least 3 orders of magnitude higher than water (**Lai et al., 2009**) (we disregard its viscoelastic nature here) and the molecule has a Stokes radius of a few nanometres, the diffusion-limited capture rate reduces to around $k_{\mathrm{cilium}} = 1\,\mathrm{nM^{-1}s^{-1}}$.

In a shear flow with a typical shear rate of $\dot{\gamma} = 10\,\mathrm{s^{-1}}$, the Péclet number of a small molecule in water is of the order of $\mathrm{Pe} \approx 1$, where the capture rate still corresponds to the stationary case. However, with larger molecules and higher viscosities, the Péclet numbers can exceed 10^4, leading to a significant enhancement of the capture rate.

When the same cilium is beating with a frequency of $25\,\mathrm{Hz}$, the Péclet number is of the order ~10, which is too small to have an effect on the capture rate. With larger molecules and higher viscosities, the Péclet numbers can be significantly higher. With a medium viscosity of $0.2\,\mathrm{Pa \cdot s}$ (200 times the water viscosity) and a Stokes radius of $10\,\mathrm{nm}$, it reaches 10^5, meaning that the motility accelerates the capture rate by one order of magnitude. For example, according to one hypothesis, motile cilia in the zebrafish left-right organizer (Kupffer's vesicle) both generate flow and detect signalling particles, possibly extracellular vesicles (**Ferreira et al., 2017**; **Ferreira et al., 2019**) similar to the proposed 'nodal vesicular parcels' (**Tanaka et al., 2005**). With a cilium length of $L = 6\,\mu\mathrm{m}$ and a particle radius of $a = 100\,\mathrm{nm}$, we obtain $\mathrm{Pe} = 1300$, showing that the capture rates can be several times higher than in a passive cilium. **Figure 5** shows how the molecular Stokes radius affects the fluid viscosity required to break the diffusion limit for a few different scenarios. However, when the particle size becomes comparable to the cilium diameter, the approximation that treats them as point particles loses validity. Indeed, it has been shown that particle size can have a direct steric effect on the capture rate (**Ding and Kanso, 2015**). Furthermore, the capture process of large particles can depend on a competition between hydrodynamic and adhesive forces (**Tripathi et al., 2013**). Steric effects can even lead to particle enrichment in flow compartments (**Nawroth et al., 2017**).

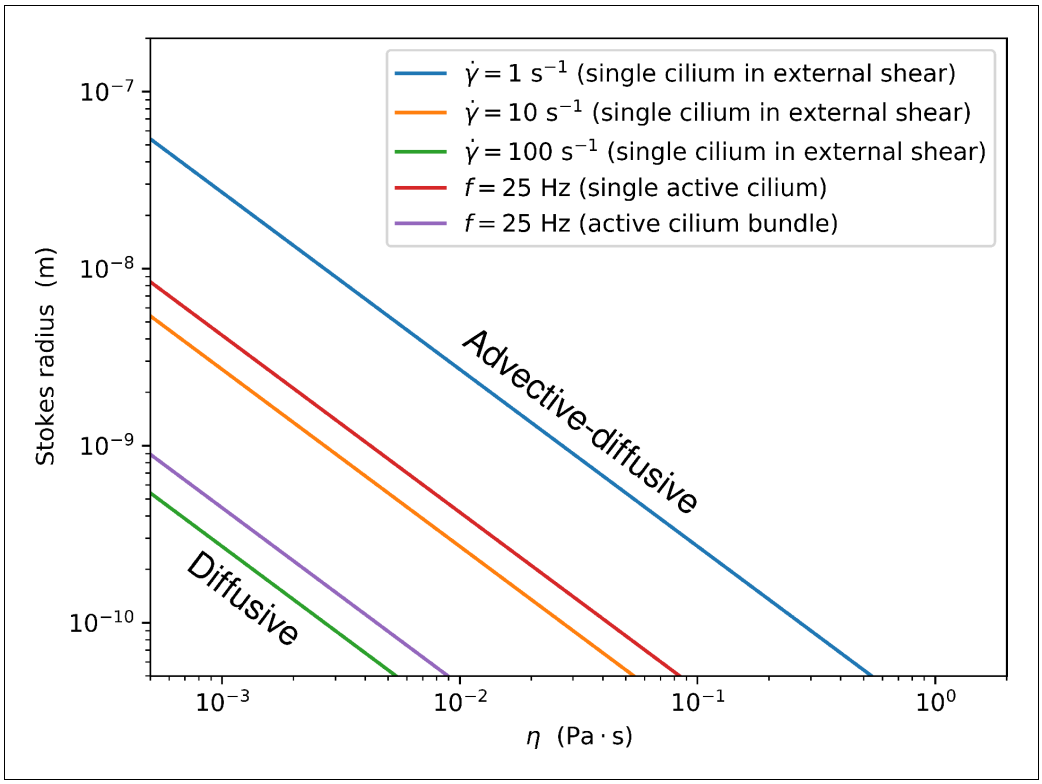

Figure 5. The demarcation between the regime where the rate constant is determined mostly by the diffusion limit and the regime in which it is enhanced by advection as a function of the fluid viscosity η and the particle Stokes radius. The blue, orange, and green lines show the results for a passive cilium in a shear flow (***Figure 2c***), the red line for an actively beatig cilium (***Figure 3c***) and the magenta line for a bundle of 7 cilia (***Figure 4e***). For all lines, the cilium dimensions are $L = 10\,\mu\mathrm{m}$ and $a = 250\,\mathrm{nm}$.

We have thus proven that for individual isolated cilia the geometry of a cilium always means an advantage in chemical sensitivity over receptors covering the same area on a flat surface (assuming they act as perfect absorbers), whether in a quiescent or moving fluid. At high Péclet numbers, which are achieved in viscous fluids, with very large particles or in very strong flows, the advantage of a cilium increases further and even confers an advantage in chemosensitivity to cilium bundles over individual cilia. These advantages can work in concert with others, such as avoiding charged surfaces and glycocalix and the provision of a closed compartment on the inside. Further work might examine the extent to which motility benefits cilia in a fluid with bulk flow, or investigate the effect of metachronal waves on ciliary chemosensitivity. Finally, our results shed light on possible engineering applications for microfluidic sensing devices based on these ideas, for example using magnetic actuation (***Vilfan et al., 2010***; ***Meng et al., 2019***; ***Matsunaga et al., 2019***).

Materials and methods

Numerically simulated point particles are injected into a finite system containing a motile cilium, and move around due to advection (resulting from the motion of the cilium) and diffusion, until they either escape from the system or are absorbed by the cilium. The proportion of particles which are captured is used to compute a rate constant.

Flow calculation

The hydrodynamics are computed using a modified Rotne-Prager mobility tensor $\mathbf{M}$ that accounts for the no-slip boundary. If there are N spheres of equal radius R in the simulation, each having a

prescribed trajectory $\mathbf{r}_i(t)$ and each acted upon by a force $\mathbf{F}_i(t)$, then these forces must satisfy (**Vilfan et al., 2010**)

$$\dot{\mathbf{r}}_i(t) = \sum_{j=1}^{N} \mathbf{M}\left[\mathbf{r}_i(t), \mathbf{r}_j(t); R, R\right] \cdot \mathbf{F}_j(t) \tag{17}$$

for every $i \in [1, N]$. Since every term except the forces is known, the forces can be determined numerically at a given t by solving this set of simultaneous equations. Then the fluid velocity at any point $\mathbf{x}$ can be determined by

$$\mathbf{u}(\mathbf{x}, t) = \sum_{i=1}^{N} \mathbf{M}[\mathbf{x}, \mathbf{r}_i(t); 0, R] \cdot \mathbf{F}_i(t). \tag{18}$$

In the simulations we used $N = 20$ spheres, corresponding to an aspect ratio $L/a = 40$. A somewhat lower value than in the analytical calculations was chosen to save computational time and also to compensate for the fact that a cylinder is replaced with a chain of spheres.

Injection

We require a particle injection procedure that satisfies the concentration boundary condition $c \to c_0$ far from the absorbing cilium. We achieve this by introducing two bounding boxes in the simulation: an inner and an outer box, separated by a thin distance d (**Figure 6**). The particles are injected at the boundary of the inner box and absorbed at the outer box. The injection rate is calculated such that it corresponds to the advective-diffusive flux through the layer between the boxes if the concentration at the inner box is c_0. Because the flux through the boundary layer is much larger than the flux of particles absorbed inside the inner box, the method is suited to ensure a constant concentration boundary condition. The method is similar to a recent algorithm using a single boundary (**Ramírez-Piscina, 2018**), but uses a simpler injection function.

To calculate the injection current density, we solve the one-dimensional steady-state advection-diffusion equation

$$0 = D\frac{\mathrm{d}^2 c}{\mathrm{d}x^2} - v\frac{\mathrm{d}c}{\mathrm{d}x}, \tag{19}$$

with the boundary conditions $c(0) = 0$ and $c(d) = c_0$. The solution is

$$c(x) = c_0 \frac{e^{vxD} - 1}{e^{vdD} - 1}. \tag{20}$$

By the application of Fick's law, this leads to an expression for the current density through the inner box:

$$j(x) = vc_0 \frac{1}{1 - e^{-vdD}}. \tag{21}$$

We assume that a test particle will take take much longer to reach the cilium than the characteristic time required for the flow to change, and hence we take $v = \langle \mathbf{u}(\mathbf{x}, t) \cdot \hat{\mathbf{n}} \rangle_t$, where $\hat{\mathbf{n}}$ is the inward pointing surface normal of the inner box. This function can then be used to probabilistically weight where particles are injected on the inner box.

Numerical integration

The test particle position is updated using an Adams-Bashforth-Milstein multistep numerical integration method in the presence of noise (**Tocino and Senosiain, 2015**):

$$\mathbf{x}_{i+1} = \mathbf{x}_i + \Delta t \left[\frac{3}{2}\mathbf{u}(\mathbf{x}_i, t) - \frac{1}{2}\mathbf{u}(\mathbf{x}_{i-1}, t - \Delta t)\right] + \xi_i. \tag{22}$$

Because the computation of the flow field $\mathbf{u}$ (see **Equation 18**) is the most demanding step, it is advantageous over methods that require additional function evaluations per step. ξ_i is a vector

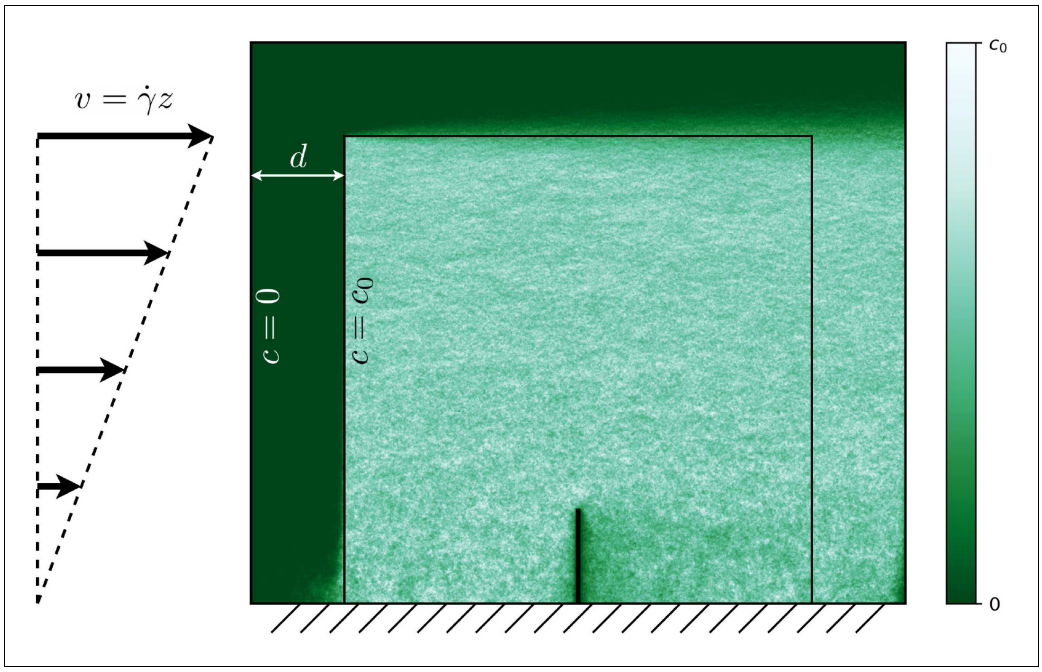

Figure 6. The boundary conditions used for injection. Since the fraction in incident particles absorbed by the cilium is small compared to the fraction absorbed by the outer surface, the concentration at the inner boundary is very close to c_0. The coloured overlay shows the concentration as recorded in an example numerical simulation of a cilium in a shear flow with $\mathrm{Pe} = 50$.

where each element is pseudorandomly generated Gaussian noise with standard deviation $\sqrt{2D\Delta t}$ and mean of zero.

Rate evaluation

We finish each simulation run when the particle position reaches the cilium (capture), or the outer box (escape). At the end, the rate constant is determined as

$$k = \frac{I}{c_0} \frac{n_{\mathrm{capture}}}{n_{\mathrm{capture}} + n_{\mathrm{escape}}}, \tag{23}$$

where I is the calculated total particle flux, obtained by integrating the flux density over the inner box, $I = \int j \mathrm{d}S$.

Numerical parameters

For all numerical simulations, we use a cilium consisting of 20 beads (thus giving a length to radius ratio $L/a = 40$). For the conical and reciprocal motion (***Figure 3a–c***), we use an opening angle (between the cone axis and surface) of 30˚, and for the titled conical motion (***Figure 3c***) the axis of the cone is tilted relative to the vertical by an angle of 55˚.

In the collective regime, the parameters are the same, with the addition of a hexagon lattice constant of $0.95L$. The cones are tilted such that their axes are perpendicular to one chosen side of the hexagon (left to right in ***Figure 4d-f***).

Acknowledgements

We thank David Zwicker for comments on the manuscript. This work has been supported by the Max Planck Society. A.V. acknowledges support from the Slovenian Research Agency (grant no. P1-0099).

Additional information

Funding

Funder	Grant reference number	Author
Max-Planck-Gesellschaft		David Hickey Andrej Vilfan Ramin Golestanian
Javna Agencija za Raziskovalno Dejavnost RS	P1-0099	Andrej Vilfan

The funders had no role in study design, data collection and interpretation, or the decision to submit the work for publication.

Author contributions

David Hickey, Data curation, Software, Formal analysis, Validation, Investigation, Visualization, Methodology, Writing - original draft, Writing - review and editing; Andrej Vilfan, Conceptualization, Software, Formal analysis, Supervision, Validation, Visualization, Methodology, Writing - original draft, Writing - review and editing; Ramin Golestanian, Conceptualization, Supervision, Funding acquisition, Methodology, Project administration, Writing - review and editing

Author ORCIDs

David Hickey https://orcid.org/0000-0003-0149-712X
Andrej Vilfan https://orcid.org/0000-0001-8985-6072
Ramin Golestanian https://orcid.org/0000-0002-3149-4002

Decision letter and Author response

Decision letter https://doi.org/10.7554/eLife.66322.sa1
Author response https://doi.org/10.7554/eLife.66322.sa2

Additional files

Supplementary files

- Transparent reporting form

Data availability

All data generated or analysed during this study are included in the manuscript and supporting files. Source data files have been provided for Figures 3 and 4.

References

Adam G, Delbruck M. 1968. Reduction of dimensionality in biological diffusion processes. In: Rich A, Davidson N (Eds). *Structural Chemistry and Molecular Biology*. San Francisco: W.H. Freeman. p. 198–215.

Berbari NF, O'Connor AK, Haycraft CJ, Yoder BK. 2009. The primary cilium as a complex signaling center. *Current Biology* **19**:R526–R535. DOI: https://doi.org/10.1016/j.cub.2009.05.025, PMID: 19602418

Berg HC, Purcell EM. 1977. Physics of chemoreception. *Biophysical Journal* **20**:193–219. DOI: https://doi.org/10.1016/S0006-3495(77)85544-6, PMID: 911982

Bhandawat V, Reisert J, Yau KW. 2010. Signaling by olfactory receptor neurons near threshold. *PNAS* **107**:18682–18687. DOI: https://doi.org/10.1073/pnas.1004571107, PMID: 20930117

Bialek W, Setayeshgar S. 2005. Physical limits to biochemical signaling. *PNAS* **102**:10040–10045. DOI: https://doi.org/10.1073/pnas.0504321102, PMID: 16006514

Bloodgood RA. 2010. Sensory reception is an attribute of both primary cilia and motile cilia. *Journal of Cell Science* **123**:505–509. DOI: https://doi.org/10.1242/jcs.066308, PMID: 20144998

Brooks ER, Wallingford JB. 2014. Multiciliated cells. *Current Biology* **24**:R973–R982. DOI: https://doi.org/10.1016/j.cub.2014.08.047, PMID: 25291643

Bustamante-Marin XM, Ostrowski LE. 2017. Cilia and mucociliary clearance. *Cold Spring Harbor Perspectives in Biology* **9**:a028241. DOI: https://doi.org/10.1101/cshperspect.a028241, PMID: 27864314

Challis RC, Tian H, Wang J, He J, Jiang J, Chen X, Yin W, Connelly T, Ma L, Yu CR, Pluznick JL, Storm DR, Huang L, Zhao K, Ma M. 2015. An olfactory cilia pattern in the mammalian nose ensures high sensitivity to odors. *Current Biology* **25**:2503–2512. DOI: https://doi.org/10.1016/j.cub.2015.07.065, PMID: 26365258

Ding Y, Kanso E. 2015. Selective particle capture by asynchronously beating cilia. *Physics of Fluids* **27**:121902. DOI: https://doi.org/10.1063/1.4938558

Elgeti J, Gompper G. 2013. Emergence of metachronal waves in cilia arrays. *PNAS* **110**:4470–4475. DOI: https://doi.org/10.1073/pnas.1218869110, PMID: 23487771

Endres RG, Wingreen NS. 2009. Maximum likelihood and the single receptor. *Physical Review Letters* **103** 158101. DOI: https://doi.org/10.1103/PhysRevLett.103.158101, PMID: 19905667

Essner JJ, Vogan KJ, Wagner MK, Tabin CJ, Yost HJ, Brueckner M. 2002. Conserved function for embryonic nodal cilia. *Nature* **418**:37–38. DOI: https://doi.org/10.1038/418037a, PMID: 12097899

Faubel R, Westendorf C, Bodenschatz E, Eichele G. 2016. Cilia-based flow network in the brain ventricles. *Science* **353**:176–178. DOI: https://doi.org/10.1126/science.aae0450, PMID: 27387952

Ferreira RR, Vilfan A, Jülicher F, Supatto W, Vermot J. 2017. Physical limits of flow sensing in the left-right organizer. *eLife* **6**:e25078. DOI: https://doi.org/10.7554/eLife.25078, PMID: 28613157

Ferreira RR, Fukui H, Chow R, Vilfan A, Vermot J. 2019. The cilium as a force sensor-myth versus reality. *Journal of Cell Science* **132**:jcs213496. DOI: https://doi.org/10.1242/jcs.213496, PMID: 31363000

Friedlander SK. 1957. Mass and heat transfer to single spheres and cylinders at low Reynolds numbers. *AIChE Journal* **3**:43–48. DOI: https://doi.org/10.1002/aic.690030109

Frings S, Lindemann B. 1990. Single unit recording from olfactory cilia. *Biophysical Journal* **57**:1091–1094. DOI: https://doi.org/10.1016/S0006-3495(90)82627-8, PMID: 2160298

Gilpin W, Bull MS, Prakash M. 2020. The multiscale physics of cilia and flagella. *Nature Reviews Physics* **2**:74–88. DOI: https://doi.org/10.1038/s42254-019-0129-0

Golestanian R, Yeomans JM, Uchida N. 2011. Hydrodynamic synchronization at low Reynolds number. *Soft Matter* **7**:3074. DOI: https://doi.org/10.1039/c0sm01121e

Guasto JS, Rusconi R, Stocker R. 2012. Fluid mechanics of planktonic microorganisms. *Annual Review of Fluid Mechanics* **44**:373–400. DOI: https://doi.org/10.1146/annurev-fluid-120710-101156

Hilgendorf KI, Johnson CT, Jackson PK. 2016. The primary cilium as a cellular receiver: organizing ciliary GPCR signaling. *Current Opinion in Cell Biology* **39**:84–92. DOI: https://doi.org/10.1016/j.ceb.2016.02.008, PMID: 26926036

Kaupp UB, Solzin J, Hildebrand E, Brown JE, Helbig A, Hagen V, Beyermann M, Pampaloni F, Weyand I. 2003. The signal flow and motor response controling chemotaxis of sea urchin sperm. *Nature Cell Biology* **5**:109–117. DOI: https://doi.org/10.1038/ncb915, PMID: 12563276

Lai SK, Wang YY, Wirtz D, Hanes J. 2009. Micro- and macrorheology of mucus. *Advanced Drug Delivery Reviews* **61**:86–100. DOI: https://doi.org/10.1016/j.addr.2008.09.012, PMID: 19166889

Lee IT, Nakayama T, Wu CT, Goltsev Y, Jiang S, Gall PA, Liao CK, Shih LC, Schürch CM, McIlwain DR, Chu P, Borchard NA, Zarabanda D, Dholakia SS, Yang A, Kim D, Chen H, Kanie T, Lin CD, Tsai MH, et al. 2020. ACE2 localizes to the respiratory cilia and is not increased by ACE inhibitors or ARBs. *Nature Communications* **11**: 5453. DOI: https://doi.org/10.1038/s41467-020-19145-6, PMID: 33116139

Leinders-Zufall T, Lane AP, Puche AC, Ma W, Novotny MV, Shipley MT, Zufall F. 2000. Ultrasensitive pheromone detection by mammalian vomeronasal neurons. *Nature* **405**:792–796. DOI: https://doi.org/10.1038/35015572, PMID: 10866200

Lisicki M, Velho Rodrigues MF, Goldstein RE, Lauga E. 2019. Swimming eukaryotic microorganisms exhibit a universal speed distribution. *eLife* **8**:e44907. DOI: https://doi.org/10.7554/eLife.44907, PMID: 31310238

Malicki JJ, Johnson CA. 2017. The cilium: cellular antenna and central processing unit. *Trends in Cell Biology* **27**: 126–140. DOI: https://doi.org/10.1016/j.tcb.2016.08.002, PMID: 27634431

Marshall WF, Nonaka S. 2006. Cilia: tuning in to the cell's antenna. *Current Biology* **16**:R604–R614. DOI: https://doi.org/10.1016/j.cub.2006.07.012, PMID: 16890522

Masoud H, Stone HA. 2019. The reciprocal theorem in fluid dynamics and transport phenomena. *Journal of Fluid Mechanics* **879**:P1. DOI: https://doi.org/10.1017/jfm.2019.553

Matsunaga D, Hamilton JK, Meng F, Bukin N, Martin EL, Ogrin FY, Yeomans JM, Golestanian R. 2019. Controlling collective rotational patterns of magnetic rotors. *Nature Communications* **10**:4696. DOI: https://doi.org/10.1038/s41467-019-12665-w, PMID: 31619673

Meng F, Matsunaga D, Yeomans JM, Golestanian R. 2019. Magnetically-actuated artificial cilium: a simple theoretical model. *Soft Matter* **15**:3864–3871. DOI: https://doi.org/10.1039/C8SM02561D, PMID: 30916679

Nachury MV, Mick DU. 2019. Establishing and regulating the composition of cilia for signal transduction. *Nature Reviews Molecular Cell Biology* **20**:389–405. DOI: https://doi.org/10.1038/s41580-019-0116-4, PMID: 30948801

Nawroth JC, Guo H, Koch E, Heath-Heckman EAC, Hermanson JC, Ruby EG, Dabiri JO, Kanso E, McFall-Ngai M. 2017. Motile cilia create fluid-mechanical microhabitats for the active recruitment of the host microbiome. *PNAS* **114**:9510–9516. DOI: https://doi.org/10.1073/pnas.1706926114, PMID: 28835539

Paffuti G. 2018. Results for capacitances and forces in cylindrical systems. *arXiv*. https://arxiv.org/abs/1801.08202.

Purcell EM. 1977. Life at low Reynolds number. *American Journal of Physics* **45**:3–11. DOI: https://doi.org/10.1119/1.10903

Ramírez-Piscina L. 2018. Fixed-density boundary conditions in overdamped Langevin simulations of diffusion in channels. *Physical Review E* **98**:013302. DOI: https://doi.org/10.1103/PhysRevE.98.013302, PMID: 30110749

Reiten I, Uslu FE, Fore S, Pelgrims R, Ringers C, Diaz Verdugo C, Hoffman M, Lal P, Kawakami K, Pekkan K, Yaksi E, Jurisch-Yaksi N. 2017. Motile-cilia-mediated flow improves sensitivity and temporal resolution of olfactory computations. *Current Biology* **27**:166–174. DOI: https://doi.org/10.1016/j.cub.2016.11.036, PMID: 28041793

Shah AS, Ben-Shahar Y, Moninger TO, Kline JN, Welsh MJ. 2009. Motile cilia of human airway epithelia are chemosensory. *Science* **325**:1131–1134. DOI: https://doi.org/10.1126/science.1173869, PMID: 19628819

Short MB, Solari CA, Ganguly S, Powers TR, Kessler JO, Goldstein RE. 2006. Flows driven by flagella of multicellular organisms enhance long-range molecular transport. *PNAS* **103**:8315–8319. DOI: https://doi.org/10.1073/pnas.0600566103, PMID: 16707579

Smith DJ, Blake JR, Gaffney EA. 2008. Fluid mechanics of nodal flow due to embryonic primary cilia. *Journal of the Royal Society Interface* **5**:567–573. DOI: https://doi.org/10.1098/rsif.2007.1306

Snow C. 1954. *Circular of the Bureau of Standards No. 544: Formulas for Computing Capacitance and Inductance*. US Government Printing Office .

Spasic M, Jacobs CR. 2017. Primary cilia: cell and molecular mechanosensors directing whole tissue function. *Seminars in Cell & Developmental Biology* **71**:42–52. DOI: https://doi.org/10.1016/j.semcdb.2017.08.036, PMID: 28843978

Spassky N, Meunier A. 2017. The development and functions of multiciliated epithelia. *Nature Reviews Molecular Cell Biology* **18**:423–436. DOI: https://doi.org/10.1038/nrm.2017.21, PMID: 28400610

Stone HA. 1989. Heat/mass transfer from surface films to shear flows at arbitrary Peclet numbers. *Physics of Fluids A: Fluid Dynamics* **1**:1112–1122. DOI: https://doi.org/10.1063/1.857335

Tanaka Y, Okada Y, Hirokawa N. 2005. FGF-induced vesicular release of sonic hedgehog and retinoic acid in leftward nodal flow is critical for left-right determination. *Nature* **435**:172–177. DOI: https://doi.org/10.1038/nature03494, PMID: 15889083

Tocino A, Senosiain MJ. 2015. Two-step Milstein schemes for stochastic differential equations. *Numerical Algorithms* **69**:643–665. DOI: https://doi.org/10.1007/s11075-014-9918-9

Tripathi A, Bhattacharya A, Balazs AC. 2013. Size selectivity in artificial cilia-particle interactions: mimicking the behavior of suspension feeders. *Langmuir* **29**:4616–4621. DOI: https://doi.org/10.1021/la400318f, PMID: 23496689

Uchida N, Golestanian R. 2010. Synchronization and collective dynamics in a carpet of microfluidic rotors. *Physical Review Letters* **104**:178103. DOI: https://doi.org/10.1103/PhysRevLett.104.178103, PMID: 20482146

Vilfan M, Potočnik A, Kavčič B, Osterman N, Poberaj I, Vilfan A, Babič D. 2010. Self-assembled artificial cilia. *PNAS* **107**:1844–1847. DOI: https://doi.org/10.1073/pnas.0906819106, PMID: 19934055

Vilfan A. 2012. Generic flow profiles induced by a beating cilium. *The European Physical Journal E* **35**:72. DOI: https://doi.org/10.1140/epje/i2012-12072-3

Williams CL, McIntyre JC, Norris SR, Jenkins PM, Zhang L, Pei Q, Verhey K, Martens JR. 2014. Direct evidence for BBSome-associated intraflagellar transport reveals distinct properties of native mammalian cilia. *Nature Communications* **5**:5813. DOI: https://doi.org/10.1038/ncomms6813, PMID: 25504142

Zhang J, Pacifico R, Cawley D, Feinstein P, Bozza T. 2013. Ultrasensitive detection of amines by a trace amine-associated receptor. *Journal of Neuroscience* **33**:3228–3239. DOI: https://doi.org/10.1523/JNEUROSCI.4299-12.2013, PMID: 23407976

Zimmermann KW. 1898. Beiträge zur Kenntniss einiger Drüsen und Epithelien. *Archiv für Mikroskopische Anatomie* **52**:552–706. DOI: https://doi.org/10.1007/BF02975837

Appendix 1

Electrostatic analogy for the capture rate

In the following we explain the analogy between the capture rate of a diffusive particles and the self-capacitance in electrostatics (***Berg and Purcell, 1977***). The diffusion equation reads

$$D\nabla^2 c = 0, \tag{24}$$

where D is the diffusion constant and c the particle concentration. The boundary conditions are $c = c_0$ at infinity and $c = 0$ at the particle surface. The diffusion equation is equivalent to the Laplace equation for source-free electrostatics, in which the electrostatic potential ϕ obeys

$$\nabla^2 \phi = 0. \tag{25}$$

If the surface of the body in the electrostatic case has a potential of $-V_0$, the boundary conditions are equivalent as well. The rate constant is determined by the integral of the current density $\mathbf{J}$ over the surface, which follows from Fick's law:

$$k = -\frac{1}{c_0}\int \mathrm{d}\mathbf{S}\cdot\mathbf{J} = \frac{1}{c_0}\int \mathrm{d}\mathbf{S}\cdot(D\nabla c). \tag{26}$$

In the electrostatic version of the problem, the equivalent expression for self-capacitance is

$$C = \frac{q}{V_0} = \frac{1}{V_0}\int \mathrm{d}\mathbf{S}\cdot(\varepsilon_0\nabla\phi), \tag{27}$$

where $-q$ is the charge on the body. By analogy, the rate constant can be expressed as:

$$k = \frac{D}{\varepsilon_0}C. \tag{28}$$

The electrostatic equivalence allows us to translate the calculation of the capture rates to a capacitance problem with a greater number of available solutions in the literature.

Appendix 2

Capture rate of a cylinder in flow

In the following, we calculate the capture rate of a cylinder, moving transversely through the flow at a high Péclet number. While defining the problem, one encounters the Stokes paradox, namely that the lateral mobility of an infinite cylinder at zero Reynolds number diverges. We avoid the problem by calculating the capture rate for a prescribed force density on the cylinder, which gives a well-defined near-field flow. Later, we can use the well established resistive force theory to estimate the force density at a given local velocity. A further simplification we make is to swap the boundary conditions (***Masoud and Stone, 2019***), such that the cylinder emits particles, leading to a concentration c_0 at its surface and 0 in the incoming fluid. We describe the flow around the cylinder with radius a with the following stream function in cylindrical coordinates

$$\psi = -\frac{af}{8\pi\eta}\left(\frac{r}{a} - \frac{a}{r} - \frac{2r}{a}\ln\left[\frac{r}{a}\right]\right)\sin(\theta), \tag{29}$$

where f is the force per unit length. The unperturbed fluid is coming from the $\theta = 0$ direction (***Appendix 2—figure 1***). The fluid velocity is determined as the curl of the stream function, e.g.:

$$v_\theta = \frac{\partial\psi}{\partial r}. \tag{30}$$

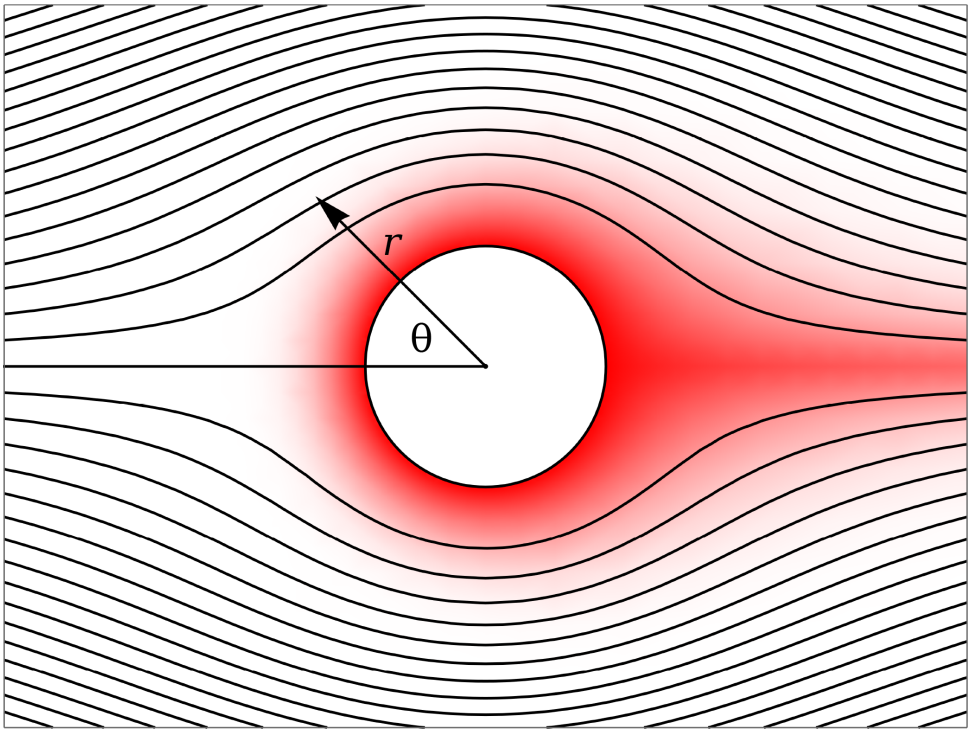

Appendix 2—figure 1. Streamlines (lines with a constant value of the stream function ψ) of the flow around a cylinder (black) and the concentration c of emitted particles (red).

In the limit of a high Péclet number, the emitted particles stay in a thin boundary layer around the cylinder before escaping at $\theta = \pi$. We can therefore use the following approximation that only takes into account the leading order contribution to the stream function

$$\psi = \frac{2af}{8\pi\eta}\left(\frac{r-a}{a}\right)^2\sin(\theta). \tag{31}$$

In the following, we derive a partial differential equation for the particle flux $\Phi(\theta)$ across a radial half-plane starting with radius r at the angle θ, defined as

$$\Phi(r,\theta)=\int_r^\infty \mathrm{d}r'\, v_\theta(r')c(r')=\int_{\psi(r)}^\infty \mathrm{d}\psi\, c(\psi). \tag{32}$$

At a high Péclet number, advection dominates over diffusion, which only needs to be considered in the direction perpendicular to the stream lines, but not along. Due to flux conservation, the variation of Φ with the angle θ is caused by the diffusive transverse flux, driven by the concentration gradient

$$\left.\frac{\partial\Phi}{\partial\theta}\right|_\psi=-rD\frac{\partial c}{\partial r}. \tag{33}$$

We finally arrive at the PDE for the particle flux

$$\frac{\partial\Phi}{\partial\theta}=-rD\frac{\partial\psi}{\partial r}\frac{\partial^2\Phi}{\partial\psi^2}=A\sqrt{\psi}\sqrt{\sin\theta}\cdot\frac{\partial^2\Phi}{\partial\psi^2} \tag{34}$$

with the constant $A=8D\sqrt{\pi\eta/af}$. The boundary conditions are $\Phi=0$ for $\theta=0$, reflecting zero flux at the inflow, while the fixed concentration at the surface, $c_0=1$, implies $\partial\Phi/\partial\psi|_{\psi=0}=-1$. A transformation of variables $t=\int\mathrm{d}\theta A\sqrt{\sin\theta}$ with $t(0)=0$ and $t(\pi)=\sqrt{8/\pi}\Gamma[3/4]^2$ leads to

$$\frac{\partial\Phi}{\partial t}=\sqrt{\psi}\frac{\partial^2\Phi}{\partial\psi^2}, \tag{35}$$

which has the solution

$$\Phi(t,\psi)=t^{2/3}\bar{\Phi}\left(\frac{\psi}{t^{2/3}}\right) \tag{36}$$

with

$$\bar{\Phi}(x)=-\frac{x\Gamma\left[-\frac{2}{3},\frac{4}{9}x^{3/2}\right]}{\Gamma\left[-\frac{2}{3}\right]}\quad\text{and}\quad\bar{\Phi}(0)=\left(\frac{3}{2}\right)^{4/3}\left(\Gamma\left[\frac{1}{3}\right]\right)^{-1}. \tag{37}$$

An example of a particle concentration c resulting from this solution is shown in ***Appendix 2—figure 1***. The emission rate (equivalent to capture rate) per unit length is given by twice the particle flux (for two sides of the cylinder):

$$\frac{dk}{dz}=2\Phi(t(\pi),0)=3\left(\frac{6}{\pi}\right)^{1/3}\frac{\Gamma(3/4)^{4/3}}{\Gamma(1/3)}D\,\mathrm{Pe}_f^{1/3}=1.822D\,\mathrm{Pe}_f^{1/3}\quad\text{with}\quad\mathrm{Pe}_f=\left(\frac{2af}{\pi\eta D}\right)^{1/3} \tag{38}$$

A previous calculation that used a similar approach, but solved the PDE with an approximate function, rather than the exact solution derived here, gave the prefactor 1.63 when converted to our units (***Friedlander, 1957***).

Finally, we can use the resistive force theory to estimate the force density per unit length as $f=C_N v\approx 1.3\pi\eta v$ and arrive at ***Equation (10)*** in the main text. The prefactor depends on the width-to-length ratio of the object and we used a value that gives a good result for typical ciliary dimensions (***Vilfan, 2012***).

,

3.4 Chapter summary

- Chemoreception is an integral part of life, found in all kinds of organisms in all kind of roles, both internal to organisms and externally.
- In eukaryotes, a lot of these chemoreceptors are found on cilia. Our work sought to understand some of the reasons why this might be the case.
- Our analysis found that all chemoreceptors found on cilia benefit from the geometry of a cilium, which acts to increase their diffusion limit. When a bulk flow is introduced, this geometry-related improvement is even more pronounced.
- Motility further increases the chemosensitivity of cilium-bound chemoreceptors. Motile cilia in cilium carpets experience a further increase in per-cilium chemosensitivity over isolated motile cilia, as long as the Péclet number of the beating cilia is high enough.

Ciliary synchronisation 4

Emergent properties, where local rules give rise to widespread global order, are everywhere in biology. The flocking behaviour of birds or sheep can be explained by rules so simple that they can be expressed in a single sentence [7, 110] but the resulting motion can look almost impossibly well-coordinated; anyone who has ever seen a thousand-strong flock of starlings knows how complex flocking behaviour can look. But emergent properties are not limited to the scales of entire herds: one very relevant example that can happen even within individual organisms is when motile cilia synchronise with their neighbours to produce globally ordered beating patterns.

[7]: Vicsek *et al.* (1995), *Novel Type of Phase Transition in a System of Self-Driven Particles*
[110]: King *et al.* (2012), *Selfish-herd behaviour of sheep under threat*

At sufficient density, motile cilia can coordinate their beating with one another, giving rise to collective motion. Sometimes this just means all cilia beating in unison, as in the fallopian tube, where motile cilia beat to move embryos and gametes [11]. However, one especially interesting coordinated beating mode arises when each cilium beats slightly ahead of its neighbours on one side, but slightly behind its neighbours on the other side. This slight phase difference gives the illusion of a travelling wave, known as a metachronal wave (see Fig. 4.1 for an illustration). Metachronal waves are not purely a cilium-related phenomenon: the motion of a millipede's legs [111], collective behaviour of worms [112], or the "Mexican waves" seen in the stands at sports events are all examples of metachronal waves, though they are less relevant to the work described in this chapter. Ciliary metachronal waves are found in the human trachea, where the waves beat metachronally in order to pump mucus [9, 113]. *Paramecium* [13] and *Volvox* [114] use metachronally synchronised cilium beating to move fluid around for swimming and feeding. Even shrimp and worms, as well as artificial swimmers like the fantastically named "krillbot", have used

[11]: Lyons *et al.* (2006), *The reproductive significance of human Fallopian tube cilia*

[111]: Garcia *et al.* (2020), *Fundamental understanding of millipede morphology and locomotion dynamics*
[112]: Peshkov *et al.* (2022), *Synchronized oscillations in swarms of nematode Turbatrix aceti*

[9]: Yaghi *et al.* (2016), *Airway Epithelial Cell Cilia and Obstructive Lung Disease*
[113]: Chateau *et al.* (2019), *Why antiplectic metachronal cilia waves are optimal to transport bronchial mucus*

[13]: Funfak *et al.* (2015), *Paramecium swimming and ciliary beating patterns: a study on four RNA interference mutations*
[114]: Brumley *et al.* (2012), *Hydrodynamic Synchronization and Metachronal Waves on the Surface of the Colonial Alga Volvox carteri*

metachronally synchronised appendages to swim [115, 116]. The list of locations where metachronal waves can be found is long, but also surprisingly varied: *Paramecium* is a single multiciliated cell, but *Volvox* is a multicellular colony, and the human trachea is a multicellular part of a larger organism.

[115]: Ford *et al.* (2021), *On the role of phase lag in multi-appendage metachronal swimming of euphausiids*
[116]: Byron *et al.* (2021), *Metachronal Motion across Scales: Current Challenges and Future Directions*

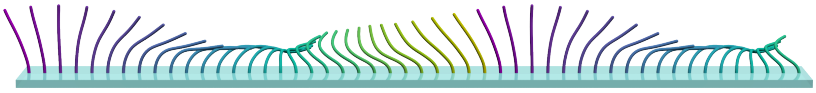

Figure 4.1: A metachronal wave in one dimension. Each cilium has a slight phase difference from both of its neighbours. The phase of each cilium is indicated by its colour.

These waves can be categorised into symplectic (meaning that the apparent motion of the wave is in the same direction as the fluid pumping), antiplectic (meaning that the wave direction is opposite the direction of pumping), or if the pumping direction is orthogonal to the wave direction, diaplectic and laeoplectic [117].

[117]: Zhang *et al.* (2022), *Metachronal patterns by magnetically-programmable artificial cilia surfaces for low Reynolds number fluid transport and mixing*

In cilia, this metachronal coordination is adaptationally advantageous because it increases pumping and swimming speed and energy efficiency [14, 15]. One can intuitively see why a metachronal wave might move more fluid than synchronous beating: if a cilium beats in phase with its neighbour, it will experience much lower hydrodynamic drag, and therefore exert lower force on the fluid, hence moving less fluid overall; metachronal waves ensure that no cilium is ever beating exactly in-phase with its neighbour. Under certain circumstances, this gain in efficiency may be much higher for certain types of metachronal waves than others: in the case of pumping of mucus in the human airway, antiplectic waves are more efficient than their symplectic equivalents [113]. Metachronal waves also reduce energy-wasting collisions between cilia [52], meaning more fluid can be moved with less energy.

[14]: Osterman *et al.* (2011), *Finding the ciliary beating pattern with optimal efficiency*
[15]: Elgeti *et al.* (2013), *Emergence of metachronal waves in cilia arrays*

[113]: Chateau *et al.* (2019), *Why antiplectic metachronal cilia waves are optimal to transport bronchial mucus*

[52]: Ringers *et al.* (2023), *Novel analytical tools reveal that local synchronization of cilia coincides with tissue-scale metachronal waves in zebrafish multiciliated epithelia*

The mechanisms underpinning the emergence of metachronal waves are varied and not completely understood. Cilia on the same cell are connected through coupling between their

basal bodies, and it has been shown that in certain cases, basal coupling between cilia on the same cell plays an important role in synchronisation, as hydrodynamically isolated cilia are still capable of synchronising [118–120]. However, in *Volvox*, the cilia are spread across multiple cells in different organisms (which means that basal coupling can be ruled out as a relevant mechanism), and they are still able to synchronise, which suggests that hydrodynamics plays the dominant role under certain circumstances [121]. Steric effects, i.e. direct collisions between cilia, have also been found to play a role [122]. Although small numbers of bacterial flagella can synchronise due to the rocking of the bacterium they are all attached to [123], this probably doesn't bear much relevance to metachronal waves in cilia, where there are often hundreds or thousands of cilia beating together.

[118]: Wan *et al.* (2016), *Coordinated beating of algal flagella is mediated by basal coupling*

[119]: Quaranta *et al.* (2015), *Hydrodynamics Versus Intracellular Coupling in the Synchronization of Eukaryotic Flagella*

[120]: Liu *et al.* (2018), *Transitions in synchronization states of model cilia through basal-connection coupling*

[121]: Goldstein *et al.* (2009), *Noise and Synchronization in Pairs of Beating Eukaryotic Flagella*

[122]: Chelakkot *et al.* (2021), *Synchronized oscillations, traveling waves, and jammed clusters induced by steric interactions in active filament arrays*

[123]: Geyer *et al.* (2013), *Cell-body rocking is a dominant mechanism for flagellar synchronization in a swimming alga*

4.1 Models of synchronisation

The literature contains many models that seek to explain ciliary synchronisation. Though some models account for things like body-rocking [123] or basal coupling [120, 124, 125], in this section we will focus on models of hydrodynamic coupling, as they are more relevant to our work.

One of the simplest models of synchronising oscillators is the Kuramoto model, wherein the oscillators have some (not necessarily identical) intrinsic frequencies ω_i and are globally coupled to one another by a function that depends upon their phase difference [126]:

$$\dot{\phi}_i = \omega_i + \frac{\epsilon}{N} \sum_{j=1}^{N} H(\phi_i - \phi_j). \tag{4.1}$$

This model is very simple, and in the large-N limit, the dynamics can be solved exactly. However, most models of hydrodynamic synchronisation are slightly more complicated than this globally-coupled Kuramoto model, because hydrodynamic interactions are dependent on distance, and

[120]: Liu *et al.* (2018), *Transitions in synchronization states of model cilia through basal-connection coupling*

[124]: Guo *et al.* (2021), *Intracellular coupling modulates biflagellar synchrony*

[125]: Klindt *et al.* (2017), *In-phase and antiphase flagellar synchronization by waveform compliance and basal coupling*

[126]: Pikovskij *et al.* (2007), *Synchronization: a universal concept in nonlinear sciences*

the coupling strength is not always purely a function of the phase difference.

Some approaches model the cilia as long filaments with active driving forces [51, 127–130]. Others consider a very detailed treatment of the cilium: Solovev *et al.* [131], for example, have developed an approach to simulation of cilia that works for arbitrary cilium shapes and trajectories, though this results in sufficient complexity that a lot of variables must be precomputed in order to be able to solve the equations of cilium motion in reasonable time.

The approach favoured by many, including us, is to model the cilium as a sphere on a fixed trajectory but with a variable speed [78, 132–139]. There are a number of advantages to this: the hydrodynamic force on a sphere in the presence of a boundary can be computed using the Rotne-Prager mobility tensor (Eqs. (2.9–2.8)) in an efficient manner, and by making simple adjustments to the trajectory, it is possible to recreate the power/recovery stroke behaviour seen in most biological motile cilia.

No matter the approach taken, it must be remembered that the Stokes flow is time-reversible, but synchronisation is by definition an irreversible process. The model must therefore find some way to break this symmetry. Possibilities that have seen success in the literature include additional degrees of freedom per cilium (which can automatically be achieved by modelling the cilia as flexible filaments that can bend in various directions), asymmetric spatial arrangements of cilia [132], driving forces or trajectories that break the right symmetries [137, 140], or (for example) nonlinear driving mechanisms that change the driving direction once a certain position is reached [15].

Most models of synchronisation make two additional simplifications: firstly, it is common for near-field hydrodynamic interactions to be neglected [133, 134]. This is an attractive simulation in many cases because it massively simplifies the computational effort required, as the far-field terms that

[51]: Gueron *et al.* (1999), *Energetic considerations of ciliary beating and the advantage of metachronal coordination*

[127]: Man *et al.* (2020), *Multisynchrony in Active Microfilaments*

[128]: Goldstein *et al.* (2016), *Elastohydrodynamic synchronization of adjacent beating flagella*

[129]: Guirao *et al.* (2007), *Spontaneous Creation of Macroscopic Flow and Metachronal Waves in an Array of Cilia*

[130]: Kim *et al.* (2006), *Pumping Fluids with Periodically Beating Grafted Elastic Filaments*

[131]: Solovev *et al.* (2021), *Lagrangian mechanics of active systems*

[78]: Uchida *et al.* (2011), *Generic Conditions for Hydrodynamic Synchronization*

[132]: Vilfan *et al.* (2006), *Hydrodynamic flow patterns and synchronization of beating cilia*

[133]: Meng *et al.* (2021), *Conditions for metachronal coordination in arrays of model cilia*

[134]: Niedermayer *et al.* (2008), *Synchronization, phase locking, and metachronal wave formation in ciliary chains*

[135]: Uchida *et al.* (2012), *Hydrodynamic synchronization between objects with cyclic rigid trajectories*

[136]: Nasouri *et al.* (2016), *Hydrodynamic interactions of cilia on a spherical body*

[137]: Kanale *et al.* (2022), *Spontaneous phase coordination and fluid pumping in model ciliary carpets*

[138]: Wollin *et al.* (2011), *Metachronal waves in a chain of rowers with hydrodynamic interactions*

[139]: Uchida *et al.* (2010), *Synchronization and collective dynamics in a carpet of microfluidic rotors*

[140]: Fruchart *et al.* (2021), *Non-reciprocal phase transitions*

[15]: Elgeti *et al.* (2013), *Emergence of metachronal waves in cilia arrays*

remain in the limit of large intercilium separation are much simpler to compute than the near-field terms, and can even be treated analytically [134]. Secondly, many modelling approaches have required the system to have periodic boundary conditions [133, 134, 138, 139], as without these, the cilia near the edges have a lower number of neighbours, which can affect their beating frequency and lead to the breaking up of order [134, 141, 142].

[141]: Kavre *et al.* (2015), *Hydrodynamic synchronization of autonomously oscillating optically trapped particles*

[142]: Hamilton *et al.* (2017), *The chimera state in colloidal phase oscillators with hydrodynamic interaction*

However, these simplifications are often biologically implausible. For example, intercilium spacing in many biological systems is much less than the cilium length [143, 144], which is at odds with assumption of a far-field limit. While there do exist periodic one-dimensional arrays of cilia, such as in starfish larvae [145] or the oral cilia of *Stentor* [146], they are far from the norm. We will later show that both of these simplifications are inadequate when considering nonreciprocal hydrodynamic coupling of cilia.

[143]: Bouhouche *et al.* (2022), *Paramecium, a Model to Study Ciliary Beating and Ciliogenesis: Insights From Cutting-Edge Approaches*

[144]: Sleigh *et al.* (1988), *The Propulsion of Mucus by Cilia*

[145]: Strathmann (1971), *The feeding behavior of planktotrophic echinoderm larvae: Mechanisms, regulation, and rates of suspension-feeding*

[146]: Wan *et al.* (2020), *Reorganization of complex ciliary flows around regenerating Stentor coeruleus*

4.2 Nonreciprocity in active systems

In active systems, the influence exerted by one body on another need not be reciprocal [140]. For example, under certain circumstances, the motion of an enzyme can be affected by a chemical gradient, which is itself affected by another enzyme. In this way, one enzyme exerts an influence on another, but the reverse is not true [147]. Similar effects can be observed in flocking behaviour [148], systems of neurons [149], artificial active particles [150], and countless others.

[140]: Fruchart *et al.* (2021), *Non-reciprocal phase transitions*

[147]: Agudo-Canalejo *et al.* (2019), *Active Phase Separation in Mixtures of Chemically Interacting Particles*

[148]: Nagy *et al.* (2010), *Hierarchical group dynamics in pigeon flocks*

[149]: Montbrió *et al.* (2018), *Kuramoto Model for Excitation-Inhibition-Based Oscillations*

[150]: Lavergne *et al.* (2019), *Group formation and cohesion of active particles with visual perception–dependent motility*

This nonreciprocal coupling can also happen in systems of hydrodynamic interactions. The Lorentz reciprocal theorem can be expressed in its integral form as

$$\iint_S \mathbf{u} \cdot (\sigma' \cdot \hat{\mathbf{n}})\, \mathrm{d}S = \iint_S \mathbf{u}' \cdot (\sigma \cdot \hat{\mathbf{n}})\, \mathrm{d}S, \tag{4.2}$$

where S is the surface of a body, σ is the hydrodynamic stress on the body's surface, and $\hat{\mathbf{n}}$ is the normal to the

body's surface [69]. This is an incredibly important result in hydrodynamics, as it means that, depending on the velocities of the two bodies, the force on each body can have the same or different signs. This differs from Newton's third law, under which the forces would always have the opposite sign, and is a consequence of hydrodynamic interactions being dissipative rather than conservative. This opens up a lot of possibilities for nonreciprocal coupling in hydrodynamics, where if two identical hydrodynamically coupled particles have very different velocities, they can experience differing forces (and vice versa: two bodies with very different active driving forces can induce differing velocities), which can be an extremely potent effect in inducing synchronisation. Some models of hydrodynamic rotor synchronisation have already included nonreciprocal hydrodynamic coupling [139] (though it should be stressed that these rotors are quite unlike cilia).

[69]: Masoud *et al.* (2019), *The reciprocal theorem in fluid dynamics and transport phenomena*

[139]: Uchida *et al.* (2010), *Synchronization and collective dynamics in a carpet of microfluidic rotors*

In the context of cilia, this means that one cilium can influence its neighbour more than vice versa. Factors such as the driving force that the cilium exerts and the nonuniformity of internal and external drag coefficients over the cilium trajectory can all make the cilium more susceptible to being perturbed by a neighbour in certain parts of its trajectory than in others. This combined with the varying velocity of the cilium relative to its neighbours can give rise to a very asymmetric interaction strength. Indeed, other work has found that asymmetric coupling can be relevant for ciliary synchronisation, such as Niedermayer *et al.* [134]. However, the model used by Niedermayer *et al.* [134] did not consider near-field hydrodynamics, rather solving in the far-field limit, and found that cilia with the same intrinsic beating frequency could only synchronise to a state with identical phases, i.e. they did not find the phase lag characteristic of metachronal waves. Our model of ciliary synchronisation, explained in the following section, relies heavily on nonreciprocal hydrodynamic coupling to synchronise.

[134]: Niedermayer *et al.* (2008), *Synchronization, phase locking, and metachronal wave formation in ciliary chains*

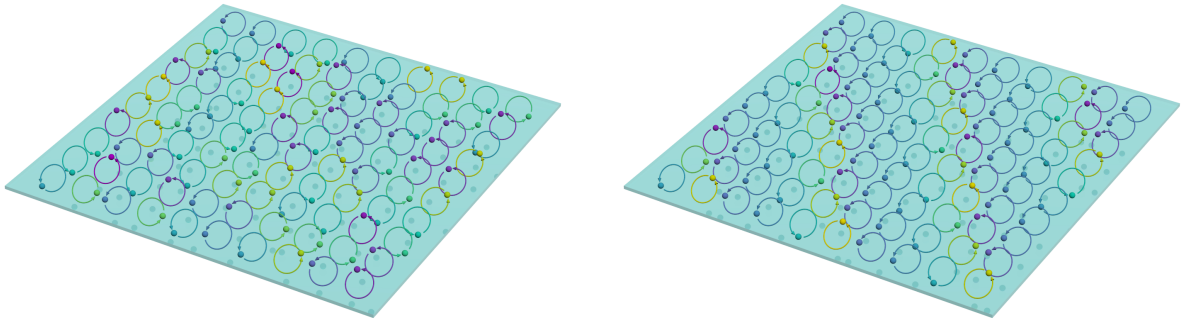

(a) Unsynchronised state

(b) Metachronally synchronised state

Figure 4.2: Potential states of the simulation, showing the phase and position of each cilium. Each cilium has an identical intrinsic frequency. Each cilium is confined to a tilted circular trajectory, where the tilt ensures that the cilia have a power and recovery stroke despite the model's simplicity. Each cilium has a driving force and friction coefficient that is a function of its phase. Hydrodynamic interactions between cilia cause some cilia to move around their trajectory slightly faster than others, eventually leading from an unsynchronised initial state (as in (a)) to a stable synchronised state (as in (b)).

4.3 Our work

In this work, we developed a simple model of ciliary synchronisation. The cilium is represented as a spherical bead on a titled circular trajectory, which despite its simplicity, still has separate power and recovery strokes. The tilting of the trajectory breaks time-reversal symmetry, meaning that the beat avoids the problem posed by scallop theorem, and is therefore able to generate a net fluid flow.

The cilium has a phase-dependent driving force $\mathbf{F}^{\mathrm{dr}}(\phi)$ and internal friction coefficient $\Gamma(\phi)$, which were tuned to give sensible cilium motion. We considered a system of many such model cilia on various lattices, where the cilia could interact with one another hydrodynamically. The governing equation for each cilium may be written as

$$0 = \mathbf{F}^{\mathrm{dr}}(\phi_i) + \mathbf{F}^{\mathrm{c}}(\phi_i) - \Gamma(\phi_i)\mathbf{v}_i - \sum_j \mathbf{\Gamma}_{ij}\mathbf{v}_j, \qquad (4.3)$$

where $\mathbf{F}^{\mathrm{c}}$ are the forces that constrain the cilium to its circular

trajectory, and are by definition always perpendicular to the trajectory, so that they don't change its speed along the trajectory. Γ_{ij} is the friction tensor, which gives the force response at cilium i due to a velocity at j – essentially, the opposite of the mobility tensor. Each cilium moves around its trajectory with some intrinsic frequency, but the motion of other cilia perturbs the fluid which in turn perturbs the cilia, causing cilia to move along their trajectory with varying speeds.

The entire system was solved numerically to find the time-evolution of the system, starting from a random initial state. We found that under normal circumstances with an open boundary, the system of cilia can quickly synchronise to a deterministic metachronal state, with a relaxation time that scales linearly with the system time – a good improvement over many other models of this same phenomenon. However, when near-field hydrodynamic effects are suppressed, the synchronisation time increases dramatically, and this linear dependence is lost; this is because of the nonreciprocal coupling that is now suppressed. Additionally, the final synchronised state can now consist of multiple wavevectors, which depends entirely on the random initial configuration. When introducing periodic boundary conditions, we found that the nonreciprocity was now counterproductive, as patches of disorder could now spread in the same way as patches of order, without being extinguished.

These results have huge implications for the importance of nonreciprocal coupling in ciliary synchronisation. Near-field effects, whereby a combination of cilium position, driving force, and hydrodynamic and internal condition make the coupling nonreciprocal, mean that a cilium can entrain its neighbour but not vice versa. This allows the order to spread extremely quickly through the system, starting from one edge and spreading linearly, and means that order is robust even at open boundaries. Without these nonreciprocal near-field effects, ciliary synchronisation takes an order of magnitude longer. The final state would no longer be deterministic, and

since antiplectic and symplectic waves pump with different speeds and efficiencies, this could have an impact on the pumping or swimming efficiency.

Secondly, these results show that hydrodynamics is sufficient for swift synchronisation in at least some circumstances, so basal coupling is not an absolute requirement for synchronisation. In real cilia, the intercilium distances can be much lower than what we have simulated, so it is possible that the hydrodynamic interactions, especially the near-field interactions, are even more relevant and can explain the extremely rapid synchronisation seen in ciliates.

This work shows that hydrodynamic interactions, in particular nonreciprocal near-field interactions, are sufficient to induce and maintain stable order in finite systems. This represents a step forward in our understanding of the emergence of metachronal waves, as most models have hitherto been unable to support stable order in finite systems, and have been forced to rely on periodic boundary conditions in order to prevent boundary effects from disrupting the order of the system. The ability to produce stable metachronal waves in finite systems is highly desirable, as open boundaries are common in experimental systems, whereas there are only a few cases where one can find unbroken lines of cilia that approximate periodic boundaries.

Nonreciprocal interactions give rise to fast cilium synchronisation in finite systems

David J Hickey[a], **Ramin Golestanian**[a,b,1], **and Andrej Vilfan**[a,c,1]

[a]Max Planck Institute for Dynamics and Self-Organization (MPI-DS), 37077 Göttingen, Germany; [b]Rudolf Peierls Centre for Theoretical Physics, University of Oxford, Oxford OX1 3PU, United Kingdom; [c]Jožef Stefan Institute, 1000 Ljubljana, Slovenia

This manuscript was compiled on May 16, 2023

Motile cilia beat in an asymmetric fashion in order to propel the surrounding fluid. When many cilia are located on a surface, their beating can synchronise such that their phases form metachronal waves. Here, we computationally study a model where each cilium is represented as a spherical particle, moving along a tilted trajectory with a position-dependent active driving force and a position-dependent internal drag coefficient. The model thus takes into account all the essential broken symmetries of the ciliary beat. We show that taking into account the near-field hydrodynamic interactions, the effective coupling between cilia can become nonreciprocal: the phase of a cilium is more strongly affected by an adjacent cilium on one side than by a cilium at the same distance in the opposite direction. As a result, synchronisation starts from a seed at the edge of a group of cilia and propagates rapidly across the system, leading to a synchronisation time that scales proportionally to the linear dimension of the system. We show that a ciliary carpet is characterised by three different velocities: the velocity of fluid transport, the phase velocity of metachronal waves and the group velocity of order propagation. Unlike in systems with reciprocal coupling, boundary effects are not detrimental for synchronisation, but rather enable the formation of the initial seed.

Cilia | Low Reynolds number hydrodynamics | Metachronal waves | Nonreciprocal interactions

Motile cilia are hairlike organelles which can move under their own power in order to fulfil roles such as fluid pumping or mixing (1). They are nigh-ubiquitous in biological systems, being found on most eukaryotic cells (2) including in the nervous system (3), the respiratory system (4), and the olfactory system (5). This makes them central to many open questions in biology, such as the precise mechanism behind the emergence of left-right differentiation during embryonic development (6). While the fascinating fluid dynamical questions involved in the dynamics of cilia and their biological function have been already highlighted by the pioneers of twentieth century fluid dynamics, such as Ludwig Prandtl (7) and G. I. Taylor (8), the subject of the collective properties of hydrodynamically active organelles at low Reynolds number continues to be an active field of research, particularly as a key component of the field of active matter (9).

When many motile cilia are located on a surface at sufficient density, their beating can synchronise with a phase lag between neighbouring cilia. The resulting phase waves are called metachronal waves. It has been shown that metachronal coordination can lead to a high energetic efficiency of swimming or fluid transport (10, 11), and that metachronal waves may reduce collisions between cilia, further raising pumping speed (12). Moreover, the coordination has been shown to be beneficial for the efficiency of the chemosensory function of motile cilia (13). Metachronal waves are found in many different organisms and systems. For example, *Paramecium* uses metachronally coordinated cilia to swim (14), as well as to feed (14). Indeed, *Paramecium*'s swimming efficiency is close to the maximum possible efficiency for an organism with cilia of that length (10). Metachronal waves are found in other systems, such as the multicellular colony *Volvox* (15) or cilia in the respiratory tract (4) where their pumping efficiency is important for moving mucus (16). Metachronal coordination also appears in animals (e.g., krill) at larger length scales with very different coordination mechanisms (17).

Metachronal waves can be classified according to the direction of the wave propagation, depending on how the phase velocity of the wave compares to the direction of fluid transport. When these two directions are parallel, the metachronal wave is said to be symplectic. If they are antiparallel, the wave is called antiplectic (18). Other wave directions are classified as dexioplectic or leoplectic.

The fact that a pair of hydrodynamically interacting cilia or flagella can synchronise their cycles, even when belonging to two separate organisms (19), suggests that hydrodynamic coupling alone can be sufficient to explain the emergence of metachronal waves. Nevertheless, some studies also point to the additional role of intracellular linkages (20–22). In fact, the metachronal waves in *Paramecium* can preserve synchrony across the wall of a micropipette that isolates them hydrodynamically (23).

A fundamental problem in understanding synchronisation via hydrodynamic interactions is the reversible nature of the

Significance Statement

Motile cilia are hairlike organelles that, at sufficient density, can synchronise hydrodynamically with their neighbours to form a metachronal wave. We use a minimal model of a ciliary carpet that accounts for near- field hydrodynamic coupling between cilia and show that the interaction between cilia can be nonreciprocal. We propose to characterize the collective dynamics of an array of cilia by three different velocities and their directions: the direction of fluid transport, the direction of metachronal waves (phase velocity) and the direction of order propagation (group velocity). The latter determines the time scale of synchronization. Near-field nonreciprocal interactions can therefore give rise to rapid emergence of metachronal waves.

R.G. and A.V. designed research; D.J.H. performed research; D.J.H. and A.V. analyzed data; D.J.H., R.G. and A.V. wrote the paper.

The authors declare no competing interests.

[1]To whom correspondence should be addressed. E-mail: ramin.golestanian@ds.mpg.de, andrej.vilfan@ds.mpg.de

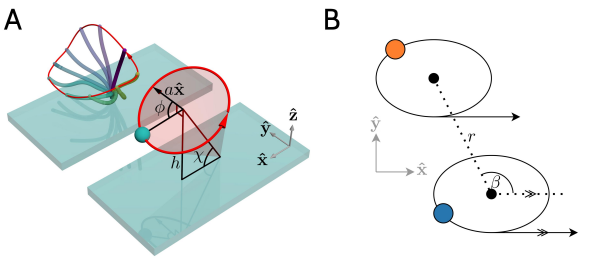

Fig. 1. Illustration of the model, showing the parameters used. (A) A realistic cilium motion with the trajectory shown in red. The power stroke (solid blue colour) gives way to a slower recovery stroke along the no-slip surface of the substrate, resulting in net fluid flow in the direction of the power stroke over a cycle. Also shown is one of our model cilia that approximates the realistic motion, with the trajectory shown in red, and relevant quantities indicated. The circular trajectory retains the essential features of a power stroke far from the substrate and a recovery stroke much closer. (B) Definition of β and the intercilium distance r. The arrows represent the direction of the power stroke of the cilium, occurring at the highest point above the surface. Feathering on lines indicates that they are parallel, so that β is the angle between the power stroke and the displacement vector connecting the lattice points of two cilia.

Stokesian hydrodynamics, i.e. the fact that the fluid flow exactly reverses its direction upon the reversal of actuating forces, whereas the tendency of a system to reach an ordered state is by definition irreversible (9). Theoretical models therefore have to take into account higher order effects that break the respective symmetries. These can include a second degree of freedom per cilium (24–29), the asymmetric spatial arrangement of cilia (30), a trajectory or driving force with sufficiently broken symmetries (28, 31–37), or a non-linear driving mechanism that, for instance, switches the direction of force when a switch point is reached (11, 38–41).

When discussing the role of symmetries for ciliary synchronisation, one has to keep in mind that reciprocity manifests itself differently for conservative or dissipative interactions. For conservative forces, Newton's third law states that opposite forces are exerted on both interacting bodies. For hydrodynamic interactions, which are dissipative in their nature, the Lorentz reciprocal theorem (42) implies that the force on one body, caused by the motion of a second one with a given velocity, is identical to the force on the second body when the first body moves with the same velocity. Hydrodynamic interactions therefore act on both bodies with the same sign. The interplay of both interaction types is one possibility to facilitate ciliary synchronisation (26). In active systems, nonreciprocal interactions can arise where the effect of the interaction on body A differs from that on body B, both in magnitude and direction (33, 43–49). For example, in the Vicsek model, particles or animals can be affected by other particles in front of them in a different way from those behind them. The orientation of hydrodynamically coupled rotors is a prime example of nonreciprocal coupling that leads to a rich phenomenology, including turbulent behaviour via defect proliferation and annihilation (31).

A major open question is related to the scaling with the system size and the role of boundaries of the ciliated region. Recent theoretical work shows that the time needed to reach synchronisation scales quadratically with the number of cilia (50). In principle, the metachronal wave vector of the final state is not uniquely determined. However, the basins of attraction of different solutions can greatly differ in size, leading to a strong preference for one state (50). Boundaries are often detrimental for synchronisation, because the cilia at the edge have a smaller number of nearest neighbours, which can affect their characteristic frequency, as demonstrated in a small 1D row of artificial oscillators (51). Boundary effects in a finite system can even lead to the emergence of a chimera state in which the oscillators split up into a coherent and an incoherent population (52). The vast majority of theoretical and computational studies focus on systems with periodic boundary conditions as a representation of generic, infinite systems (11, 26, 31, 32, 34, 38, 50, 53, 54). In nature, periodic circular 1D chains of cilia exist, for instance the oral cilia of *Stentor* (55) or in starfish larvae (56). However, for topological reasons 2D arrangements of cilia need open boundaries or topological defects, as it is impossible to have a polar field on the topology of a sphere without discontinuities.

In this paper, we show that the near-field effects between hydrodynamically coupled cilia can lead to an effective nonreciprocal interaction, where cilium A can affect the phase of cilium B more strongly than vice versa. As a result of this nonreciprocity, the metachronal order propagates through the array of cilia with a group velocity, which is not directly related to the velocity of the fluid transport or the phase velocity of metachronal waves. In a finite group of cilia, order then emerges at a boundary and propagates across the group in a time that scales linearly with the system dimension, an order of magnitude faster than an equivalent system without near-field hydrodynamics. We suggest that nonreciprocal coupling is key to understanding the fast emergence of synchronisation in large ciliary carpets. The dynamics of the tissue are then characterised by three independent velocities: the velocity of fluid transport above the surface, the phase velocity of metachronal waves, and the group velocity with which the order propagates.

Results. Cilia are long and thin, and beat with a time-irreversible whip-like stroke (1). Because of the complexity of the ciliary stroke, its description quickly leads to an intractable number of parameters. We therefore take a simplified approach common to many theoretical models (e.g., 30, 34, 35) and replace the cilium with a small sphere, pushed along a fixed trajectory by a position-dependent active force. The position of the sphere represents the tip position of a cilium and the active driving force represents the activity of dynein motors of the cilium's axoneme. We thus consider a sphere of radius b moving on a fixed circular trajectory of radius a, with its centre a distance h above a surface. The sphere is driven by an internal driving force $F^{\mathrm{dr}}(\phi)$ and has an internal friction coefficient $\Gamma(\phi)$, both of which act in the tangential direction of the trajectory. The tilt of the trajectory is controlled by an angle χ such that when $\chi = \pi/2$, the trajectory lies in a plane parallel to the substrate beneath the cilium, shown in Fig. 1A.

This choice to model the cilia as single spheres on fixed tilted circular trajectories means that we neglect much of the fluid flow driven by the cilium closer to the surface, while preserving the irreversibility of the cilium beat – essential given the inherent irreversibility of synchronisation. This approximation also replicates the pumping ability of the cilium: when the cilium is closer to the no-slip surface, it produces less fluid flow, and when it is further away it produces more. Over a cycle, the cilium moves a positive net amount of fluid in the direction of its 'power stroke'. At distances from the cilium

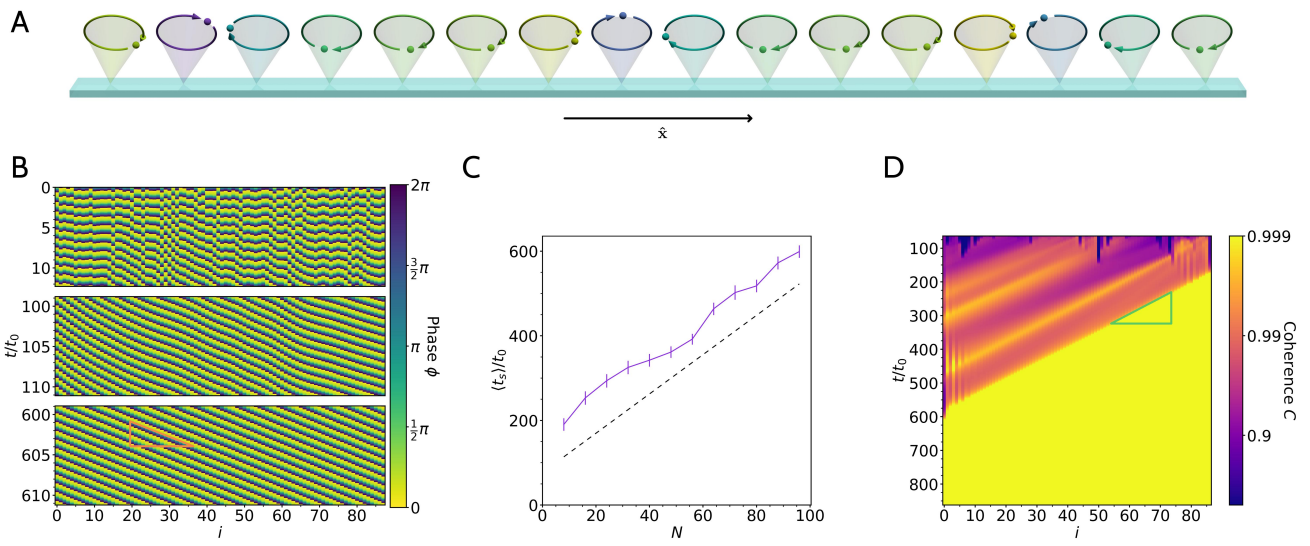

Fig. 2. Synchronisation in a one-dimensional row of cilia. (A) A snapshot from the simulation. The colours indicate the phases. (B) A kymograph showing the metachronal waves in the system at different times. The simulation starts with random phases, but patches of order quickly assert themselves and give rise to waves that are initially uneven but eventually become completely uniform. The waves travel with the phase velocity v_{ph} (orange triangle) in the direction of fluid transport, and are hence symplectic waves. (C) The mean synchronisation time $\langle t_{\mathrm{s}} \rangle$ vs. the number of cilia N. The mean is calculated by simulating many systems at each size with different random initial phase configurations, and measuring how long it takes to synchronise using a metric based on standard deviation of cilium frequencies. The figure shows that the synchronisation time scales approximately linearly in the system size. Error bars are standard error of the mean, based on ≥ 92 simulations. (D) A kymograph showing the coherence between adjacent pairs of cilia. On this graph each value of i on the abscissa corresponds to the coherence between cilium i and $i+1$. Once an ordered patch forms on the right edge it spreads across the row with the group velocity v_{g} (green triangle) in the negative x direction. The fact that the synchronisation time is mainly limited by the propagation across the system explains the linear size-dependence in panel (C).

that are several times greater than h, this approximation gives almost identical fluid flow to a more detailed treatment of the cilium (57). In the following, we orient the pumping direction in the positive x-direction.

To study synchronisation and the emergence of metachronal waves, we now consider many cilia arranged on a two-dimensional surface. Each point $\mathbf{r}_i = (x_i, y_i, 0)$ represents the position on the substrate directly below the centre of a cilium's trajectory. A pair of cilia (i and j) is characterised by the angle β_{ij}, which is the angle between the working stroke of cilium i (along the x-axis, Fig. 1) and the line pointing from $\mathbf{r}_i$ to $\mathbf{r}_j$. These quantities are illustrated in Fig. 1B.

The position $\mathbf{R}_i$ of the sphere representing cilium i is parameterised as a function of its phase ϕ_i following the notation used by Meng et al. (34):

$$\mathbf{R}_i(\phi_i) = \mathbf{r}_i + \begin{pmatrix} a\cos\phi_i \\ a\sin\phi_i\sin\chi \\ h - a\sin\phi_i\cos\chi \end{pmatrix} . \qquad [1]$$

To replicate the beating cycle of a cilium, which consists of a fast working stroke followed by a slower sweeping recovery stroke, we introduce a position-dependent force and an internal drag coefficient, which together determine the force-velocity relationship of the active driving force $F^{\mathrm{dr}}(\phi_i) - \Gamma(\phi_i)v$. Both can be expanded in a Fourier series as:

$$F^{\mathrm{dr}}(\phi_i) = F_0^{\mathrm{dr}}\left[1 + \sum_n^{\infty} A_n\cos(n\phi_i) + B_n\sin(n\phi_i)\right], \qquad [2]$$

$$\Gamma(\phi_i) = \Gamma_0\left[1 + \sum_n^{\infty} C_n\cos(n\phi_i) + D_n\sin(n\phi_i)\right]. \qquad [3]$$

In the following, we only account for terms where $n \leq 2$. This simplification is justified, as the first harmonic is known to be essential for synchronisation (and indeed is well-placed to replicate the cilium's beating pattern of a fast power stroke and a slower recovery stroke) but the second harmonic is much more effective at driving the onset of synchronisation and ensuring a more stable synchronised state (28, 35, 36).

Due to the linearity of the Stokes flow, the hydrodynamic force $\mathbf{F}_i^{\mathrm{h}}$ on a particle is a linear function of the particle's own velocity and the velocities of all other particles it hydrodynamically interacts with. It can be expressed with a generalised friction tensor in the presence of a no-slip boundary, $\mathbf{\Gamma}(\phi_i, \phi_j)$, as $\mathbf{F}_i^{\mathrm{h}} = -\sum_j \mathbf{\Gamma}(\phi_i, \phi_j)\cdot\mathbf{v}_j$. Along with the driving force, which is always tangential to the trajectory, and a perpendicular constraint force $\mathbf{F}^{\mathrm{cstr}}$ which keeps the particle on the trajectory, the force balance on cilium i states:

$$\mathbf{F}^{\mathrm{dr}}(\phi_i) + \mathbf{F}^{\mathrm{cstr}} - \Gamma(\phi_i)\mathbf{v}_i - \sum_j \mathbf{\Gamma}(\phi_i, \phi_j)\cdot\mathbf{v}_j = 0\,. \qquad [4]$$

By considering only its tangential component (i.e., multiplying the above equation with the tangent vector $\mathbf{t}(\phi_i)$), we obtain the equations of motion for each cilium:

$$F^{\mathrm{dr}}(\phi_i) = \Gamma(\phi_t)v_i + \sum_j \mathbf{t}(\phi_i)\cdot\mathbf{\Gamma}(\phi_i, \phi_j)\cdot\mathbf{t}(\phi_j)v_j. \qquad [5]$$

Here, the velocities are related to the phase derivatives as $\mathbf{v}_i = (\partial\mathbf{R}_i/\partial\phi_i)\dot{\phi}_i$. By solving these equations numerically, we can simulate the evolution of the cilium phases ϕ_i over time. In the following, we non-dimensionalise all time units using the time period of an isolated cilium t_0, which can

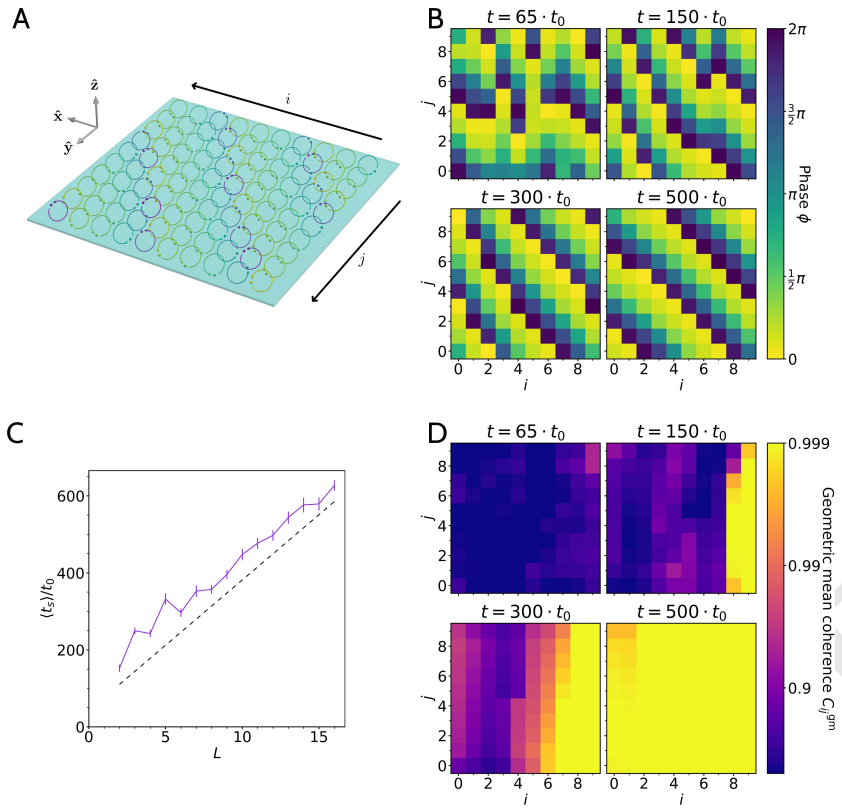

Fig. 3. Synchronisation in a two-dimensional square lattice. (A) A schematic of the simulation of the square $L \times L$ lattice at a synchronised state for the specific case L = 10. The colour of each model cilium indicates its phase, making the order clearly visible. See also Movie S1 for an animated representation. (B) A series of snapshots showing the phases of the cilia in the square lattice, for the specific case of L = 10 (see movie S2 for a complete time series). (C) The mean synchronisation time $\langle t_s \rangle$ vs. the linear dimension of the system L. The mean is calculated by simulating many systems at each size with different random initial phase configurations, and measuring how long it takes for the standard deviation of the cilium frequencies in each system to drop below a certain threshold value. The synchronisation time scales approximately linearly in L. Error bars are standard error of the mean, based on $\geq$ 31 samples. (D) The geometric mean of the coherence between each cilium and all of its neighbours for a specific simulation with L = 10. The order emerges on the right side and spreads across the system in negative x direction, leading to the observed linear dependence between the synchronisation time and the length L.

be determined as $t_0 = \int_0^{2\pi} \left(\dot{\phi}_i\right)^{-1} \mathrm{d}\phi_i$ using Eq. (5) without interacting neighbours.

Symmetries. Before discussing the numerical solutions, it is instructive to consider the symmetries of the system and their effect on synchronisation and formation of metachronal waves. Our model contains the following symmetries:

(i) Swapping. Because all cilia are intrinsically equal, the equations of motion stay the same when exchanging two cilia ($\phi_1 \leftrightarrow \phi_2$) and re-arranging them such that $\beta \leftrightarrow \beta + \pi$.

(ii) Mirror symmetry. The trajectories of cilia (but not their drag and driving force) are symmetric with respect to $y \leftrightarrow -y$. The equations of motion therefore contain the symmetry $\beta \leftrightarrow \pi - \beta$, $\phi \leftrightarrow \pi - \phi$, $F_0^{\mathrm{dr}} \leftrightarrow -F_0^{\mathrm{dr}}$ with the adjustment of the coefficients defined in Eqs. (2, 3): $(A_n, C_n) \leftrightarrow (-1)^n (A_n, C_n)$ and $(B_n, D_n) \leftrightarrow -(-1)^n (B_n, D_n)$.

(iii) Time reversal. Due to the time-reversibility of the Stokes equation, the equations of motion also remain invariant under the transformation $F_0^{\mathrm{dr}} \leftrightarrow -F_0^{\mathrm{dr}}$ and $t \to -t$. Because of the time-reversal, a solution that is stable in the original system becomes unstable in the transformed system.

(iv) Without near-field hydrodynamics: axial reflection. If the distance between cilia is sufficient that the near-field hydrodynamic interactions can be neglected ($r \gg h$), the mobility tensor ($\mathbf{M} = \mathbf{\Gamma}^{-1}$) for two particles at a distance $\Delta\mathbf{x} = (\Delta x, \Delta y, 0)$, where $\Delta x = x_j - x_i$ and $\Delta y = y_j - y_i$, can be approximated as (30)

$$\mathbf{M}(\mathbf{x}_i, \mathbf{x}_j) = \frac{3}{2\pi\eta} \cdot \frac{z_i z_j}{|\Delta\mathbf{x}|^5} \begin{pmatrix} (\Delta x)^2 & \Delta x \Delta y & 0 \\ \Delta y \Delta x & (\Delta y)^2 & 0 \\ 0 & 0 & 0 \end{pmatrix}. \quad [6]$$

At the same time, the variation of the horizontal positions (x, y) of a cilium during a cycle can be neglected such that the motion along the trajectory only affects the vertical distances z_i and z_j. The far-field mobility tensor is therefore symmetric with respect to $\beta \leftrightarrow \beta + \pi$.

The above symmetry properties have bold consequences for the synchronisation. Consider a row of cilia arranged along the x axis, in the direction of pumping. In such a row, the angles β can only have values 0 and π. Without any of the coefficients that change sign under (ii), i.e., $A_1, C_1, B_2, \ldots$, the motion is symmetric upon the combination of transformations (i), (ii) and (iii). Because the combined transformation contains time reversal which renders a stable solution unstable, no stable states are possible under these assumptions. The notion is consistent with the result in (30) if two cilia are arranged along the pumping direction. The existence of a stable solution requires at least one of the terms $A_1, C_1, B_2, D_2, A_3, C_3$, etc. to be nonzero. The same argument also holds for a row of cilia arranged along the y axis (perpendicular to the pumping direction) when the symmetries (ii) and (iii) are employed (see related arguments in (9, 58)).

Without near-field effects (NFEs) in the hydrodynamic coupling, the symmetry property (iv) immediately implies the equivalence of metachronal waves with wave vectors $\mathbf{k}$ and

$-\mathbf{k}$, as seen in (34). We therefore expect such systems to show the emergence of multiple long-lived domains with different metachronal wave vectors.

Near-field effects in combination with (for instance) the rotational motion of cilia can break the spatial symmetry, and lead to antisymmetric coupling terms that synchronise the cilia into a state with a non-zero phase difference (9, 30, 58–60). Here, we point out that the interactions are not only asymmetric with respect to the phase difference, but also nonreciprocal with respect to their strength. In a given configuration, the response of cilium i to the phase of cilium j can differ from the response of cilium j to cilium i both in the magnitude and in the phase dependence. This nonreciprocity has profound implications for the emergence of metachronal waves.

Synchronisation in one dimension. We first consider a one-dimensional row of cilia with uniform spacing d and open boundaries such that cilium i is located at position $\mathbf{r}_i = (id, 0, 0)$ (see Fig. 2A). This means that $\beta_{ij} = 0$ or π for every cilium pair $i \neq j$. We used numerical simulations to see how order emerged in the system when the cilia were initialised with random initial phases.

Figure 1B shows the phases of the cilia on a kymograph. The initially random phases quickly coalesce into mostly-ordered waves, which slowly become more ordered over time until the waves are completely uniform. The average time t_s to reach a synchronised state scales approximately linearly with the system length (Fig. 1C). We consider the state as synchronised when the standard deviation of all cilium frequencies falls below a fixed threshold. The linear dependence can be understood by looking at the signal coherence between adjacent pairs of cilia (Fig. 1D). The signal coherence is a measure of the degree of linear dependence between two signals, given as a function of the frequency, with values between 0 and 1. For two signals in the time domain $x(t)$ and $x'(t)$, the coherence is calculated as

$$C_{xx'}(f) = \frac{|\tilde{x}^*(f)\tilde{x}'(f)|^2}{\tilde{x}(f)\tilde{x}'(f)}, \qquad [7]$$

where $\tilde{x}(f)$ and $\tilde{x}'(f)$ indicate the Fourier transforms of $x(t)$ and $x'(t)$, respectively. For every pair of cilia, we calculate the coherence between $\cos(\phi_i(t))$ and $\cos(\phi_j(t))$ at the frequency with the strongest cross-spectral density between the two signals (i.e., the frequency f that maximises the numerator in Eq. (7)).

Random patches of order sometimes emerge and travel against the pumping direction (in this case the pumping direction is rightwards), as the nonreciprocal nature of the hydrodynamic interactions causes the order to expand on one side and be extinguished by the disorder on its other side. However, when an ordered patch occurs close enough to the rightmost edge, there is no disorder to its right to extinguish it, so it spreads throughout the system. This explains why we see that the synchronisation time has a roughly affine relationship with the system length.

Synchronisation in two dimensions. The vast majority of motile cilia are found in two-dimensional bundles on multiciliated cells, where the cells themselves are sparsely distributed (61). Hence, we consider a two-dimensional square lattice with side length L and lattice constant d (so that the total number of cilia is $N = L \times L$). We enforce open boundaries, and run a very similar simulation to the one described in the previous section. Figure 3A shows the lattice, with the cilium trajectories marked according to their phase, rendering the structure of the metachronal wave clearly visible. Figure 3B shows how the order of the cilia emerges over time: initially there is no correlation between phases, but over time some order emerges, which eventually solidifies into well-ordered metachronal waves.

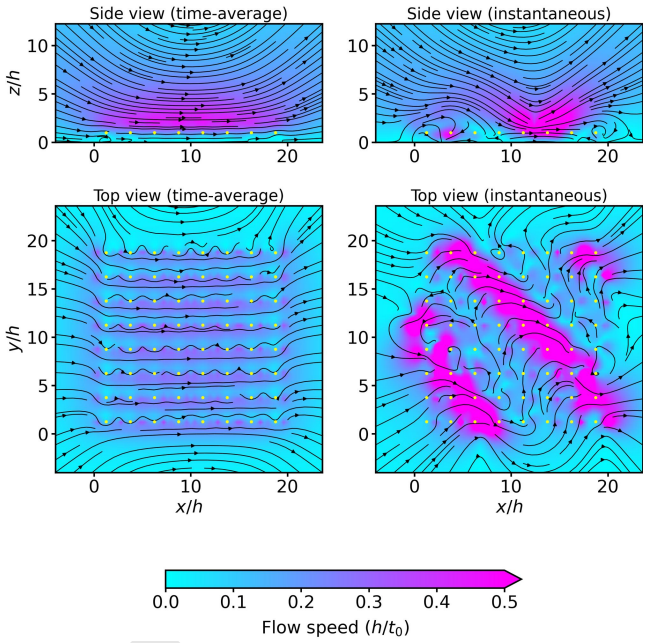

Fig. 4. Time-averaged and instantaneous flow in a system of 8×8 cilia after reaching a synchronised metachronal state. The background colour indicates the flow speed in units of h/t_0 and the yellow dots represent the centre of cilium orbits. The side view corresponds to a vertical cross-section through the middle of the array of cilia (x/h = 10) and the top view to a slice at $z = h$. The structure of the metachronal wave is clearly visible in the instantaneous flow fields.

Figure 3C shows that the synchronisation time scales approximately linearly with the linear dimension of the system L (i.e. $\langle t_s \rangle \sim L \sim \sqrt{N}$), just as in the one-dimensional case. This is explained by Fig. 3D, which illustrates the coherence of each cilium with its neighbours. For each cilium i the value is given by the geometric mean of coherence values with all directly adjacent (not including diagonally adjacent) cilia:

$$C_i^{\mathrm{gm}} = \left[\prod_{j \in \{\mathrm{n.n.}\}} C\left(\{\phi_i\}, \{\phi_j\}\right) \right]^{(1/N_{\mathrm{n.n.}})}, \qquad [8]$$

where $C(\{\phi\}, \{\phi'\})$ is the coherence, defined over two time series of phases. The resulting graph explains the linearity: the order emerges along one edge and gradually spreads across the entire lattice. Since the limiting factor to synchronisation is the time taken for the order to spread through the length of the system, this time depends on the linear dimension as L/v_g.

The flow field induced by a carpet of cilia that has reached the synchronised state with steady metachronal waves is shown in Figure 4. The time-averaged flows show a region of largely homogeneous flow above the carpet where the fluid is pumped

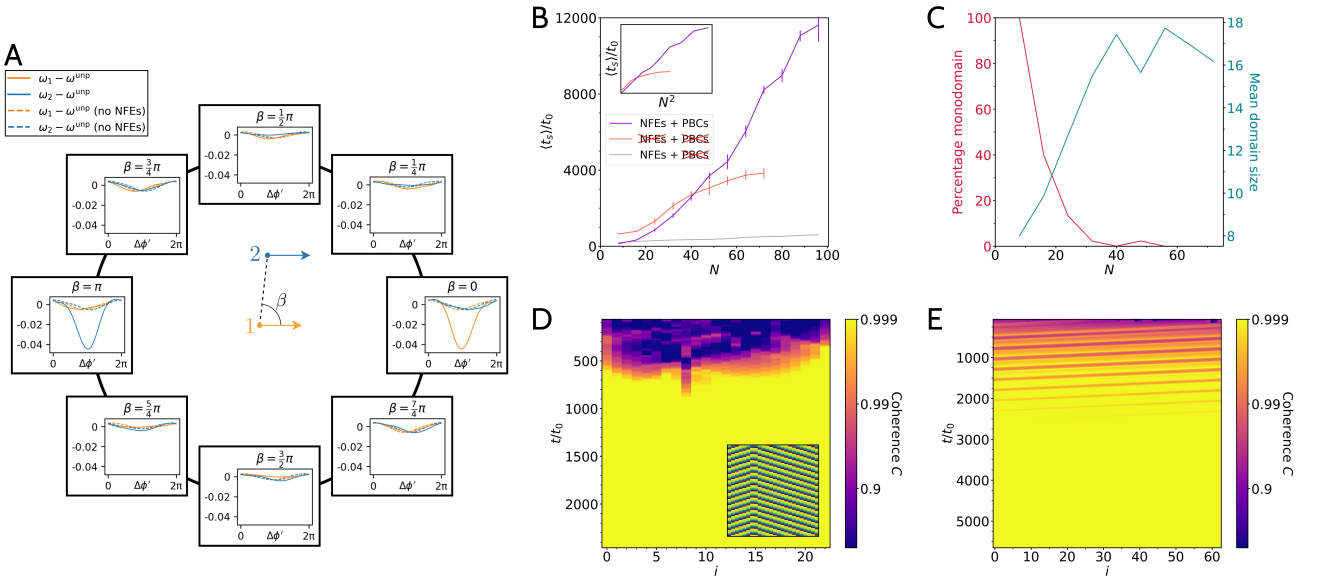

Fig. 5. The role of nonreciprocal hydrodynamic interactions and near-field effects in synchronisation. (A) The effective angular frequencies ω_1 and ω_2 of two interacting cilia (in dimensionless units) as a function of the adjusted difference $\Delta\phi'$. The cilia are positioned at a fixed distance ($r = 2.5h$) in different directions β. When the cilia are arranged in the x-direction ($\beta = 0, \pi$) there is a stark difference between ω_1 and ω_2, showing that the interaction is highly nonreciprocal. The nonreciprocity is much weaker when the cilia are arranged y direction ($\beta = \pi/2$), and the nonreciprocity vanishes entirely when near-field hydrodynamic effects are disabled (dashed lines). (B) The mean time to reach the synchronised state $\langle t_s \rangle$ in a 1D row of N cilia with near-field effects disabled (orange) and with periodic boundary conditions (magenta). The synchronisation time is dramatically longer in both of these cases than in the one-dimensional open boundary case (grey line, data from Fig. 2C). The inset indicates that the scaling of these synchronisation times is close to $\langle t_s \rangle \sim N^2$. With open boundaries and no near-field effects, however, the synchronisation time reaches a plateau when the final state consists of multiple domains with different wave vectors. Error bars are standard error of the mean, based on 9 samples for the periodic boundary case and ≥ 44 for the case without near-field effects. (C) With near-field effects disabled, the final state typically contains multiple domains with different wave vectors. The red line (left scale) shows the percentage of simulation runs that end in a monodomain state and cyan line (right scale) the average domain size as a function of the system size N. (D) Kymograph showing the coherence between adjacent cilia with near-field effects disabled, with the phase kymograph as an inset. Unlike in the case of nonreciprocal coupling (see Fig. 2D), defects between domains with different wave vectors remain after synchronisation (the example shows one defect). (E) Coherence kymograph of the system with near-field effects and periodic boundary conditions. Defects between coherent regions move with the group velocity, but do not get extinguished at the boundaries, again resulting in a long synchronisation time.

in the positive x-direction, the direction of the cilium power stroke. The instantaneous flows, on the other hand, show a periodic structure that follows the movement of metachronal wavefronts.

Although we used a square lattice as an example, the ability of cilia to synchronise is robust against the lattice type and the shape of the arrangement. Similar dynamics is obtained on a hexagonal lattice, as well as on an array with boundaries in the shape of an octagon (Fig. S1).

Role of nonreciprocity and near-field effects. Our model shows strong nonreciprocity in the hydrodynamic interactions between cilia. This can be seen by calculating the shift of beating frequencies caused by hydrodynamic interactions, relative to the unperturbed cilium ($\omega - \omega^{\mathrm{unp}}$). The frequency shifts, averaged over one cycle, are shown in Fig. 5A as a function of the phase difference $\Delta\phi'$ and the relative position of the two cilia, represented by the angle β. Nonreciprocity manifests itself as shifts in the beating frequency of the two interacting cilia. The two cilia can experience dramatically different frequency shifts, with very different magnitudes and functional forms. The degree of this nonreciprocity is highly anisotropic, being much greater in the pumping direction than perpendicular to it (Fig. 5A).

As shown in the section Symmetries, nonreciprocal interactions are not possible when the hydrodynamic interactions are treated in the far-field approximation. In the far-field, the interaction with a cilium at position β has to be identical to the interaction with a cilium at the opposite position $\beta + \pi$. We demonstrate this by disabling the near-field effects and replacing the off-diagonal elements of the mobility matrix with the approximation given by Eq. (6). The resulting frequency shifts (dashed lines in Fig. 5A) become reciprocal, as they fulfil $\omega_1(\Delta\phi') = \omega_2(-\Delta\phi')$.

To investigate the role of near-field effects in the formation of metachronal waves, we simulated the dynamics of a row of cilia (analogous to the results in Fig. 2) with only far-field interactions. The resulting synchronisation times are significantly longer (orange line in Fig. 5B) than with near-field effects (grey line). In small systems, the scaling with size becomes quadratic (inset in Fig. 5B), whereas we showed them to be linear in the presence of nonreciprocal coupling. However, in larger systems, the synchronisation times saturate, as the final state no longer consists of a uniform metachronal wave. Rather, the system evolves into a long-lived state consisting of multiple domains with distinct wave vectors. An example with two domains, separated by one defect, is shown in Fig. 5D. The mean domain size and the likelihood that the system evolves into a mono-domain metachronal wave are shown in Fig. 5C.

To understand the role of open boundaries in our system, we compared the results to the same system with periodic boundary conditions. Periodic boundary conditions are typical in other hydrodynamic models of ciliary or flagellar synchro-

nisation (11, 12, 26, 31, 32, 34, 38, 50, 53, 54, 62) when there are many cilia present (though with rare exceptions (e.g. 41)), as they ensure that no cilia exist at an open boundary which could cause order to break down – indeed, when such models are subjected to open boundary conditions, they often find only intermittent synchronisation (38). Our results show that introducing periodic boundaries, while preserving the nonreciprocal coupling, strongly increases the synchronisation timescale, which again scales quadratically with the system size (Fig. 5B). The reason why periodic boundary conditions become deleterious to synchronisation can be seen in the coherence kymograph in Fig. 5E. It shows a number of defects, each propagating with the group velocity v_g, that travel periodically across the system, so the system only slowly reaches a coherent state with a single metachronal wave.

Discussion. In our study we used a strongly simplified model of a cilium. We replaced the cilium with a single particle moving along a tilted circular trajectory. The tilted trajectory breaks the most important symmetry of the cilium, namely that between the power stroke, when the distance to the surface is larger, and the recovery stroke, when the distance is smaller. This asymmetry is at the core of fluid transport, which does not rely on metachronal coordination, although the metachronal waves can improve the energetic efficiency of cilia (10, 11). At the same time, the driving force and the internal friction are modulated such that they reproduce a power stroke that is faster than the recovery stroke and also reproduce the fore-aft asymmetry that is present in cilia. The modulation of both parameters represents both the cyclic activity of dynein motors and the variations in the shape of the cilium, which is stretched during the power stroke and bent during the recovery stroke. Unlike theoretical models with fewer broken symmetries (35), our model allows the emergence of metachronal waves that are not directly linked to the fluid transport.

The numerical solution of the model equations takes into account not only the the far-field hydrodynamics, as in (34), but also the near-field effects that become relevant when the size of a cilium becomes comparable to the distance between adjacent cilia. Near-field effects are definitely important in most ciliary systems that show metachronal coordination. For example, in *Paramecium* the intercilium distance is in the micrometre range, which is several times less than the cilium length (63). In respiratory epithelia the distances are even shorter at fractions of a micrometre (64). On the other hand, in *Volvox* colonies, pairs of flagella (one on each cell) are spaced at a distance comparable to their length and still form metachronal waves (15). The intermediate densities we chose here allow us to take a generic approach that does not depend on fine details of the trajectory, while qualitatively capturing the near-field interactions. We therefore expect that the magnitude of near-field effects, as well as interactions in general in our study, is underestimated, and that the underlying principles can account for significantly faster synchronisation in natural cilia.

Our main finding is that the near-field effects can make the coupling nonreciprocal. The nonreciprocity goes beyond the asymmetry discussed in (50), which implies that two cilia tend to synchronise with a phase difference that depends on their relative orientation. The nonreciprocal magnitude of the interaction means that a cilium tends to follow a neighbour on one side and to entrain the neighbour in the opposite direction. An easy-to-understand mechanism that contributes to nonreciprocity is that the periodically modulated driving force and internal drag make the cilium more susceptible to hydrodynamic interactions in certain parts of the trajectory, which are in turn closer to some neighbours than the others. The nonreciprocal coupling introduces a third direction in the plane, after the direction of fluid transport and the direction of the preferred metachronal wave, which dictates the propagation of order. We therefore refer to it as a group velocity. However, we note that unlike in classical waves in linear media with energy conservation, the group velocity is not related to the phase velocity in a straightforward way (e.g. through a dispersion relation).

Nonreciprocal coupling has two major effects on the formation of metachronal waves. First, it produces robust waves in finite systems with open boundaries. While open boundaries are the standard in real systems, they are detrimental in many models of synchronisation, and also in experimental model systems (51). The majority of theoretical works on cilia synchronisation therefore only investigate systems with periodic boundary conditions. In the presence of nonreciprocal coupling, the situation reverses and boundaries help seed the order which then rapidly spreads across the system. With nonreciprocal interactions, it is actually the periodic boundary conditions that significantly slow down the convergence to an ordered metachronal wave. The second major effect of nonreciprocal coupling is that the timescale of metachronal wave formation scales linearly with linear dimension of the system. This holds in both one and two dimensions, due to the linear spreading of order through the system from a boundary. At each system size tested, as long as near-field effects are not suppressed, the system always converges to the same metachronal wavevector regardless of the random initial conditions, meaning that the basin of attraction is effectively as large as the phase space of the system. We have demonstrated that suppressing the near-field hydrodynamic interactions (and therefore the nonreciprocal coupling) gives rise to unfavourable synchronisation time scaling and unpredictable final states with long-living defects remaining.

Our model does not account for non-hydrodynamic interactions which have been shown to be relevant for cilium synchronisation, such as steric effects (65) and basal coupling (22). Because it has been shown that hydrodynamic interactions alone are sufficient to achieve synchronisation (66), one can consider these other effects as intercilium coupling to fine-tune the interactions rather than being an absolute requirement. In particular, basal coupling could provide a means to align metachronal waves in order to optimise efficiency (67). Finally, we neglected any inertial effects which are known to be small compared to viscous forces in systems of cilia. Nevertheless, it is still possible that a small inertial effect can be decisive for synchronisation in situations where other effects cancel out (68, 69).

Our results leave some open questions that could be addressed in future work. For example, in real biological systems there are a great many sources of noise (70), and at the scale of cilia, noise may be very relevant for synchronisation (60) so future extensions to our model could examine the role of noise in the motion of the cilia. Additionally, we have assumed that all cilia are of identical lengths, but in reality there can be

variation in the lengths of cilia, and some studies have found that this can affect synchronisation (71). Similarly, even in healthy humans there are some cilia with structural abnormalities (72), which means that the influence on synchronisation of nonidentical cilia may be significant. Our circular trajectory retains many key features of the stroke of real cilia, but it is possible that some crucial feature is lost in this simplification, so future work could integrate realistic cilium strokes with elongated cilia. This would also enable a more realistic driving engine for the cilia: in our model the cilia have a time-varying driving force that always points along the tangent of the trajectory, but real cilia are driven by creating shear forces between pairs of dynein tubes that make up the internal structure of the cilium (73). It is possible that in the future, artificial or lab-grown cilia may have applications in microfluidic pumping, given the advancing state of the fields of growing artificial lab-on-a-chip cilia (74) and nanoscale artificial cilium production (75), which could offer real-world applications for our work and the future work proposed here.

Materials and Methods

Fluid flow. At the scale of cilia, the behaviour of the fluid flow field $\mathbf{u}$ is well-approximated by the incompressible Stokes equations:

$$\eta\nabla^2\mathbf{u} - \nabla p = 0,$$
$$\nabla\cdot\mathbf{u} = 0,$$

where η is the fluid dynamic viscosity and p is the pressure.

The hydrodynamic interactions between two particles are calculated using a modified Rotne-Prager approximation with corrections to account for the no-slip fluid boundary on the surface below the cilium. The Rotne-Prager tensor takes into account terms up to the order $\sim r^{-3}$ and is equivalent to averaging the Green's function (Oseen tensor) over the surfaces of both spheres. To take into account the presence of the no-slip boundary at $z=0$, we use the method of images and replace the free-space Green's function by the Blake tensor (76), defined as

$$\mathbf{M}_{ij}^{\mathrm{Blake}} = \frac{1}{8\pi\eta}\Big[\mathbf{G}^{\mathrm{S}}(\mathbf{x}_i-\mathbf{x}_j) - \mathbf{G}^{\mathrm{S}}(\mathbf{x}_i-\bar{\mathbf{x}}_j) + 2z_j^2\mathbf{G}^{\mathrm{D}}(\mathbf{x}_i-\bar{\mathbf{x}}_j) - 2z_j\mathbf{G}^{\mathrm{SD}}(\mathbf{x}_i-\bar{\mathbf{x}}_j)\Big], \quad [9]$$

where $\mathbf{x}_k$ is the position of particles k, and $\bar{\mathbf{x}}_k$ is the position of the image of particle k reflected in the no-slip boundary at $z=0$, and where

$$\mathbf{G}^{\mathrm{S}}_{\alpha\beta}(\mathbf{r}) = \frac{\delta_{\alpha\beta}}{r} + \frac{r_\alpha r_\beta}{r^3}, \quad [10]$$

$$\mathbf{G}^{\mathrm{D}}_{\alpha\beta}(\mathbf{r}) = (1-2\delta_{\beta z})\frac{\partial}{\partial r_\beta}\left(\frac{r_\alpha}{r^3}\right), \quad [11]$$

$$\mathbf{G}^{\mathrm{SD}}_{\alpha\beta}(\mathbf{r}) = (1-2\delta_{\beta z})\frac{\partial}{\partial r_\beta}G^{\mathrm{S}}_{\alpha z}(\mathbf{r}). \quad [12]$$

The Rotne-Prager tensor corrected for the no-slip boundary follows by including the leading corrections that result from surface-averaging over each sphere. The non-diagonal terms, describing the interaction between two particles $i\neq j$, can be calculated as

$$\mathbf{M}_{ij} = \left(1+\frac{a^2}{6}\nabla^2_{\mathbf{x}_i}\right)\left(1+\frac{a^2}{6}\nabla^2_{\mathbf{x}_j}\right)\mathbf{M}^{\mathrm{Blake}}_{ij}. \quad [13]$$

Explicit expressions for the elements of the mobility matrix can be found in (77).

Solving equations of motion. The equations of motion as stated in Eq. (5) give a complete description of the system. However, they require the knowledge of the many-particle drag matrix $\mathbf{\Gamma}$, whereas the Rotne-Prager approximation gives us the mobility matrix $\mathbf{M}=\mathbf{\Gamma}^{-1}$. Simulating Eq. (5) directly for N cilia would therefore require the inversion of a $3N\times 3N$ matrix at each simulation step, in addition to solving a linear equation system with N unknowns.

To accelerate the numerical solution, we therefore rewrite the equations of motion based on the mobility matrix $\mathbf{M}(\phi_i,\phi_j)$ which gives the velocity response at the position of cilium i to a force at cilium j. We can express the force balance and the hydrodynamic equations with the hydrodynamic force $\mathbf{F}^{\mathrm{h}}_i$ acting on the cilium:

$$0 = \mathbf{t}_i\cdot\mathbf{F}^{\mathrm{h}}_i(\{j\}) + F^{\mathrm{dr}}_i(\phi_i) - \Gamma(\phi_i)v_i, \quad [14]$$

$$\mathbf{v}_i = -\mathbf{M}(\phi_i,\phi_i)\cdot\mathbf{F}^{\mathrm{h}}_i - \sum_{j\neq i}\mathbf{M}(\phi_i,\phi_j)\cdot\mathbf{F}^{\mathrm{h}}_j. \quad [15]$$

By multiplying the first equation with $\mathbf{t}_i$ and inserting it into the second, we can derive a coupled set of $3N$ equations which allow us to solve for all hydrodynamic force vectors simultaneously (assuming that $\Gamma(\phi)$ is never zero):

$$\left(\mathbf{M}(\phi_i,\phi_i) + \frac{\mathbf{t}_i\mathbf{t}_i^T}{\Gamma(\phi_i)}\right)\cdot\mathbf{F}^{\mathrm{h}}_i + \sum_{j\neq i}\mathbf{M}(\phi_i,\phi_j)\cdot\mathbf{F}^{\mathrm{h}}_j = -\frac{F^{\mathrm{dr}}(\phi_i)}{\Gamma(\phi_i)}\mathbf{t}_i.$$

In the above equation system the first term describing the self-interaction of cilium i is always dominant, whereas the second term describing the hydrodynamic interactions between cilia is weaker and can be treated in a perturbative way. In matrix form the equation is always block-diagonally dominant, which means that it can be solved efficiently using an adapted Successive Over-Relaxation (SOR) algorithm (78) that works on 3×3 blocks rather than individual elements. In the initial time step of the simulation, we use the solution to the purely diagonal matrix equation as the first iteration, but in subsequent step it is more efficient to start iterating with the solution of the previous step. In this way only a very small number of iterations ($N_{\mathrm{it}}=3$) is required to converge to remarkably good accuracy with a relative error $\varepsilon<10^{-6}$. Once the hydrodynamic forces have been obtained, they can be substituted back into Eq. (14) to find the cilium speeds v_i, and this can be trivially transformed into the time derivatives of the phases $\dot{\phi}_i$.

Numerical integration. The phase of each cilium is updated using the standard Runge-Kutta method (RK4). Unlike implicit methods, Runge-Kutta algorithms require a single calculation of the hydrodynamic forces at each timestep, which is by far the most computationally demanding simulation step. The timestep used was approximately $0.001\,t_0$.

Quantifying synchronisation. To determine whether the entire system has reached a synchronised state, we find the average frequencies of each cilium in a moving window of 50 time periods. We take the standard deviation of these frequencies to be the order parameter of the system.

When considering pairs of cilia, as in Figs. 2C, 3D, and 5D-E, standard deviations were less useful. Instead, the signal coherence was computed using the phases of adjacent pairs of cilia using Welch's method (79), with a moving window in the time domain representing approximately 50 unperturbed cilium cycles. In the 2D case, we instead used the geometric mean of the coherence with all neighbouring cilia.

Uniform phase angle. In Fig. 5 we used a transformed phase difference $\Delta\phi' = \phi'_2 - \phi'_1$. These angles have the property that for a single isolated cilium, $\dot{\phi}'$ is constant. The transformed phase can be derived from the original phase angle using

$$\phi'(\phi) = \frac{2\pi}{t_0}\int_0^{\phi}\frac{1}{\dot{\phi}(\phi'')}\,\mathrm{d}\phi'', \quad [16]$$

where all quantities on the right hand side are for an isolated cilium.

Periodic boundary conditions. When considering the effect of cilium j on cilium i, only the closest instance of j was considered. In simple terms, if j were right next to i, then we would proceed in the same way as if we had no periodic boundaries. However, if j were more than half of the system length away from i, then we would instead consider a copy of j translated by the system length, putting it closer to i. Since the mobility tensor decays quickly along the surface as $1/r^3$, neglecting the distant cilia does not have any effect on the results.

Numerical parameters. In all simulations, we took the lattice constant to be $d = 2.5h = 2.5a$, and $b = a/10$. χ was always $\pi/6$ and we used $A_1 = -0.55$, $A_2 = -0.2$, $B_1 = -0.2$, $B_2 = 0.35$, $C_1 = 0.3$, $C_2 = -0.4$, $D_1 = -0.1$, and $D_2 = -0.55$. These parameters give a fast working stroke and a slower recovery stroke which break the fore-aft symmetry, consistent with the behaviour of real cilia. The slowest part of the stroke is just before the lowest part of the recovery stroke, where the cilium would be curling up and the tip would therefore be travelling at its minimum speed.

ACKNOWLEDGMENTS. This work has received support from the Max Planck School Matter to Life and the MaxSynBio Consortium, which are jointly funded by the Federal Ministry of Education and Research (BMBF) of Germany, and the Max Planck Society. A.V. acknowledges support from the Slovenian Research Agency (grant no. P1-0099)

1. C Brennen, H Winet, Fluid mechanics of propulsion by cilia and flagella. *Annu. Rev. Fluid Mech.* **9**, 339–398 (1977).
2. MV Nachury, DU Mick, Establishing and regulating the composition of cilia for signal transduction. *Nat. Rev. Mol. Cell Biol.* **20**, 389–405 (2019).
3. R Faubel, C Westendorf, E Bodenschatz, G Eichele, Cilia-based flow network in the brain ventricles. *Science* **353**, 176–178 (2016).
4. A Yaghi, MB Dolovich, Airway epithelial cell cilia and obstructive lung disease. *Cells* **5**, 40 (2016).
5. V Bhandawat, J Reisert, KW Yau, Signaling by olfactory receptor neurons near threshold. *Proc. Natl. Acad. Sci. U.S.A.* **107**, 18682–18687 (2010).
6. A Dasgupta, JD Amack, Cilia in vertebrate left–right patterning. *Phil. Trans. Royal Soc. B: Biol. Sci.* **371**, 20150410 (2016).
7. L Prandtl, Aufgaben der Strömungsforschung (lecture delivered at the inauguration of the Kaiser Wilhelm Institute for Flow Research in Göttingen, 16 July 1925). *Naturwissenschaften* **14**, 335–338 (1926).
8. GI Taylor, Analysis of the swimming of microscopic organisms. *Proc. R. Soc. Lond. A* **209**, 447–461 (1951).
9. R Golestanian, JM Yeomans, N Uchida, Hydrodynamic synchronization at low Reynolds number. *Soft Matter* **7**, 3074 (2011).
10. N Osterman, A Vilfan, Finding the ciliary beating pattern with optimal efficiency. *Proc. Natl. Acad. Sci. U.S.A.* **108**, 15727–15732 (2011).
11. J Elgeti, G Gompper, Emergence of metachronal waves in cilia arrays. *Proc. Natl. Acad. Sci. U.S.A.* **110**, 4470–4475 (2013).
12. C Ringers, et al., Novel analytical tools reveal that local synchronization of cilia coincides with tissue-scale metachronal waves in zebrafish multiciliated epithelia. *eLife* **12**, e77701 (2023).
13. D Hickey, A Vilfan, R Golestanian, Ciliary chemosensitivity is enhanced by cilium geometry and motility. *eLife* **10**, e66322 (2021).
14. A Funfak, et al., *Paramecium* swimming and ciliary beating patterns: a study on four RNA interference mutations. *Integr. Biol.* **7**, 90–100 (2015).
15. DR Brumley, M Polin, TJ Pedley, RE Goldstein, Hydrodynamic synchronization and metachronal waves on the surface of the colonial alga *Volvox carteri*. *Phys. Rev. Lett.* **109**, 268102 (2012).
16. S Chateau, J Favier, S Poncet, U D'Ortona, Why antiplectic metachronal cilia waves are optimal to transport bronchial mucus. *Phys. Rev. E* **100**, 791 (2019).
17. ML Byron, et al., Metachronal motion across scales: Current challenges and future directions. *Integr. Comp. Biol.* **61**, 1674–1688 (2021).
18. EW Knight-Jones, Relations between metachronism and the direction of ciliary beat in metazoa. *J. Cell Sci.* **3**, 503–521 (1954).
19. RE Goldstein, M Polin, I Tuval, Noise and synchronization in pairs of beating eukaryotic flagella. *Phys. Rev. Lett.* **103**, 168103 (2009).
20. KY Wan, RE Goldstein, Coordinated beating of algal flagella is mediated by basal coupling. *Proc. Natl. Acad. Sci. U.S.A.* **113**, E2784–E2793 (2016).
21. G Quaranta, ME Aubin-Tam, D Tam, Hydrodynamics versus intracellular coupling in the synchronization of eukaryotic flagella. *Phys. Rev. Lett.* **115**, 238101 (2015).
22. Y Liu, R Claydon, M Polin, DR Brumley, Transitions in synchronization states of model cilia through basal-connection coupling. *J. Royal Soc. Interface* **15**, 20180450 (2018).
23. N Narematsu, R Quek, KH Chiam, Y Iwadate, Ciliary metachronal wave propagation on the compliant surface of *Paramecium* cells. *Cytoskeleton* **72**, 633–646 (2015).
24. M Reichert, H Stark, Synchronization of rotating helices by hydrodynamic interactions. *Eur. Phys. J. E* **17**, 493–500 (2005).
25. B Guirao, JF Joanny, Spontaneous creation of macroscopic flow and metachronal waves in an array of cilia. *Biophys. J.* **92**, 1900–1917 (2007).
26. T Niedermayer, B Eckhardt, P Lenz, Synchronization, phase locking, and metachronal wave formation in ciliary chains. *Chaos* **18**, 037128 (2008).
27. B Qian, H Jiang, DA Gagnon, KS Breuer, TR Powers, Minimal model for synchronization induced by hydrodynamic interactions. *Phys. Rev. E* **80**, 061919 (2009).
28. N Uchida, R Golestanian, Hydrodynamic synchronization between objects with cyclic rigid trajectories. *Eur. Phys. J. E* **35**, 135 (2012).
29. Y Man, E Kanso, Multisynchrony in Active Microfilaments. *Phys. Rev. Lett.* **125**, 148101 (2020).
30. A Vilfan, F Jülicher, Hydrodynamic flow patterns and synchronization of beating cilia. *Phys. Rev. Lett.* **96**, 1–4 (2006).
31. N Uchida, R Golestanian, Synchronization and collective dynamics in a carpet of microfluidic rotors. *Phys. Rev. Lett.* **104**, 178103 (2010).
32. N Uchida, R Golestanian, Synchronization in a carpet of hydrodynamically coupled rotors with random intrinsic frequency. *Europhys. Lett.* **89**, 50011 (2010).
33. S Saha, S Ramaswamy, R Golestanian, Pairing, waltzing and scattering of chemotactic active colloids. *New J. Phys.* **21**, 063006 (2019).
34. F Meng, RR Bennett, N Uchida, R Golestanian, Conditions for metachronal coordination in arrays of model cilia. *Proc. Natl. Acad. Sci. U.S.A.* **118** (2021).
35. AV Kanale, F Ling, H Guo, S Fürthauer, E Kanso, Spontaneous phase coordination and fluid pumping in model ciliary carpets. *Proc. Natl. Acad. Sci. U.S.A.* **119**, e2214413119 (2022).
36. N Uchida, R Golestanian, Generic conditions for hydrodynamic synchronization. *Phys. Rev. Lett.* **106**, 058104 (2011).
37. A Maestro, et al., Control of synchronization in models of hydrodynamically coupled motile cilia. *Commun. Phys.* **1**, 1–8 (2018).
38. C Wollin, H Stark, Metachronal waves in a chain of rowers with hydrodynamic interactions. *Eur. Phys. J. E* **34**, 42 (2011).
39. H Guo, L Fauci, M Shelley, E Kanso, Bistability in the synchronization of actuated microfilaments. *J. Fluid Mech.* **836**, 304–323 (2018).
40. B Chakrabarti, D Saintillan, Hydrodynamic synchronization of spontaneously beating filaments. *Phys. Rev. Lett.* **123**, 208101 (2019).
41. B Chakrabarti, S Fürthauer, MJ Shelley, A multiscale biophysical model gives quantized metachronal waves in a lattice of cilia. *Proc. Natl. Acad. Sci. U.S.A.* **119**, e2113539119 (2022).
42. H Masoud, HA Stone, The reciprocal theorem in fluid dynamics and transport phenomena. *J. Fluid Mech.* **879**, P1 (2019).
43. R Soto, R Golestanian, Self-assembly of catalytically active colloidal molecules: Tailoring activity through surface chemistry. *Phys. Rev. Lett.* **112**, 068301 (2014).
44. R Soto, R Golestanian, Self-assembly of active colloidal molecules with dynamic function. *Phys. Rev. E* **91**, 052304 (2015).
45. J Agudo-Canalejo, R Golestanian, Active phase separation in mixtures of chemically interacting particles. *Phys. Rev. Lett.* **123**, 018101 (2019).
46. S Saha, J Agudo-Canalejo, R Golestanian, Scalar active mixtures: The nonreciprocal Cahn-Hilliard model. *Phys. Rev. X* **10**, 041009 (2020).
47. SAM Loos, SHL Klapp, Irreversibility, heat and information flows induced by non-reciprocal interactions. *New J. Phys.* **22**, 123051 (2020).
48. M Fruchart, R Hanai, PB Littlewood, V Vitelli, Non-reciprocal phase transitions. *Nature* **592**, 363–369 (2021).
49. S Osat, R Golestanian, Non-reciprocal multifarious self-organization. *Nat. Nanotechnol.* **18**, 79–85 (2023).
50. A Solovev, BM Friedrich, Synchronization in cilia carpets: multiple metachronal waves are stable, but one wave dominates. *New J. Phys.* **24**, 013015 (2022).
51. I Kavre, A Vilfan, D Babič, Hydrodynamic synchronization of autonomously oscillating optically trapped particles. *Phys. Rev. E* **91**, 031002 (2015).
52. E Hamilton, N Bruot, P Cicuta, The chimera state in colloidal phase oscillators with hydrodynamic interaction. *Chaos* **27**, 123108 (2017).
53. B Nasouri, GJ Elfring, Hydrodynamic interactions of cilia on a spherical body. *Phys. Rev. E* **93**, 033111 (2016).
54. FO Mannan, M Jarvela, K Leiderman, Minimal model of the hydrodynamical coupling of flagella on a spherical body with application to *Volvox*. *Phys. Rev. E* **102**, 033114 (2020).
55. KY Wan, et al., Reorganization of complex ciliary flows around regenerating Stentor coeruleus. *Phil. Trans. Royal Soc. B: Biol. Sci.* **375**, 20190167 (2020).
56. RR Strathmann, The feeding behavior of planktotrophic echinoderm larvae: Mechanisms, regulation, and rates of suspension-feeding. *J. Exp. Mar. Biol. Ecol.* **6**, 109–160 (1971).
57. A Vilfan, Generic flow profiles induced by a beating cilium. *Eur. Phys. J. E* **35**, 72 (2012).
58. GJ Elfring, E Lauga, Hydrodynamic phase locking of swimming microorganisms. *Phys. Rev. Lett.* **103**, 088101 (2009).
59. A Solovev, BM Friedrich, Lagrangian mechanics of active systems. *Eur. Phys. J. E* **44**, 49 (2021).
60. A Solovev, BM Friedrich, Synchronization in cilia carpets and the Kuramoto model with local coupling: Breakup of global synchronization in the presence of noise. *Chaos* **32**, 013124 (2022).
61. F Boselli, J Jullien, E Lauga, RE Goldstein, Fluid mechanics of mosaic ciliated tissues. *Phys. Rev. Lett.* **127**, 198102 (2021).
62. A Ghorbani, A Najafi, Symplectic and antiplectic waves in an array of beating cilia attached to a closed body. *Phys. Rev. E* **95**, 052412 (2017).
63. K Bouhouche, et al., Paramecium, a model to study ciliary beating and ciliogenesis: Insights from cutting-edge approaches. *Front. Cell Dev. Biol.* **10**, 847908 (2022).
64. MA Sleigh, JR Blake, N Liron, The propulsion of mucus by cilia. *Am. Rev. Respir. Dis.* **137**, 726–741 (1988).
65. R Chelakkot, M F. Hagan, A Gopinath, Synchronized oscillations, traveling waves, and jammed clusters induced by steric interactions in active filament arrays. *Soft Matter* **17**, 1091–1104 (2021).
66. DR Brumley, KY Wan, M Polin, RE Goldstein, Flagellar synchronization through direct hydrodynamic interactions. *eLife* **3**, e02750 (2014).
67. AWJ Soh, et al., Intracellular connections between basal bodies promote the coordinated behavior of motile cilia. *Mol. Biol. Cell* **33**, br18 (2022).
68. M Theers, RG Winkler, Synchronization of rigid microrotors by time-dependent hydrodynamic interactions. *Phys. Rev. E* **88**, 023012 (2013).
69. D Wei, PG Dehnavi, ME Aubin-Tam, D Tam, Measurements of the unsteady flow field around beating cilia. *J. Fluid Mech.* **915**, A70 (2021).
70. W Gilpin, MS Bull, M Prakash, The multiscale physics of cilia and flagella. *Nat. Rev. Phys.* **2**, 74–88 (2020).
71. M Bottier, KA Thomas, SK Dutcher, PV Bayly, How does cilium length affect beating? *Biophys. J.* **116**, 1292–1304 (2019).
72. F Verra, et al., Ciliary abnormalities in bronchial epithelium of smokers, ex-smokers, and nonsmokers. *Am. J. Respir. Crit. Care Med.* **151** (2013).
73. A Horani, TW Ferkol, Advances in the genetics of primary ciliary dyskinesia. *Chest* **154**,

645–652 (2018).
74. JC Nawroth, et al., Stem cell-based lung-on-chips: The best of both worlds? *Adv. Drug Deliv. Rev.* **140**, 12–32 (2019).
75. JMJ den Toonder, PR Onck, Microfluidic manipulation with artificial/bioinspired cilia. *Trends Biotechnol.* **31**, 85–91 (2013).
76. JR Blake, A note on the image system for a stokeslet in a no-slip boundary. *Proc. Camb. Phil. Soc.* **70**, 303–310 (1971).
77. M Vilfan, et al., Self-assembled artificial cilia. *Proc. Natl. Acad. Sci. U.S.A.* **107**, 1844–1847 (2010).
78. DM Young, *Iterative Solution of Large Linear Systems.* (Academic Press, Orlando, FL), (1971).
79. P Welch, The use of fast Fourier transform for the estimation of power spectra: A method based on time averaging over short, modified periodograms. *IEEE Trans. Audio Electroacoust.* **15**, 70–73 (1967).

4.5 Chapter summary

- Metachronal waves are relatively common phenomena that lead to increased pumping effectiveness in cilia.
- Even in finite systems, hydrodynamic interactions are sufficient to give fast stable metachronal waves.
- Nonreciprocity of hydrodynamic interactions is crucial to retain this fast synchronisation. If the nonreciprocity is somehow suppressed, synchronisation is now much slower and the final synchronised state is no longer deterministic, which (given that research has shown that antiplectic waves are more efficient than symplectic ones [113]) could lead to decreased pumping efficiency even in the steady-state.

[113]: Chateau *et al.* (2019), *Why antiplectic metachronal cilia waves are optimal to transport bronchial mucus*

5 Conclusion

Treacle nodded. "I hadn't looked at it like that," he said, "but you're absolutely right. He's really pushed back the boundaries of ignorance. There's so much about the universe we don't know."

Sir Terry Pratchett, *Equal Rites*

Given the ubiquity of cilia, and their centrality to so many biological processes, it is partly a shame, but mostly a fantastic opportunity, that we still don't fully understand why they are built the way they are and act the way they do, and they continue to be the source of so many interesting open questions. We have tried to make some progress towards closing some of these open questions, and in the process we have opened a few new ones – as Pratchett put it, in this work we have pushed the boundaries of ignorance, continuing a process that presumably began when the first organism with eyes looked up at the stars and wondered what they were.

In Chapter 3, by considering the mass transport to a perfectly reactive cilium, we found that the geometry of the cilium confers a chemosensory advantage over a chemosensory patch, and that motility confers a chemosensory advantage over immotility, even when motile cilia are bunched together in groups. These results were robust at a wide range of biologically plausible values of the cilium beating frequency, and would go some way towards explaining why chemoreceptors are often found on cilia (both motile and primary).

That said, the model considered in this chapter has some limitations. We assumed that particles are absorbed by the cilium immediately upon first touching it, which is only justified if the receptors cover a sufficient fraction of the surface area (though the required fraction is extremely low: in the absence of advection, only 1% of the surface must be

covered by receptors to achieve near-perfect sensitivity [66]). The Rotne-Prager mobility tensor that we used does not perfectly satisfy the no-slip boundary, especially at high Péclet numbers, which should not change the qualitative story told by the results but could have a quantitative impact. We have also assumed that the signalling molecules being detected are extremely small relative to the cilium, which may not be completely true for large protein complexes or vesicles.

[66]: Berg *et al.* (1977), *Physics of chemoreception*

Then, in Chapter 4, we considered the interactions of a lattice of cilia, and found that stable order could emerge in linear time even in finite systems with open boundaries, provided the hydrodynamic intercilium coupling was nonreciprocal. Without this nonreciprocal coupling, the order emerged in nonlinear time, and the final state was non-deterministic. This suggests that for cilia, nonreciprocal coupling is incredibly important.

Possibly the primary limitation in the model in this chapter is that it does not consider the role of non-identical cilium forms and noisy behaviour. Thermal noise will play a role in cilium motion simply due to their small size, but additionally the driving process for the motile cilium is itself stochastic, i.e. there are active fluctuations [186]. In biological systems, ciliary synchronisation is highly resistant to noise [77] and it would be useful to know if this behaviour is reproduced by our model. Different cilia, even on the same cell, can have differing intrinsic beat frequencies [121], and there is no reason we would necessarily expect every cilium to be identical in length, especially when they have been subject to damage or disease [187]. The simplification of the entire cilium to a single sphere on a circular trajectory simplified the calculations and simulation to a huge degree, and probably does not qualitatively affect the results, but it does remove certain near-field effects. Given that we found near-field hydrodynamic interactions to be incredibly important to synchronisation, it is possible that the synchronisation would be even faster with a cilium model more akin to the chain

[186]: Ma *et al.* (2014), *Active Phase and Amplitude Fluctuations of Flagellar Beating*

[77]: Gilpin *et al.* (2020), *The multiscale physics of cilia and flagella*

[121]: Goldstein *et al.* (2009), *Noise and Synchronization in Pairs of Beating Eukaryotic Flagella*

[187]: Leopold *et al.* (2009), *Smoking Is Associated with Shortened Airway Cilia*

of beads used in Ch. 3, so this is another avenue worth exploring.

Considering the work as a whole, we see that interactions between motile cilia are extremely beneficial, increasing sensing and pumping efficiency. It should therefore come as no surprise that motile cilia are often found in carpets, as the close proximity ensures that per-cilium chemosensitivity sees an improvement, as well as permitting the cilia to benefit from near-field hydrodynamic interactions so that they can coordinate their beating.

Other than addressing the limitations discussed above, there is plenty of additional research to be done on these and similar models. For example, we showed that motile cilia in close proximity can quickly synchronise to form a metachronal wave, and we also showed that a bundle of motile cilia with random phases can be more chemosensitive per cilium than a single motile cilium on its own. It would be interesting to see whether this increase is retained if the cilium phases are metachronally synchronised rather than randomised, which seems probable given that the high volume flow rates achieved by metachronal waves could draw a large amount of signalling molecules into the cilium carpet.

Coronaviruses in general frequently attack and damage ciliated cells [188], and patients with SARS-CoV-2 are known to have ciliated cells that have lost their cilia entirely [189], resulting in a reduced rate of mucus clearance from the lungs and airway by cilia [190]. Since this mucociliary clearance is one of the first lines of defence against airborne pathogens and particulates, this results in higher susceptibility to disease and damage [191]. It is possible that the lower cilium density results in a loss of metachronal coordination, which in turn causes this decreased pumping efficiency seen in SARS-CoV-2 patients, but it could simply be the case that a lower cilium density results in impeded clearance of mucus from the airways due to fewer cilia moving mucus. Better understanding the mechanisms underlying this reduced

[188]: Jonsdottir *et al.* (2016), *Coronaviruses and the human airway: A universal system for virus-host interaction studies*

[189]: Buqaileh *et al.* (2021), *Can cilia provide an entry gateway for SARS-CoV-2 to human ciliated cells?*

[190]: Robinot *et al.* (2021), *SARS-CoV-2 infection induces the dedifferentiation of multiciliated cells and impairs mucociliary clearance*

[191]: Tilley *et al.* (2015), *Cilia Dysfunction in Lung Disease*

pumping efficiency could be of significant value, and could be achieved by using a version of our model to investigate how the loss or damage of cilia affects the ability of ciliary carpets to synchronise, though it would need to be adapted to account for the non-Newtonian nature of the mucus.

It has been mentioned several times in this work that the left-right differentiation in many vertebrates originates with cilia. The exact mechanism isn't known, but it is known that motile cilia can generate asymmetrical fluid flows in structures generally referred to as 'left-right organisers'. One hypothesis is that these asymmetric flows create nonuniform distributions of signalling molecules that are then detected by other cilia, but it has also been proposed that mechanosensitive cilia detect these asymmetrical flows directly [152]. We could potentially adapt our models to the geometry of the left-right organiser, and thus try to better understand the origins of left-right differentiation.

[152]: Dasgupta *et al.* (2016), *Cilia in vertebrate left-right patterning*

One recent paper suggested a role for organisms like *Paramecium* in surgery [56]. *Paramecium* can sense chemical gradients and swim along them, so if *Paramecium* were inserted into a human body, perhaps it could be guided around by injecting inert calcium salts in the right places in the body. This obviously all remains highly speculative, but perhaps in the future artificial chemosensing microswimmers could see actual clinical use, and in this case it would be helpful if they were able to sense and swim effectively, perhaps by taking advantage of the efficiency afforded by cilium synchronisation and the chemosensitivity afforded by cilium geometry and motility.

[56]: Sarvestani *et al.* (2016), *Simulation of Paramecium Chemotaxis Exposed to Calcium Gradients*

This thesis began by imagining the surprise that our predecessors experienced when they came across something as shocking and inexplicable as *situs inversus*, something that was completely contrary to their experiences and expectations. While we were carrying out the work we have described, we were often surprised by what we found out. Even with centuries of scientific progress, the bizarre be-

haviour of cilia and the wonderful world they inhabit have clearly still not run out of surprises waiting for the interested researcher.

Appendices

A

A.1 Supplementary figures: Ciliary chemosensitivity is enhanced by cilium geometry and motility

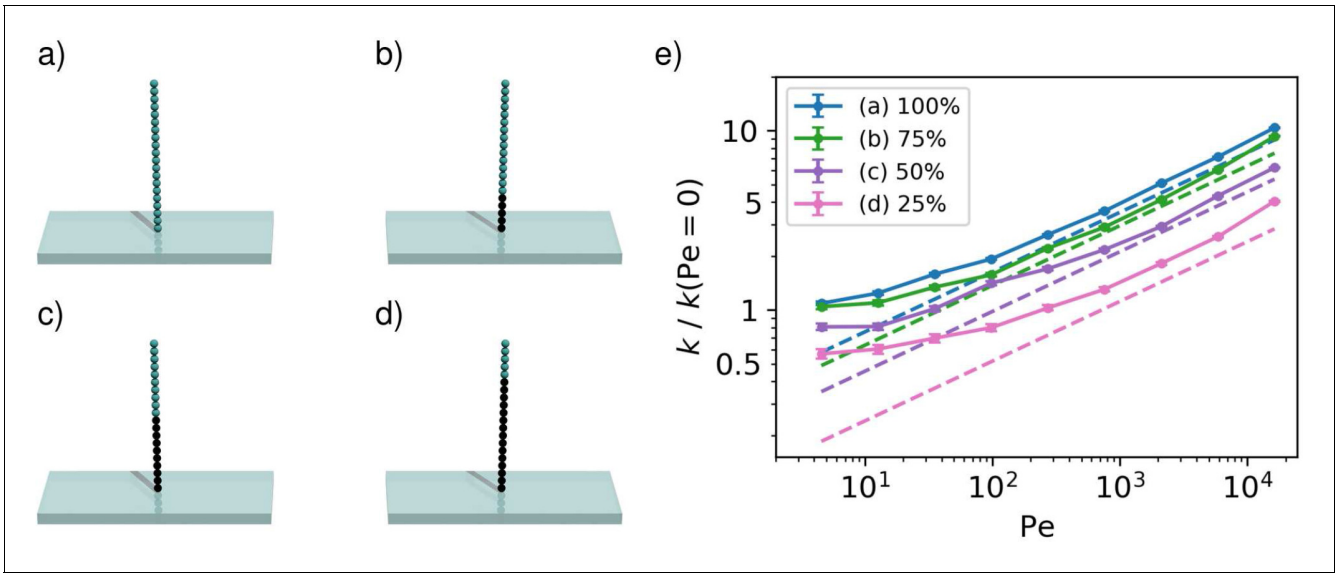

Figure 2—figure supplement 1. Capture rate as a function of the Péclet number for passive cilia in a shear flow, obtained from numerical simulations. The lines show the capture rates for cilia that absorb particles only on a fraction of their length, starting from the tip. The schematics indicate the absorbing part of the cilium in blue and the non-absorbing part in black.

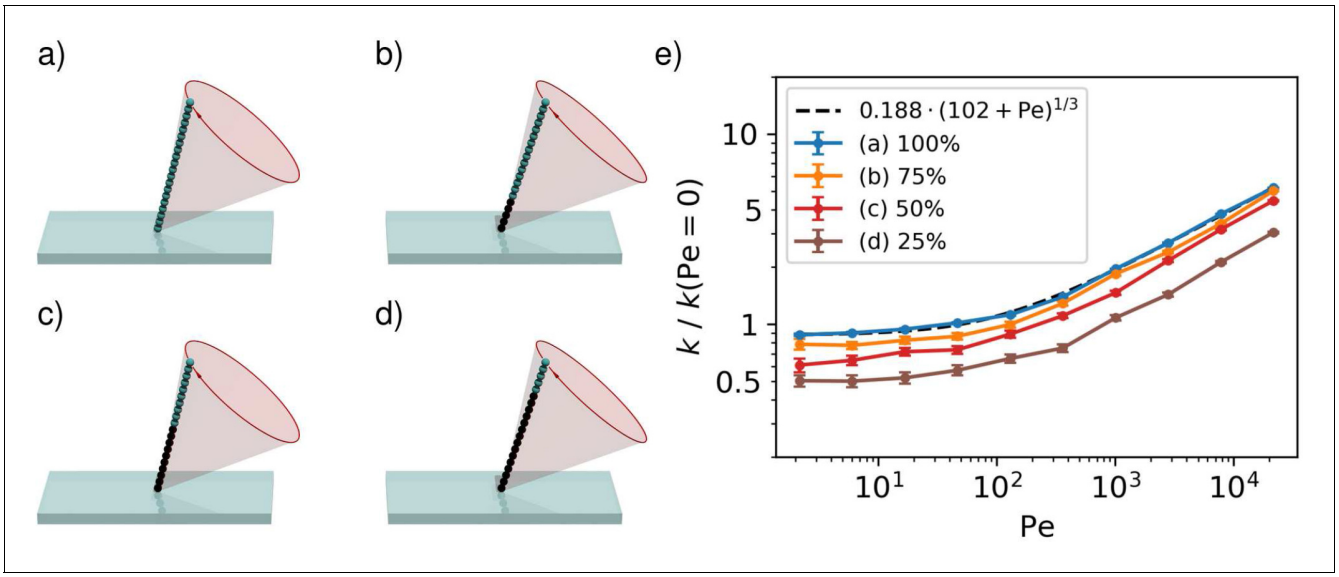

Figure 3—figure supplement 1. Capture rate of an actively beating cilium tracing out a tilted cone, plotted as a function of the Péclet number. These results were obtained from numerical simulations. The lines show the capture rates for cilia that absorb particles only on a fraction of their length, starting from the tip. The schematics indicate the absorbing part of the cilium in blue and the non-absorbing part in black.

B

B.1 Supplementary information: Nonreciprocal interactions give rise to fast cilium synchronisation in finite systems

Supporting Information for

Nonreciprocal interactions give rise to fast cilium synchronisation in finite systems

David J Hickey, Ramin Golestanian and Andrej Vilfan

E-mail: ramin.golestanian@ds.mpg.de, andrej.vilfan@ds.mpg.de

This PDF file includes:

Figs. S1 to S2
Legends for Movies S1 to S2

Other supporting materials for this manuscript include the following:

Movies S1 to S2

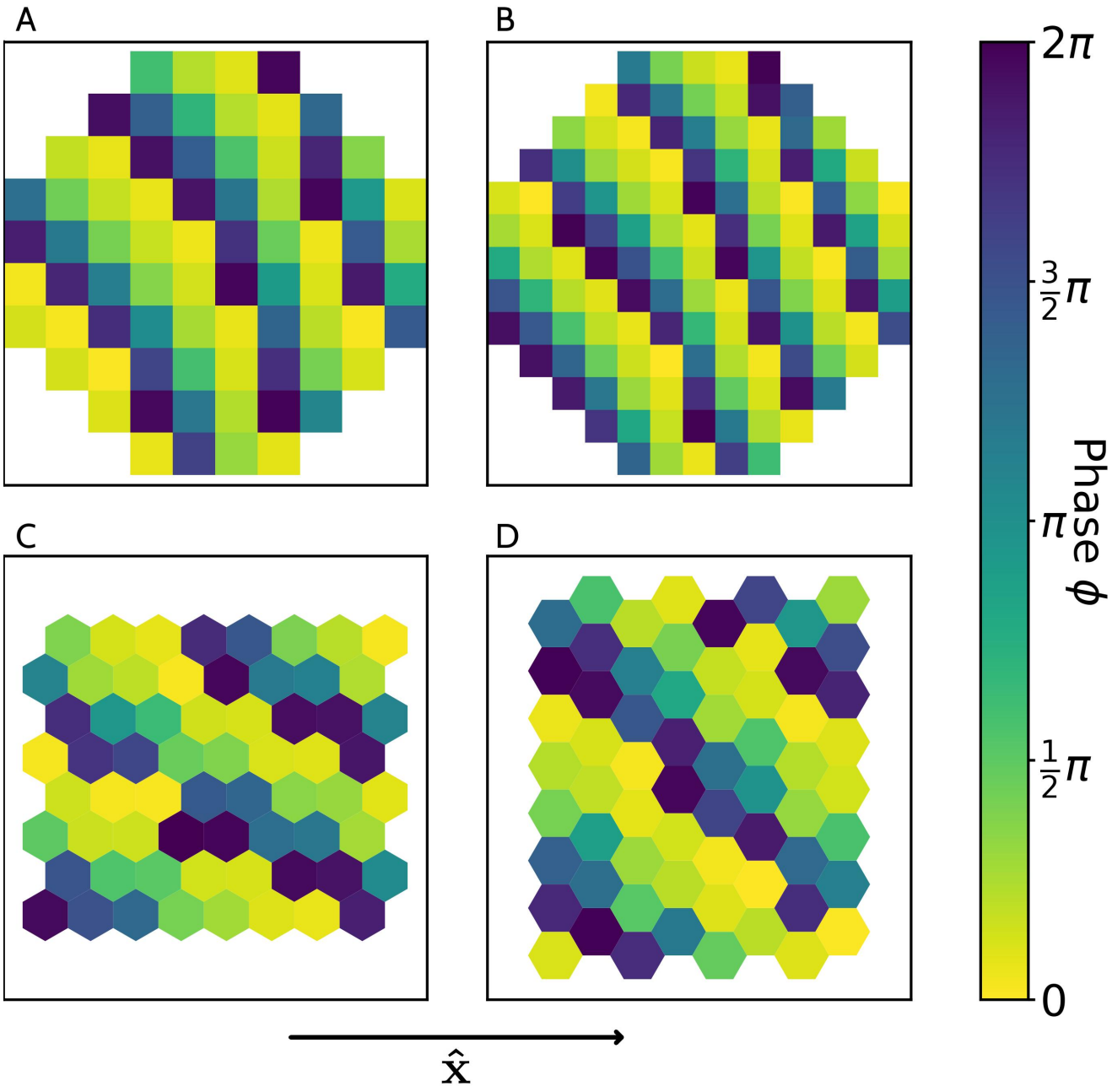

Fig. S1. Emergent metachronal waves on different lattices, with pumping direction in the x-direction (indicated). (A) 64 cilia arranged on a square lattice forming an octagon. (B) 144 cilia in the same arrangement. (C) 64 cilia on a hexagonal lattice, oriented such that one base vector is aligned with the direction of the power stroke. (D) as in (C), but with a lattice that is rotated by 90°.

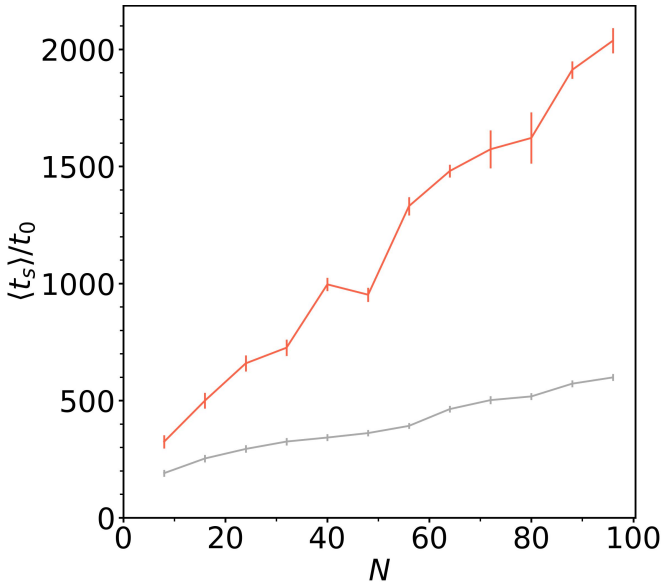

Fig. S2. Synchronisation times on a 1D lattice. The orange line shows cilia arranged along the y-axis (i.e. in the direction of weaker nonreciprocity). The grey line shows cilia arranged along the x-axis, as in Fig. 2C (main text). Synchronisation times still scale linearly when cilia are arranged in the y-direction, but are higher by some numerical factor, as expected from the weaker (but still present) nonreciprocity.

Movie S1. Animation of a metachronal wave in 2D.

Movie S2. Emergence of a metachronal wave on a lattice of 8×8 cilia.

Bibliography

1. Pennekamp, P., Menchen, T., Dworniczak, B. & Hamada, H. Situs inversus and ciliary abnormalities: 20 years later, what is the connection? *Cilia* **4,** 1. doi:10.1186/s13630-014-0010-9 (2015).
2. Ogunlade, O. *et al.* The role of electrocardiogram in the diagnosis of dextrocardia with mirror image atrial arrangement and ventricular position in a young adult Nigerian in Ile-Ife: a case report. *Journal of Medical Case Reports* **9,** 222. doi:10.1186/s13256-015-0695-4 (2015).
3. Baillie, M. XXI. An account of a remarkable transposition of the viscera. By Matthew Baillie, M. D. In a letter to John Hunter, Esq. F. R. S. *Philosophical Transactions of the Royal Society of London* **78,** 350–363. doi:10.1098/rstl.1788.0023 (1788).
4. Eitler, K., Bibok, A. & Telkes, G. Situs Inversus Totalis: A Clinical Review. *International Journal of General Medicine* **15,** 2437–2449. doi:10.2147/IJGM.S295444 (2022).
5. Essner, J. J., Vogan, K. J., Wagner, M. K., Tabin, C. J., Yost, H. J. & Brueckner, M. Conserved function for embryonic nodal cilia. *Nature* **418,** 37–38. doi:10.1038/418037a (2002).
6. McGrath, J. & Brueckner, M. Cilia are at the heart of vertebrate left–right asymmetry. *Current Opinion in Genetics & Development* **13,** 385–392. doi:10.1016/S0959-437X(03)00091-1 (2003).
7. Vicsek, T., Czirók, A., Ben-Jacob, E., Cohen, I. & Shochet, O. Novel Type of Phase Transition in a System of Self-Driven Particles. *Physical Review Letters* **75,** 1226–1229. doi:10.1103/PhysRevLett.75.1226 (1995).
8. Nachury, M. V. & Mick, D. U. Establishing and regulating the composition of cilia for signal transduction. *Nature Reviews Molecular Cell Biology* **20,** 389–405. doi:10.1038/s41580-019-0116-4 (2019).
9. Yaghi, A. & Dolovich, M. B. Airway Epithelial Cell Cilia and Obstructive Lung Disease. *Cells* **5,** 40. doi:10.3390/cells5040040 (2016).
10. Faubel, R., Westendorf, C., Bodenschatz, E. & Eichele, G. Cilia-based flow network in the brain ventricles. *Science* **353,** 176–178. doi:10.1126/science.aae0450 (2016).
11. Lyons, R. A., Saridogan, E. & Djahanbakhch, O. The reproductive significance of human Fallopian tube cilia. *Human Reproduction Update* **12.** doi:10.1093/humupd/dml012 (2006).

12. Girardet, L., Augière, C., Asselin, M.-P. & Belleannée, C. Primary cilia: biosensors of the male reproductive tract. *Andrology* **7,** 588–602. doi:10.1111/andr.12650 (2019).

13. Funfak, A. *et al. Paramecium* swimming and ciliary beating patterns: a study on four RNA interference mutations. *Integrative Biology* **7,** 90–100. doi:10.1039/c4ib00181h (2015).

14. Osterman, N. & Vilfan, A. Finding the ciliary beating pattern with optimal efficiency. *Proceedings of the National Academy of Sciences* **108,** 15727–15732. doi:10.1073/pnas.1107889108 (2011).

15. Elgeti, J. & Gompper, G. Emergence of metachronal waves in cilia arrays. *Proceedings of the National Academy of Sciences* **110,** 4470–4475. doi:10.1073/pnas.1218869110 (2013).

16. Bloodgood, R. A. Sensory reception is an attribute of both primary cilia and motile cilia. *Journal of Cell Science* **123,** 505–509. doi:10.1242/jcs.066308 (2010).

17. Saggese, T., Young, A. A., Huang, C., Braeckmans, K. & McGlashan, S. R. Development of a method for the measurement of primary cilia length in 3D. *Cilia* **1,** 11. doi:10.1186/2046-2530-1-11 (2012).

18. Purcell, E. M. Life at low Reynolds number. *American Journal of Physics* **45,** 3–11. doi:10.1119/1.10903 (1977).

19. Zhang, S.-D. *et al.* Swimming behaviour and magnetotaxis function of the marine bacterium strain MO-1. *Environmental Microbiology Reports* **6,** 14–20. doi:10.1111/1758-2229.12102 (2014).

20. Citerne, G. P., Carreau, P. J. & Moan, M. Rheological properties of peanut butter. *Rheologica Acta* **40,** 86–96. doi:10.1007/s003970000120 (2001).

21. Day, M. A. The no-slip condition of fluid dynamics. *Erkenntnis* **33,** 285–296. doi:10.1007/BF00717588 (1990).

22. Blake, J. R. A note on the image system for a stokeslet in a no-slip boundary. *Proceedings of the Cambridge Philosophical Society* **70,** 303–310. doi:10.1017/S0305004100049902 (1971).

23. Vilfan, A. Generic flow profiles induced by a beating cilium. *European Physical Journal E* **35,** 72. doi:10.1140/epje/i2012-12072-3 (2012).

24. Gauger, E. M., Downton, M. T. & Stark, H. Fluid transport at low Reynolds number with magnetically actuated artificial cilia. *The European Physical Journal E* **28,** 231–242. doi:10.1140/epje/i2008-10388-1 (2009).

25. Vilfan, M. *et al.* Self-assembled artificial cilia. *Proceedings of the National Academy of Sciences* **107,** 1844–1847. doi:10.1073/pnas.0906819106 (2010).

26. Guazzelli, É. & Morris, J. F. *A Physical Introduction to Suspension Dynamics* (Cambridge University Press, 2011).

27. Borker, N. S. & Koch, D. L. Slender body theory for particles with non-circular cross-sections with application to particle dynamics in shear flows. *Journal of Fluid Mechanics* **877,** 1098–1133. doi:10.1017/jfm.2019.625 (2019).

28. Koens, L. Tubular-body theory for viscous flows. *Physical Review Fluids* **7,** 034101. doi:10.1103/PhysRevFluids.7.034101 (2022).

29. Lauga, E. Bacterial Hydrodynamics. *Annual Review of Fluid Mechanics* **48,** 105–130. doi:10.1146/annurev-fluid-122414-034606 (2016).

30. Fulford, G. R. & Blake, J. R. Muco-ciliary transport in the lung. *Journal of Theoretical Biology* **121,** 381–402. doi:10.1016/S0022-5193(86)80098-4 (1986).

31. Johnson, R. E. & Brokaw, C. J. Flagellar hydrodynamics. A comparison between resistive-force theory and slender-body theory. *Biophysical Journal* **25,** 113–127 (1979).

32. Gueron, S. & Liron, N. Ciliary motion modeling, and dynamic multicilia interactions. *Biophysical Journal* **63,** 1045–1058. doi:10.1016/S0006-3495(92)81683-1 (1992).

33. Cortez, R. Regularized Stokeslet segments. *Journal of Computational Physics* **375,** 783–796. doi:10.1016/j.jcp.2018.08.055 (2018).

34. Smith, D. J. A boundary element regularized Stokeslet method applied to cilia- and flagella-driven flow. *Proceedings of the Royal Society A: Mathematical, Physical and Engineering Sciences* **465,** 3605–3626. doi:10.1098/rspa.2009.0295 (2009).

35. Pedley, T. J. & Kessler, J. O. Hydrodynamic Phenomena in Suspensions of Swimming Microorganisms. *Annual Review of Fluid Mechanics* **24,** 313–358. doi:10.1146/annurev.fl.24.010192.001525 (1992).

36. McGlashan, S. R., Jensen, C. G. & Poole, C. A. Localization of Extracellular Matrix Receptors on the Chondrocyte Primary Cilium. *Journal of Histochemistry & Cytochemistry* **54,** 1005–1014. doi:10.1369/jhc.5A6866.2006 (2006).

37. Goetz, J. G. *et al.* Endothelial Cilia Mediate Low Flow Sensing during Zebrafish Vascular Development. *Cell Reports* **6,** 799–808. doi:10.1016/j.celrep.2014.01.032 (2014).

38. Nauli, S. M., Kawanabe, Y., Kaminski, J. J., Pearce, W. J., Ingber, D. E. & Zhou, J. Endothelial Cilia Are Fluid Shear Sensors That Regulate Calcium Signaling and Nitric Oxide Production Through Polycystin-1. *Circulation* **117,** 1161–1171. doi:10.1161/CIRCULATIONAHA.107.710111 (Mar. 2008).

39. Brailov, I., Bancila, M., Brisorgueil, M.-J., Miquel, M.-C., Hamon, M. & Vergé, D. Localization of 5-HT6 receptors at the plasma membrane of neuronal cilia in the rat brain. *Brain Research* **872,** 271–275. doi:10.1016/S0006-8993(00)02519-1 (2000).

40. Marshall, W. F. & Nonaka, S. Cilia: Tuning in to the Cell's Antenna. *Current Biology* **16,** R604–R614. doi:10.1016/j.cub.2006.07.012 (2006).

41. Insinna, C. & Besharse, J. C. Intraflagellar transport and the sensory outer segment of vertebrate photoreceptors. *Developmental Dynamics* **237,** 1982–1992. doi:10.1002/dvdy.21554 (2008).

42. Kuhara, A. *et al.* Temperature Sensing by an Olfactory Neuron in a Circuit Controlling Behavior of C. elegans. *Science* **320,** 803–807. doi:10.1126/science.1148922 (2008).

43. Malicki, J. J. & Johnson, C. A. The Cilium: Cellular Antenna and Central Processing Unit. *Trends in Cell Biology* **27,** 126–140. doi:10.1016/j.tcb.2016.08.002 (2017).

44. Waters, A. M. & Beales, P. L. Ciliopathies: an expanding disease spectrum. *Pediatric Nephrology* **26,** 1039–1056. doi:10.1007/s00467-010-1731-7 (2011).

45. Van der Heiden, K. *et al.* Monocilia on chicken embryonic endocardium in low shear stress areas. *Developmental Dynamics* **235,** 19–28. doi:10.1002/dvdy.20557 (2006).

46. Horani, A. & Ferkol, T. W. Advances in the Genetics of Primary Ciliary Dyskinesia. *Chest* **154,** 645–652. doi:10.1016/j.chest.2018.05.007 (2018).

47. Olstad, E. W. *et al.* Ciliary Beating Compartmentalizes Cerebrospinal Fluid Flow in the Brain and Regulates Ventricular Development. *Current Biology* **29,** 229–241.e6. doi:10.1016/j.cub.2018.11.059 (2019).

48. Yuan, S. *et al.* Motile cilia of the male reproductive system require miR-34/miR-449 for development and function to generate luminal turbulence. *Proceedings of the National Academy of Sciences* **116,** 3584–3593. doi:10.1073/pnas.1817018116 (2019).

49. Mannan, F. O., Jarvela, M. & Leiderman, K. Minimal model of the hydrodynamical coupling of flagella on a spherical body with application to *Volvox*. *Physical Review E* **102,** 033114. doi:10.1103/PhysRevE.102.033114 (2020).

50. Afzelius, B. Cilia-related diseases. *The Journal of Pathology* **204,** 470–477. doi:10.1002/path.1652 (2004).

51. Gueron, S. & Levit-Gurevich, K. Energetic considerations of ciliary beating and the advantage of metachronal coordination. *Proceedings of the National Academy of Sciences* **96,** 12240–12245. doi:10.1073/pnas.96.22.12240 (1999).

52. Ringers, C. *et al.* Novel analytical tools reveal that local synchronization of cilia coincides with tissue-scale metachronal waves in zebrafish multiciliated epithelia. *eLife* **12,** e77701. doi:10.7554/eLife.77701 (2023).

53. Falk, N., Lösl, M., Schröder, N. & Gießl, A. Specialized Cilia in Mammalian Sensory Systems. *Cells* **4,** 500–519. doi:10.3390/cells4030500 (2015).

54. Sokolinskaya, E. L., Kolesov, D. V., Lukyanov, K. A. & Bogdanov, A. M. Molecular principles of insect chemoreception. *Acta Naturae* **12,** 81–91. doi:10.32607/actanaturae.11038 (2020).

55. Cummins, E. P., Strowitzki, M. J. & Taylor, C. T. Mechanisms and Consequences of Oxygen and Carbon Dioxide Sensing in Mammals. *Physiological Reviews* **100,** 463–488. doi:10.1152/physrev.00003.2019 (2020).

56. Sarvestani, A. N., Shamloo, A. & Ahmadian, M. T. Simulation of Paramecium Chemotaxis Exposed to Calcium Gradients. *Cell Biochemistry and Biophysics* **74,** 241–252. doi:10.1007/s12013-016-0727-8 (2016).

57. Zipfel, C. Plant pattern-recognition receptors. *Trends in Immunology* **35,** 345–351. doi:10.1016/j.it.2014.05.004 (2014).

58. Zimmermann, K. W. Beiträge zur Kenntniss einiger Drüsen und Epithelien. *Archiv für mikroskopische Anatomie* **52,** 552–706. doi:10.1007/BF02975837 (1898).

59. Mykytyn, K. & Askwith, C. G-Protein-Coupled receptor signaling in cilia. *Cold Spring Harbor Perspectives in Biology* **9.** doi:10.1101/cshperspect.a028183 (2017).

60. Cheng, Z., Garvin, D., Paguio, A., Stecha, P., Wood, K. & Fan, F. Luciferase Reporter Assay System for Deciphering GPCR Pathways. *Current Chemical Genomics* **4,** 84–91. doi:10.2174/1875397301004010084 (2010).

61. Ebong, E. E., Macaluso, F. P., Spray, D. C. & Tarbell, J. M. Imaging the Endothelial Glycocalyx In Vitro by Rapid Freezing/Freeze Substitution Transmission Electron Microscopy. *Arteriosclerosis, Thrombosis, and Vascular Biology* **31,** 1908–1915. doi:10.1161/ATVBAHA.111.225268 (2011).

62. Reitsma, S., Slaaf, D. W., Vink, H., van Zandvoort, M. A. M. J. & oude Egbrink, M. G. A. The endothelial glycocalyx: composition, functions, and visualization. *Pflugers Archiv* **454,** 345–359. doi:10.1007/s00424-007-0212-8 (2007).

63. Feynman, R. P., Leighton, R. B. & Sands, M. L. *The Feynman lectures on physics* (Pearson Addison Wesley, San Francisco, 2006).

64. Einstein, A. Über die von der molekularkinetischen Theorie der Wärme geforderte Bewegung von in ruhenden Flüssigkeiten suspendierten Teilchen. *Annalen der Physik* **322.** doi:10.1002/andp.19053220806 (1905).

65. Widrow, B., Kim, Y., Park, D. & Perin, J. K. in *Artificial Intelligence in the Age of Neural Networks and Brain Computing* (eds Kozma, R., Alippi, C., Choe, Y. & Morabito, F. C.) 1–30 (Academic Press, 2019). doi:10.1016/B978-0-12-815480-9.00001-3.

66. Berg, H. & Purcell, E. Physics of chemoreception. *Biophysical Journal* **20,** 193–219. doi:10.1016/S0006-3495(77)85544-6 (1977).

67. Bowman, C. W., Ward, D. M., Johnson, A. I. & Trass, O. Mass transfer from fluid and solid spheres at low Reynolds numbers. *The Canadian Journal of Chemical Engineering* **39,** 9–13. doi:10.1002/cjce.5450390104 (1961).

68. Friedlander, S. K. Mass and heat transfer to single spheres and cylinders at low Reynolds numbers. *AIChE Journal* **3,** 43–48. doi:10.1002/aic.690030109 (1957).

69. Masoud, H. & Stone, H. A. The reciprocal theorem in fluid dynamics and transport phenomena. *Journal of Fluid Mechanics* **879,** P1. doi:10.1017/jfm.2019.553 (2019).

70. Berbari, N. F., O'Connor, A. K., Haycraft, C. J. & Yoder, B. K. The Primary Cilium as a Complex Signaling Center. *Current Biology* **19.** doi:10.1016/j.cub.2009.05.025 (2009).

71. Hilgendorf, K. I., Johnson, C. T. & Jackson, P. K. The primary cilium as a cellular receiver: organizing ciliary GPCR signaling. *Current Opinion in Cell Biology* **39,** S0955067416300151. doi:10.1016/j.ceb.2016.02.008 (2016).

72. Spasic, M. & Jacobs, C. R. Primary cilia: Cell and molecular mechanosensors directing whole tissue function. *Seminars in Cell & Developmental Biology* **71,** 42–52. doi:10.1016/j.semcdb.2017.08.036 (2017).

73. Ferreira, R. R., Fukui, H., Chow, R., Vilfan, A. & Vermot, J. The cilium as a force sensor – myth versus reality. *Journal of Cell Science* **132,** jcs213496. doi:10.1242/jcs.213496 (2019).

74. Brooks, E. R. & Wallingford, J. B. Multiciliated Cells. *Current Biology* **24,** R973–R982. doi:10.1016/j.cub.2014.08.047 (2014).

75. Spassky, N. & Meunier, A. The development and functions of multiciliated epithelia. *Nature Reviews Molecular Cell Biology* **18,** 423–436. doi:10.1038/nrm.2017.21 (2017).

76. Golestanian, R., Yeomans, J. M. & Uchida, N. Hydrodynamic synchronization at low Reynolds number. *Soft Matter* **7,** 3074. doi:10.1039/c0sm01121e (2011).

77. Gilpin, W., Bull, M. S. & Prakash, M. The multiscale physics of cilia and flagella. *Nature Reviews Physics* **2,** 74–88. doi:10.1038/s42254-019-0129-0 (2020).

78. Uchida, N. & Golestanian, R. Generic Conditions for Hydrodynamic Synchronization. *Physical Review Letters* **106,** 058104. doi:10.1103/PhysRevLett.106.058104 (2011).

79. Guasto, J. S., Rusconi, R. & Stocker, R. Fluid Mechanics of Planktonic Microorganisms. *Annual Review of Fluid Mechanics* **44,** 373–400. doi:10.1146/annurev-fluid-120710-101156 (2012).

80. Lisicki, M., Velho Rodrigues, M. F., Goldstein, R. E. & Lauga, E. Swimming eukaryotic microorganisms exhibit a universal speed distribution. *eLife* **8,** 447. doi:10.7554/eLife.44907 (2019).

81. Bustamante-Marin, X. M. & Ostrowski, L. E. Cilia and Mucociliary Clearance. *Cold Spring Harbor Perspectives in Biology* **9,** a028241. doi:10.1101/cshperspect.a028241 (2017).

82. Shah, A. S., Yehuda, B. S., Moninger, T. O., Kline, J. N. & Welsh, M. J. Motile cilia of human airway epithelia are chemosensory. *Science* **325,** 1131–1134. doi:10.1126/science.1173869 (2009).

83. Lee, I. T. *et al.* ACE2 localizes to the respiratory cilia and is not increased by ACE inhibitors or ARBs. *Nature Communications* **11,** 265. doi:10.1038/s41467-020-19145-6 (2020).

84. Leinders-Zufall, T. *et al.* Ultrasensitive pheromone detection by mammalian vomeronasal neurons. *Nature* **405,** 792–796. doi:10.1038/35015572 (2000).

85. Bhandawat, V., Reisert, J. & Yau, K.-W. Signaling by olfactory receptor neurons near threshold. *Proceedings of the National Academy of Sciences* **107,** 18682–18687. doi:10.1073/pnas.1004571107 (2010).

86. Kaupp, U. B. *et al.* The signal flow and motor response controling chemotaxis of sea urchin sperm. *Nature Cell Biology* **5,** 109–117. doi:10.1038/ncb915 (2003).

87. Bialek, W. & Setayeshgar, S. Physical limits to biochemical signaling. *Proceedings of the National Academy of Sciences* **102,** 0504321102. doi:10.1073/pnas.0504321102 (2005).

88. Endres, R. G. & Wingreen, N. S. Maximum Likelihood and the Single Receptor. *Physical Review Letters* **103,** 158101. doi:10.1103/PhysRevLett.103.158101 (2009).

89. Adam, G. & Delbrück, M. in *Structural Chemistry and Molecular Biology* (eds Rich, A. & Davidson, N.) 198–215 (W.H. Freeman, San Francisco, 1968). doi:10.1016/S0378-4371(99)00485-9.

90. Short, M. B., Solari, C. A., Ganguly, S., Powers, T. R., Kessler, J. O. & Goldstein, R. E. Flows driven by flagella of multicellular organisms enhance long-range molecular transport. *Proceedings of the National Academy of Sciences* **103,** 8315–8319. doi:10.1073/pnas.0600566103 (2006).

91. Reiten, I. *et al.* Motile-Cilia-Mediated Flow Improves Sensitivity and Temporal Resolution of Olfactory Computations. *Current Biology* **27,** 166–174. doi:10.1016/j.cub.2016.11.036 (2017).

92. Snow, C. *Formulas for Computing Capacitance and Inductance* (U.S. Government Printing Office, 1954).

93. Challis, R. C. *et al.* An olfactory cilia pattern in the mammalian nose ensures high sensitivity to odors. *Current Biology* **25,** 2503–2512. doi:10.1016/j.cub.2015.07.065 (2015).

94. Williams, C. L. *et al.* Direct evidence for BBSome-associated intraflagellar transport reveals distinct properties of native mammalian cilia. *Nature Communications* **5,** 444. doi:10.1038/ncomms6813 (2014).

95. Paffuti, G. *Results for Capacitances and Forces in cylindrical systems* 2018.

96. Stone, H. A. Heat/mass transfer from surface films to shear flows at arbitrary Peclet numbers. *Physics of Fluids A* **1,** 1112–1122. doi:10.1063/1.857335 (1989).

97. Smith, D. J., Blake, J. R. & Gaffney, E. A. Fluid mechanics of nodal flow due to embryonic primary cilia. *Journal of the Royal Society Interface* **5,** 567–573. doi:10.1098/rsif.2007.1306 (2008).

98. Ding, Y. & Kanso, E. Selective particle capture by asynchronously beating cilia. *Physics of Fluids* **27,** 121902. doi:10.1063/1.4938558 (2015).

99. Nawroth, J. C. *et al.* Motile cilia create fluid-mechanical microhabitats for the active recruitment of the host microbiome. *Proceedings of the National Academy of Sciences* **114,** 9510–9516. doi:10.1073/pnas.1706926114 (2017).

100. Frings, S. & Lindemann, B. Single unit recording from olfactory cilia. *Biophysical Journal* **57,** S0006349590826278. doi:10.1016/S0006-3495(90)82627-8 (1990).

101. Zhang, J., Pacifico, R., Cawley, D., Feinstein, P. & Bozza, T. Ultrasensitive Detection of Amines by a Trace Amine-Associated Receptor. *Journal of Neuroscience* **33,** 33/7/3228. doi:10.1523/JNEUROSCI.4299-12.2013 (2013).

102. Lai, S. K., Wang, Y.-Y., Wirtz, D. & Hanes, J. Micro- and macrorheology of mucus. *Advanced Drug Delivery Reviews* **61,** 86–100. doi:10.1016/j.addr.2008.09.012 (2009).

103. Ferreira, R. R., Vilfan, A., Jülicher, F., Supatto, W. & Vermot, J. Physical limits of flow sensing in the left-right organizer. *eLife* **6,** e25078. doi:10.7554/eLife.25078 (2017).

104. Tanaka, Y., Okada, Y. & Hirokawa, N. FGF-induced vesicular release of Sonic hedgehog and retinoic acid in leftward nodal flow is critical for left–right determination. *Nature* **435,** 172–177. doi:10.1038/nature03494 (2005).

105. Tripathi, A., Bhattacharya, A. & Balazs, A. C. Size Selectivity in Artificial Cilia–Particle Interactions: Mimicking the Behavior of Suspension Feeders. *Langmuir* **29,** 4616–4621. doi:10.1021/la400318f (2013).

106. Meng, F., Matsunaga, D., Yeomans, J. M. & Golestanian, R. Magnetically-actuated artificial cilium: a simple theoretical model. *Soft Matter* **15,** 3864–3871. doi:10.1039/c8sm02561d (2019).

107. Matsunaga, D. *et al.* Controlling collective rotational patterns of magnetic rotors. *Nature Communications* **10,** 4696. doi:10.1038/s41467-019-12665-w (2019).

108. Ramírez-Piscina, L. Fixed-density boundary conditions in overdamped Langevin simulations of diffusion in channels. *Physical Review E* **98,** 013302. doi:10.1103/physreve.98.013302 (2018).

109. Tocino, A. & Senosiain, M. J. Two-step Milstein schemes for stochastic differential equations. *Numerical Algorithms* **69,** 643–665. doi:10.1007/s11075-014-9918-9 (2015).

110. King, A. J. *et al.* Selfish-herd behaviour of sheep under threat. *Current Biology* **22,** R561–R562. doi:10.1016/j.cub.2012.05.008 (2012).

111. Garcia, A., Krummel, G. & Priya, S. Fundamental understanding of millipede morphology and locomotion dynamics. *Bioinspiration & Biomimetics* **16,** 026003. doi:10.1088/1748-3190/abbdcc (2020).

112. Peshkov, A., McGaffigan, S. & Quillen, A. C. Synchronized oscillations in swarms of nematode Turbatrix aceti. *Soft Matter* **18,** 1174–1182. doi:10.1039/D1SM01572A (2022).

113. Chateau, S., Favier, J., Poncet, S. & D'Ortona, U. Why antiplectic metachronal cilia waves are optimal to transport bronchial mucus. *Physical Review E* **100,** 791. doi:10.1103/PhysRevE.100.042405 (2019).

114. Brumley, D. R., Polin, M., Pedley, T. J. & Goldstein, R. E. Hydrodynamic Synchronization and Metachronal Waves on the Surface of the Colonial Alga *Volvox* carteri. *Physical Review Letters* **109,** 268102. doi:10.1103/PhysRevLett.109.268102 (2012).

115. Ford, M. P. & Santhanakrishnan, A. On the role of phase lag in multi-appendage metachronal swimming of euphausiids. *Bioinspiration & Biomimetics* **16,** 066007. doi:10.1088/1748-3190/abc930 (Sept. 2021).

116. Byron, M. L. *et al.* Metachronal Motion across Scales: Current Challenges and Future Directions. *Integrative and Comparative Biology* **61,** 1674–1688. doi:10.1093/icb/icab105 (2021).

117. Zhang, R., den Toonder, J. & R. Onck, P. Metachronal patterns by magnetically-programmable artificial cilia surfaces for low Reynolds number fluid transport and mixing. *Soft Matter* **18,** 3902–3909. doi:10.1039/D1SM01680F (2022).

118. Wan, K. Y. & Goldstein, R. E. Coordinated beating of algal flagella is mediated by basal coupling. *Proceedings of the National Academy of Sciences* **113.** doi:10.1073/pnas.1518527113 (2016).

119. Quaranta, G., Aubin-Tam, M.-E. & Tam, D. Hydrodynamics Versus Intracellular Coupling in the Synchronization of Eukaryotic Flagella. *Physical Review Letters* **115,** 238101. doi:10.1103/PhysRevLett.115.238101 (2015).

120. Liu, Y., Claydon, R., Polin, M. & Brumley, D. R. Transitions in synchronization states of model cilia through basal-connection coupling. *Journal of the Royal Society Interface* **15,** 20180450. doi:10.1098/rsif.2018.0450 (2018).

121. Goldstein, R. E., Polin, M. & Tuval, I. Noise and Synchronization in Pairs of Beating Eukaryotic Flagella. *Physical Review Letters* **103,** 168103. doi:10.1103/PhysRevLett.103.168103 (2009).

122. Chelakkot, R., F. Hagan, M. & Gopinath, A. Synchronized oscillations, traveling waves, and jammed clusters induced by steric interactions in active filament arrays. *Soft Matter* **17,** 1091–1104. doi:10.1039/D0SM01162B (2021).

123. Geyer, V. F., Jülicher, F., Howard, J. & Friedrich, B. M. Cell-body rocking is a dominant mechanism for flagellar synchronization in a swimming alga. *Proceedings of the National Academy of Sciences* **110,** 18058–18063. doi:10.1073/pnas.1300895110 (2013).

124. Guo, H., Man, Y., Wan, K. Y. & Kanso, E. Intracellular coupling modulates biflagellar synchrony. *Journal of the Royal Society Interface* **18,** 20200660. doi:10.1098/rsif.2020.0660 (2021).

125. Klindt, G. S., Ruloff, C., Wagner, C. & Friedrich, B. M. In-phase and anti-phase flagellar synchronization by waveform compliance and basal coupling. *New Journal of Physics* **19,** 113052. doi:10.1088/1367-2630/aa9031 (2017).

126. Pikovskij, A., Rosenblum, M. & Kurths, J. *Synchronization: a universal concept in nonlinear sciences* (Cambridge Univ. Press, 2007).

127. Man, Y. & Kanso, E. Multisynchrony in Active Microfilaments. *Physical Review Letters* **125,** 148101. doi:10.1103/PhysRevLett.125.148101 (2020).

128. Goldstein, R. E., Lauga, E., Pesci, A. I. & Proctor, M. R. E. Elastohydrodynamic synchronization of adjacent beating flagella. *Physical Review Fluids* **1,** 73201. doi:10.1103/PhysRevFluids.1.073201 (2016).

129. Guirao, B. & Joanny, J.-F. Spontaneous Creation of Macroscopic Flow and Metachronal Waves in an Array of Cilia. *Biophysical Journal* **92,** 1900–1917. doi:10.1529/biophysj.106.084897 (2007).

130. Kim, Y. W. & Netz, R. R. Pumping Fluids with Periodically Beating Grafted Elastic Filaments. *Physical Review Letters* **96,** 158101. doi:10.1103/PhysRevLett.96.158101 (2006).

131. Solovev, A. & Friedrich, B. M. Lagrangian mechanics of active systems. *European Physical Journal E* **44,** 49. doi:10.1140/epje/s10189-021-00016-x (2021).

132. Vilfan, A. & Jülicher, F. Hydrodynamic flow patterns and synchronization of beating cilia. *Physical Review Letters* **96,** 1–4. doi:10.1103/PhysRevLett.96.058102 (2006).

133. Meng, F., Bennett, R. R., Uchida, N. & Golestanian, R. Conditions for metachronal coordination in arrays of model cilia. *Proceedings of the National Academy of Sciences* **118.** doi:10.1073/pnas.2102828118 (2021).

134. Niedermayer, T., Eckhardt, B. & Lenz, P. Synchronization, phase locking, and metachronal wave formation in ciliary chains. *Chaos* **18,** 037128. doi:10.1063/1.2956984 (2008).

135. Uchida, N. & Golestanian, R. Hydrodynamic synchronization between objects with cyclic rigid trajectories. *European Physical Journal E* **35,** 135. doi:10.1140/epje/i2012-12135-5 (2012).

136. Nasouri, B. & Elfring, G. J. Hydrodynamic interactions of cilia on a spherical body. *Physical Review E* **93,** 033111. doi:10.1103/PhysRevE.93.033111 (2016).

137. Kanale, A. V., Ling, F., Guo, H., Fürthauer, S. & Kanso, E. Spontaneous phase coordination and fluid pumping in model ciliary carpets. *Proceedings of the National Academy of Sciences* **119,** e2214413119. doi:10.1073/pnas.2214413119 (2022).

138. Wollin, C. & Stark, H. Metachronal waves in a chain of rowers with hydrodynamic interactions. *European Physical Journal E* **34,** 42. doi:10.1140/epje/i2011-11042-7 (2011).

139. Uchida, N. & Golestanian, R. Synchronization and collective dynamics in a carpet of microfluidic rotors. *Physical Review Letters* **104,** 178103. doi:10.1103/PhysRevLett.104.178103 (2010).

140. Fruchart, M., Hanai, R., Littlewood, P. B. & Vitelli, V. Non-reciprocal phase transitions. *Nature* **592,** 363–369. doi:10.1038/s41586-021-03375-9 (2021).

141. Kavre, I., Vilfan, A. & Babič, D. Hydrodynamic synchronization of autonomously oscillating optically trapped particles. *Physical Review E* **91,** 031002. doi:10.1103/PhysRevE.91.031002 (2015).

142. Hamilton, E., Bruot, N. & Cicuta, P. The chimera state in colloidal phase oscillators with hydrodynamic interaction. *Chaos* **27,** 123108. doi:10.1063/1.4989466 (2017).

143. Bouhouche, K. *et al.* Paramecium, a Model to Study Ciliary Beating and Ciliogenesis: Insights From Cutting-Edge Approaches. *Frontiers in Cell and Developmental Biology* **10,** 847908. doi:10.3389/fcell.2022.847908 (2022).

144. Sleigh, M. A., Blake, J. R. & Liron, N. The Propulsion of Mucus by Cilia. *American Review of Respiratory Disease* **137,** 726–741. doi:10.1164/ajrccm/137.3.726 (1988).

145. Strathmann, R. R. The feeding behavior of planktotrophic echinoderm larvae: Mechanisms, regulation, and rates of suspension-feeding. *Journal of Experimental Marine Biology and Ecology* **6,** 109–160. doi:10.1016/0022-0981(71)90054-2 (1971).

146. Wan, K. Y. *et al.* Reorganization of complex ciliary flows around regenerating Stentor coeruleus. *Philosophical Transactions of the Royal Society B: Biological Sciences* **375,** 20190167. doi:10.1098/rstb.2019.0167 (2020).

147. Agudo-Canalejo, J. & Golestanian, R. Active Phase Separation in Mixtures of Chemically Interacting Particles. *Physical Review Letters* **123,** 018101. doi:10.1103/PhysRevLett.123.018101 (2019).

148. Nagy, M., Ákos, Z., Biro, D. & Vicsek, T. Hierarchical group dynamics in pigeon flocks. *Nature* **464,** 890–893. doi:10.1038/nature08891 (2010).

149. Montbrió, E. & Pazó, D. Kuramoto Model for Excitation-Inhibition-Based Oscillations. *Physical Review Letters* **120,** 244101. doi:10.1103/PhysRevLett.120.244101 (2018).

150. Lavergne, F. A., Wendehenne, H., Bäuerle, T. & Bechinger, C. Group formation and cohesion of active particles with visual perception–dependent motility. *Science* **364,** 70–74. doi:10.1126/science.aau5347 (2019).

151. Brennen, C. & Winet, H. Fluid Mechanics of Propulsion by Cilia and Flagella. *Annual Review of Fluid Mechanics* **9,** 339–398. doi:10.1146/annurev.fl.09.010177.002011 (1977).

152. Dasgupta, A. & Amack, J. D. Cilia in vertebrate left-right patterning. *Philosophical Transactions of the Royal Society B: Biological Sciences* **371.** doi:10.1098/rstb.2015.0410 (2016).

153. Prandtl, L. Aufgaben der Strömungsforschung (Lecture delivered at the inauguration of the Kaiser Wilhelm Institute for Flow Research in Göttingen, 16 July 1925). *Naturwissenschaften* **14,** 335–338. doi:10.1007/BF01506967 (1926).

154. Taylor, G. I. Analysis of the swimming of microscopic organisms. *Proc. R. Soc. Lond. A* **209,** 447–461. doi:10.1098/rspa.1951.0218 (1951).

155. Hickey, D., Vilfan, A. & Golestanian, R. Ciliary chemosensitivity is enhanced by cilium geometry and motility. *eLife* **10,** e66322. doi:10.7554/eLife.66322 (2021).

156. Knight-Jones, E. W. Relations between Metachronism and the Direction of Ciliary Beat in Metazoa. *Journal of Cell Science* **3,** 503–521. doi:10.1242/jcs.s3-95.32.503 (1954).

157. Narematsu, N., Quek, R., Chiam, K.-H. & Iwadate, Y. Ciliary metachronal wave propagation on the compliant surface of *Paramecium* cells. *Cytoskeleton* **72,** 633–646. doi:10.1002/cm.21266 (2015).

158. Reichert, M. & Stark, H. Synchronization of rotating helices by hydrodynamic interactions. *European Physical Journal E* **17,** 493–500. doi:10.1140/epje/i2004-10152-7 (2005).

159. Qian, B., Jiang, H., Gagnon, D. A., Breuer, K. S. & Powers, T. R. Minimal model for synchronization induced by hydrodynamic interactions. *Physical Review E* **80,** 061919. doi:10.1103/PhysRevE.80.061919 (2009).

160. Uchida, N. & Golestanian, R. Synchronization in a carpet of hydrodynamically coupled rotors with random intrinsic frequency. *Europhysics Letters* **89,** 50011. doi:10.1209/0295-5075/89/50011 (2010).

161. Saha, S., Ramaswamy, S. & Golestanian, R. Pairing, waltzing and scattering of chemotactic active colloids. *New Journal of Physics* **21,** 063006. doi:10.1088/1367-2630/ab20fd (2019).

162. Maestro, A., Bruot, N., Kotar, J., Uchida, N., Golestanian, R. & Cicuta, P. Control of synchronization in models of hydrodynamically coupled motile cilia. *Communications Physics* **1,** 1–8. doi:10.1038/s42005-018-0031-6 (2018).

163. Guo, H., Fauci, L., Shelley, M. & Kanso, E. Bistability in the synchronization of actuated microfilaments. *Journal of Fluid Mechanics* **836,** 304–323. doi:10.1017/jfm.2017.816 (2018).

164. Chakrabarti, B. & Saintillan, D. Hydrodynamic Synchronization of Spontaneously Beating Filaments. *Physical Review Letters* **123,** 208101. doi:10.1103/PhysRevLett.123.208101 (2019).

165. Chakrabarti, B., Fürthauer, S. & Shelley, M. J. A multiscale biophysical model gives quantized metachronal waves in a lattice of cilia. *Proceedings of the National Academy of Sciences* **119,** e2113539119. doi:10.1073/pnas.2113539119 (2022).

166. Soto, R. & Golestanian, R. Self-Assembly of Catalytically Active Colloidal Molecules: Tailoring Activity Through Surface Chemistry. *Phys. Rev. Lett.* **112,** 068301. doi:10.1103/physrevlett.112.068301 (2014).

167. Soto, R. & Golestanian, R. Self-assembly of active colloidal molecules with dynamic function. *Phys. Rev. E* **91,** 052304. doi:10.1103/physreve.91.052304 (2015).

168. Saha, S., Agudo-Canalejo, J. & Golestanian, R. Scalar Active Mixtures: The Nonreciprocal Cahn-Hilliard Model. *Physical Review X* **10,** 041009. doi:10.1103/PhysRevX.10.041009 (2020).

169. Loos, S. A. M. & Klapp, S. H. L. Irreversibility, heat and information flows induced by non-reciprocal interactions. *New Journal of Physics* **22,** 123051. doi:10.1088/1367-2630/abcc1e (2020).

170. Osat, S. & Golestanian, R. Non-reciprocal multifarious self-organization. *Nature Nanotechnology* **18,** 79–85. doi:10.1038/s41565-022-01258-2 (2023).

171. Solovev, A. & Friedrich, B. M. Synchronization in cilia carpets: multiple metachronal waves are stable, but one wave dominates. *New Journal of Physics* **24,** 013015. doi:10.1088/1367-2630/ac2ae4 (2022).

172. Elfring, G. J. & Lauga, E. Hydrodynamic Phase Locking of Swimming Microorganisms. *Phys. Rev. Lett.* **103,** 088101. doi:10.1103/PhysRevLett.103.088101 (8 2009).

173. Solovev, A. & Friedrich, B. M. Synchronization in cilia carpets and the Kuramoto model with local coupling: Breakup of global synchronization in the presence of noise. *Chaos* **32,** 013124. doi:10.1063/5.0075095 (2022).

174. Boselli, F., Jullien, J., Lauga, E. & Goldstein, R. E. Fluid Mechanics of Mosaic Ciliated Tissues. *Physical Review Letters* **127,** 198102. doi:10.1103/PhysRevLett.127.198102 (2021).

175. Ghorbani, A. & Najafi, A. Symplectic and antiplectic waves in an array of beating cilia attached to a closed body. *Physical Review E* **95,** 052412. doi:10.1103/PhysRevE.95.052412 (2017).

176. Brumley, D. R., Wan, K. Y., Polin, M. & Goldstein, R. E. Flagellar synchronization through direct hydrodynamic interactions. *eLife* **3,** e02750. doi:10.7554/eLife.02750 (2014).

177. Soh, A. W. J. *et al.* Intracellular connections between basal bodies promote the coordinated behavior of motile cilia. *Molecular Biology of the Cell* **33,** br18. doi:10.1091/mbc.E22-05-0150 (2022).

178. Theers, M. & Winkler, R. G. Synchronization of rigid microrotors by time-dependent hydrodynamic interactions. *Physical Review E* **88,** 023012. doi:10.1103/PhysRevE.88.023012 (2013).

179. Wei, D., Dehnavi, P. G., Aubin-Tam, M.-E. & Tam, D. Measurements of the unsteady flow field around beating cilia. *Journal of Fluid Mechanics* **915,** A70. doi:10.1017/jfm.2021.149 (2021).

180. Bottier, M., Thomas, K. A., Dutcher, S. K. & Bayly, P. V. How Does Cilium Length Affect Beating? *Biophysical Journal* **116,** 1292–1304. doi:10.1016/j.bpj.2019.02.012 (2019).

181. Verra, F., Escudier, E., Lebargy, F., Bernaudin, J. F., Crémoux, H. d. & Bignon, J. Ciliary Abnormalities in Bronchial Epithelium of Smokers, Ex-smokers, and Nonsmokers. *American Journal of Respiratory and Critical Care Medicine* **151.** doi:10.1164/ajrccm/151.3_Pt_1.630 (2013).

182. Nawroth, J. C., Barrile, R., Conegliano, D., van Riet, S., Hiemstra, P. S. & Villenave, R. Stem cell-based Lung-on-Chips: The best of both worlds? *Advanced Drug Delivery Reviews* **140,** 12–32. doi:10.1016/j.addr.2018.07.005 (2019).

183. Den Toonder, J. M. J. & Onck, P. R. Microfluidic manipulation with artificial/bioinspired cilia. *Trends in Biotechnology* **31,** 85–91. doi:10.1016/j.tibtech.2012.11.005 (2013).

184. Young, D. M. *Iterative Solution of Large Linear Systems* (Academic Press, Orlando, FL, 1971).

185. Welch, P. The use of fast Fourier transform for the estimation of power spectra: A method based on time averaging over short, modified periodograms. *IEEE Transactions on Audio and Electroacoustics* **15,** 70–73. doi:10.1109/TAU.1967.1161901 (1967).

186. Ma, R., Klindt, G. S., Riedel-Kruse, I. H., Jülicher, F. & Friedrich, B. M. Active Phase and Amplitude Fluctuations of Flagellar Beating. *Physical Review Letters* **113,** 048101. doi:10.1103/PhysRevLett.113.048101 (July 2014).

187. Leopold, P. L., O'Mahony, M. J., Lian, X. J., Tilley, A. E., Harvey, B.-G. & Crystal, R. G. Smoking Is Associated with Shortened Airway Cilia. *PLoS ONE* **4,** e8157. doi:10.1371/journal.pone.0008157 (2009).

188. Jonsdottir, H. R. & Dijkman, R. Coronaviruses and the human airway: A universal system for virus-host interaction studies. *Virology Journal* **13.** doi:10.1186/s12985-016-0479-5 (2016).

189. Buqaileh, R., Saternos, H., Ley, S., Aranda, A., Forero, K. & AbouAlaiwi, W. A. Can cilia provide an entry gateway for SARS-CoV-2 to human ciliated cells? *Physiological Genomics* **53,** 249–258. doi:10.1152/physiolgenomics.00015.2021 (2021).

190. Robinot, R. *et al.* SARS-CoV-2 infection induces the dedifferentiation of multiciliated cells and impairs mucociliary clearance. *Nature Communications* **12,** 4354. doi:10.1038/s41467-021-24521-x (2021).

191. Tilley, A. E., Walters, M. S., Shaykhiev, R. & Crystal, R. G. Cilia Dysfunction in Lung Disease. *Annual Review of Physiology* **77,** 379–406. doi:10.1146/annurev-physiol-021014-071931 (2015).